Los Angeles-Long Beach Harbors and San Pedro Bay Hydrodynamic and Sediment-Contaminant Transport Model Calibration

DRAFT

February 2009

Prepared for:
USEPA Region 9
Los Angeles Regional Water Quality Control Board

Prepared by:
Tetra Tech, Inc.

Table of Contents

Appendix D: Sediment and Contaminant Transport Model Sensitivity to Long-Term Load Reductions

Appendix E: Analysis of Additional Water Column Metals and Suspended Solids Data

List of Figures

List of Tables

1. Introduction

This report summarizes the development and calibration of the hydrodynamic and sediment transport model components of a coupled hydrodynamic and water quality modeling system under development to support TMDLs in the greater Los Angeles and Long Beach Harbors, including the Los Angeles River estuary and San Pedro Bay. The report presents the overall modeling framework to support TMDL development, observational data to support the hydrodynamic and sediment transport model configuration and calibration, and calibration results.

Areas of the Los Angeles and Long Beach Harbors and San Pedro Bay, including their tributaries, the Los Angeles and San Gabriel Rivers and Dominguez Channel, are currently on the State of California's 303(d) list of impaired waters. A variety of toxic inorganic and organic contaminants contribute to benthic effects and sediment toxicity impairments. Specific inorganic metal contaminants on the list include cadmium, chromium, copper, lead, mercury, nickel, and zinc. Organic contaminants listed include chlordane, DDT, dieldrin, PAHs, PCBs, and toxaphene. The fate and transport of metals and organic contaminants in surface water systems is strongly coupled with the fate and transport of organic and inorganic sediments and dissolved organic material due to their affinity to adsorb to sediment particles and bond with dissolved organic carbon to form complexes.

Hydrodynamic and water quality models provide an important tool to evaluate existing conditions, including identifying non-point source load contributions, source controls, and TMDL allocation alternatives. A modeling system that includes hydrodynamic, sediment transport, and contaminant transport and fate is necessary to assess current conditions and potential load reduction scenarios for the listed waterbodies. This report provides an update on the status of the development of the hydrodynamic component of this modeling system, including calibration results (Section 5, Section 6, and Appendix A), and describes the sediment transport and contaminant transport and fate components. The report is organized as follows:

- *Modeling Framework*. Summarizes the overall modeling framework including model selection and the sequence of steps leading to the decision support modeling system for TMDL development.
- *Observational Data for Model Configuration and Calibration*. Summarizes available observational data for configuration and calibration of the hydrodynamic model component.
- *Hydrodynamic Model Configuration*. Describes general and hydrodynamic configuration of the model for the greater Los Angeles and Long Beach Harbors system.
- *Hydrodynamic Calibration*. Outlines the approach used and presents results for the hydrodynamic and transport calibration.

- *Sediment and Contaminant Transport Configuration.* Describes the configuration of the sediment and contaminant transport and fate components of the modeling including analysis of field observations.
- *Sediment and Contaminant Transport Calibration*. Outlines the approach used and presents calibration results.
- *Summary and Recommendations*. Summarizes the status of the calibration and makes recommendations for use of the model for TMDL development.
- *Appendix A*. Provides time series plots of the salinity calibration.
- *Appendix B*. Describes the model performance measures used to compare model output and observed data during model calibration.
- *Appendix C.* Presents dry season model sensitivity analyses.
- *Appendix D*. Presents model sensitivity to long-term load reductions.
- *Appendix E.* Provides analyses of additional water column data.

2. Modeling Framework

A modeling system to support TMDL development for metals and hydrophobic organic compounds in the greater Los Angeles and Long Beach Harbors system requires three primary components: hydrodynamic, sediment transport, and contaminant transport and fate. The U. S. Army Corps of Engineers (ACOE) has conducted numerous hydrodynamic and eutrophication modeling studies in the greater harbors area (Seabergh and Outlaw, 1984; Seabergh, 1985; CERC, 1990; Hall, 1990; Hall, 1995; Wang et al., 1995; Miller et al., 1998; Bunch, et al., 2000, 2002, 2003) using the proprietary CH3D hydrodynamic and CE-QAUL-IC water quality models. No previous modeling efforts have addressed the fate and transport of sediment adsorbed toxic metals and organic compounds in the greater harbor waters.

The Environmental Fluid Dynamics Code (EFDC) (Hamrick, 1992; Hamrick and Wu; 1997; Park et al., 1995) was selected for this study for a number of reasons. The EFDC model includes all required model components (hydrodynamic, sediment transport, and contaminant transport and fate) and is in the public domain, as well as being supported by the U. S. Environmental Protection Agency (EPA). The EFDC model has been used for more than 100 surface water modeling applications including nutrient TMDL development (Wool et al., 2003; Zou et al., 2006) and metals and organic contaminant fate and transport at conventional (Ji et al., 2002; King County, 1999) and superfund sites (U. S. EPA, Region 1, 2006; U. S. EPA Region 10, 2006). An EFDC model was developed by the Port of Los Angeles for the Dominguez Channel estuary and the Consolidated Slips.

The EFDC modeling framework to support TMDL development in the greater harbors systems was undertaken in a sequence of steps. The first step was configuration and calibration of the model hydrodynamic component, including

salinity and temperature transport. This step was followed by the configuration and calibration of the sediment transport and contaminant fate and transport components. Both of these steps utilized results from two complimentary studies. Fresh water inflow and associated sediment and contaminant loads were provided by LSPC models of the near shore watersheds and the three larger watersheds (Dominguez Channel, Los Angeles River, and San Gabriel River watersheds) (Tetra Tech, 2006). The EFDC model had previously been applied to simulate sediment and metals transport in the tidal region of Dominguez Channel (Everest, 2006). The model grid used in the Dominguez study was adopted for this study. Field observations collected during that study were also used for model calibration and validation in this current effort. This report summarizes the configuration and calibration of the hydrodynamic, sediment transport, and contaminant transport and fate components of this modeling system.

3. Observational Data for Model Configuration and Calibration

Observational data for the hydrodynamic model falls within two general classes: data used for model configuration and data used for model calibration. Model configuration data includes the water body shoreline, bathymetry, data used for specifying hydrodynamic and salinity and temperature boundary conditions, atmospheric wind and thermal forcing, and inflows. Calibration data includes observations of hydrodynamic variables predicted by the modeling including water surface elevation, horizontal currents, salinity, temperature, and dye tracer concentration.

Table 1 summarizes the observational data currently used for hydrodynamic model configuration and calibration. Data listed in Table 1 and used for the hydrodynamic model configuration and calibration are discussed later in this report. It is useful to summarize that the available observational data for hydrodynamic model configuration are very adequate, while the data for model calibration could be judged as less adequate. The available data being used for calibration are limited to two tide gauges, four current meters within the breakwater, six current meters outside the breakwater in San Pedro Bay, and approximately 120 salinity and temperature monitoring stations.

The adequacy of the data for calibration relates strongly to the hydrodynamic characteristics of the greater harbors system. Previous modeling studies by the ACOE indicated that water surface elevation amplitude and phase vary insignificantly in the system and that the long-term NOAA tide gauge record is representative of the entire system. Recent current meter observations within the breakwater (POLA Prop 13, Table 1) have been confined to the inner regions of Los Angeles Harbor. Current meter observations outside the breakwater (LSCSD Palos Verde Shelf, Table 1) were useful in developing boundary conditions, but are far removed from the primary area of interest.

Table 1. Data Used for Hydrodynamic Model Configuration and Calibration

Data Type	Use	Source
Shoreline, Breakwaters and Fairways	Model Grid Generation	NOAA Electronic Navigation Charts
Bathymetry	Primary Model Bathymetry Configuration	NOAA High Resolution Coastal Relief Bathymetric Data Set
Bathymetry	Local Model Bathymetry Configuration	NOAA Electronic Navigation Charts
Bathymetry	Local Model Bathymetry Configuration	Port of Los Angeles
Tide Gauge Record at Port of Los Angeles	Development of Tidal Boundary Conditions and Tidal Elevation Calibration	NOAA Center for Operational Oceanographic Products and Services
Port of Los Angeles Prop 13 Current Meter Record	Tidal Elevation Calibration	Electronic Data Provided to US EPA by Study Contractor
LSCSD Palo Verde Shelf Study Current Meter and CTD Records	Development of Tidal and Temperature Boundary Conditions and Tidal Current Calibration	Electronic Data Provided to US EPA by Study Contractor (SAIC, 2004)
Port of Los Angeles Prop 13 Current Meter Record	Tidal Current Calibration	Electronic Data Provided to US EPA by Study Contractor
Stream Flow Records	Dominguez Channel Los Angeles and San Gabriel River Inflows	County of Los Angeles, Department of Public Works
WWTP Discharge Record	Terminal Island Treatment Plant Discharge	City of Los Angeles
Wind Speed and Direction Records	Wind Forcing	NOAA National Climate Data Center LAX Airport Station
Wind Speed and Direction Records	Wind Forcing	California Irrigation Management System, Long Beach and Santa Monica Station
Wind Speed and Direction Records	Wind Forcing	NOAA National Data Buoy Center Stations 46025, 46086
Atmospheric Temperature, Relative Humidity, Solar Radiation and Cloud Cover Records	Atmospheric Thermal Forcing	NOAA National Climate Data Center LAX Airport Station
Atmospheric Temperature, Relative Humidity, Solar Radiation and Cloud Cover Records	Atmospheric Thermal Forcing	California Irrigation Management System, Long Beach and Santa Monica Stations
Salinity and Temperature Monitoring Data	Transport Calibration and Temperature Calibration	City of Los Angeles
Salinity and Temperature Monitoring Data	Transport Calibration and Temperature Calibration	Harbor Generating Station
Salinity and Temperature Monitoring Data	Transport Calibration and Temperature Calibration	Port of Los Angeles
Salinity and Temperature Monitoring Data	Transport Calibration and Temperature Calibration	Port of Los Angeles & Port of Long Beach Biological Baseline Study
Port of Los Angeles Prop 13 Salinity, Temperature and Dye Data	Transport Calibration	Electronic Data Provided to US EPA by Study Contractor
Port of Long Beach Tide Gauge and Current Meter Data	Tidal Elevation	Horizontal ADCP Monitoring Pier J Basin Winter Monitoring Report (Moffatt & Nichol, 2004)
Salinity and Temperature Monitoring Data (Bight 03 data on stormwater runoff and dispersion)	Transport Calibration and Temperature Calibration	SCCWRP and others

Table 1 lists a number of discrete salinity and temperature monitoring studies, representing approximately 120 stations. With respect to temperature, these data are very adequate. However because temperature variability is primarily temporal, model temperature prediction is more of a measure of correctness of atmospheric thermal forcing rather than hydrodynamic transport. The adequacy of the salinity observations in these monitoring data sets is very limited. This is due to the climate and hydrology of the area that results in significant salinity variability being associated with episodic freshwater inflow events. Of the 120 monitoring stations, only 20 have observations corresponding to times when the salinity is significantly less than the 32 to 33 ppt level characteristic of the greater harbors system. Further, at these 20 stations, there are only three observations per station showing depressed salinity.

Table 2 summarizes data used for sediment transport and contaminant fate and transport configuration and calibration. These data are described in detail throughout sections 7 and 8 and their associated appendices.

Table 2. Data Used for Sediment and Contaminant Model Configuration and Calibration

Data Description	Use	Source
POLA/POLB – Sediment bed physical data (2006)	Sediment Bed Physical Model Initialization	Electronic Data Provided to US EPA by Study Contractor
Bight 03 – Sediment bed physical data (2003)	Sediment Bed Physical Model Initialization	Electronic Data Provided by SCCWRP
Bight 94 – Sediment bed physical data (1994)	Sediment Bed Physical Model Initialization	Contaminated Sediments Task Force Database
Bight 98 – Sediment bed physical data (1998)	Sediment Bed Physical Model Initialization	Contaminated Sediments Task Force Database
POLA/POLB Biological Baseline Study – Sediment bed physical data (2000)	Sediment Bed Physical Model Initialization	Electronic Reports Provided to US EPA
Bay Protection and Toxic Cleanup – Sediment bed physical data (1997)	Sediment Bed Physical Model Initialization	Contaminated Sediments Task Force Database
Western EMAP – Sediment bed physical data (1999)	Sediment Bed Physical Model Initialization	Contaminated Sediments Task Force Database
POLA/POLB Special Studies (1998-2001) POLA Berth 100 Final Report POLA Berth 121, 122-124 Final Rprt 2/2 POLA Berth 240B Final Report POLA Berths 148-151 Sed Test POLA Berths 167-169 Sed Tests POLA Berths 212-215 Sed Tests POLA Berths 263-264 Sed Tests POLA Slip 5 Sed Tests POLA West Ch B40-44 Sed Testing POLB Contract HD5951 POLB Pier J, East Channel Dredge POLB Pier S Dredging, Final Report POLB West Basin, 8/98 Sed Testing	Sediment Bed Physical Model Initialization	Contaminated Sediments Task Force Database

Data Description	Use	Source
Harbor Generating Station - Sediment chemistry data (2001-2003)	Sediment Bed Chemistry Model Initialization	Electronic Data Provided to US EPA by Contractor during 303(d) data compilation efforts
Terminal Island Treatment Plant - Sediment chemistry data (2001-2003)	Sediment Bed Chemistry Model Initialization	Electronic Data Provided to US EPA by City of Los Angeles, Environmental Monitoring Division
EPA/POLA/AMEC - Sediment chemistry data (2002)	Sediment Bed Chemistry Model Initialization	Electronic Data Provided to US EPA by Study Contractor
Bight 03 – Sediment chemistry data (2003)	Sediment Bed Chemistry Model Initialization	Electronic Data Provided by SCCWRP
POLA/POLB – Sediment chemistry data (2006)	Sediment Bed Chemistry Model Initialization	Electronic Data Provided to US EPA by Study Contractor
POLA/POLB – Overlying water chemistry data (2006)	Water Column Chemistry Calibration	Electronic Data Provided to US EPA by Study Contractor
POLA/POLB – Mid-column water chemistry data at POLB stations (2006)	Water Column Chemistry Calibration	Electronic Data Provided to US EPA by Study Contractor
POLA - Mid-column water chemistry data at POLA stations (2005)	Water Column Chemistry Calibration	Electronic Data Provided to US EPA by Port of Los Angeles

4. Model Configuration

The following subsections outline the steps conducted to configure the EFDC hydrodynamic model.

4.1. Model Grid System

A multi-resolution, curvilinear spatial grid of the greater harbors and San Pedro Bay was constructed using the using the Visual Orthogonal Grid Generation (VOGG) grid generation system (Tetra Tech, 2002). Shoreline boundaries for the grid were based on the NOAA/NOS electronic navigation charts in GIS format. The grid and shoreline, with the exception of the Dominguez Channel area, are shown in Figure 1. The Dominguez Channel grid from a previous study was incorporated into the model (Everest, 2006). The grid system uses a multi-domain mapping, unique to the EFDC model, which allow a course resolution outside the breakwater in San Pedro Bay and a finer resolution in the harbors system. The grid has 2,568 horizontal cells. In the vertical, the number of sigma layers is readily changed to allow for use of an optimum number of layers to represent hydrodynamic and transport processes. For this study four vertical layers were used.

4.2. Bathymetry and Topography

Bathymetric data were interpolated on to the model grid using an average of the bathymetric data points falling within a cell. The primary bathymetric data set

used was the NOAA High Resolution Coastal Relief Data, which has a horizontal resolution of approximately 90 meters. This data set was supplemented by recent bathymetric survey data provided by the Port of Los Angeles. Additional bathymetry adjustments were made by visual comparison of gridded bathymetry with NOAA/NOS electronic navigation charts. Model bathymetry is shown in Figure 2.

4.3. Selection of Temporal Simulation Period

The hydrodynamic and transport model was configured for a four-year historical simulation period spanning January 2002 through December 2005, since this period encompasses the greatest density of observational data for model calibration.

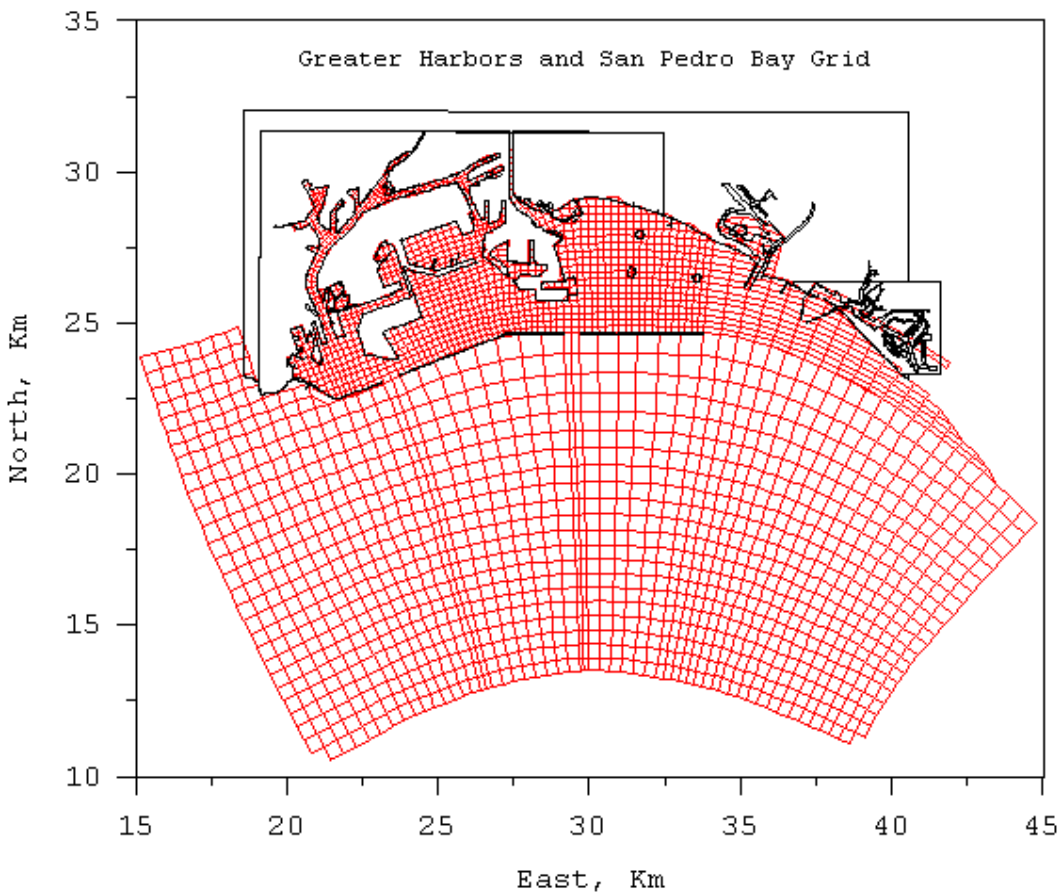

Note: The portion of the grid in Dominguez Channel extending to Vermont Avenue is not shown. The grid for this area was represented by a previous study (Everest, 2006).

Figure 1. Greater harbors and San Pedro Bay grid

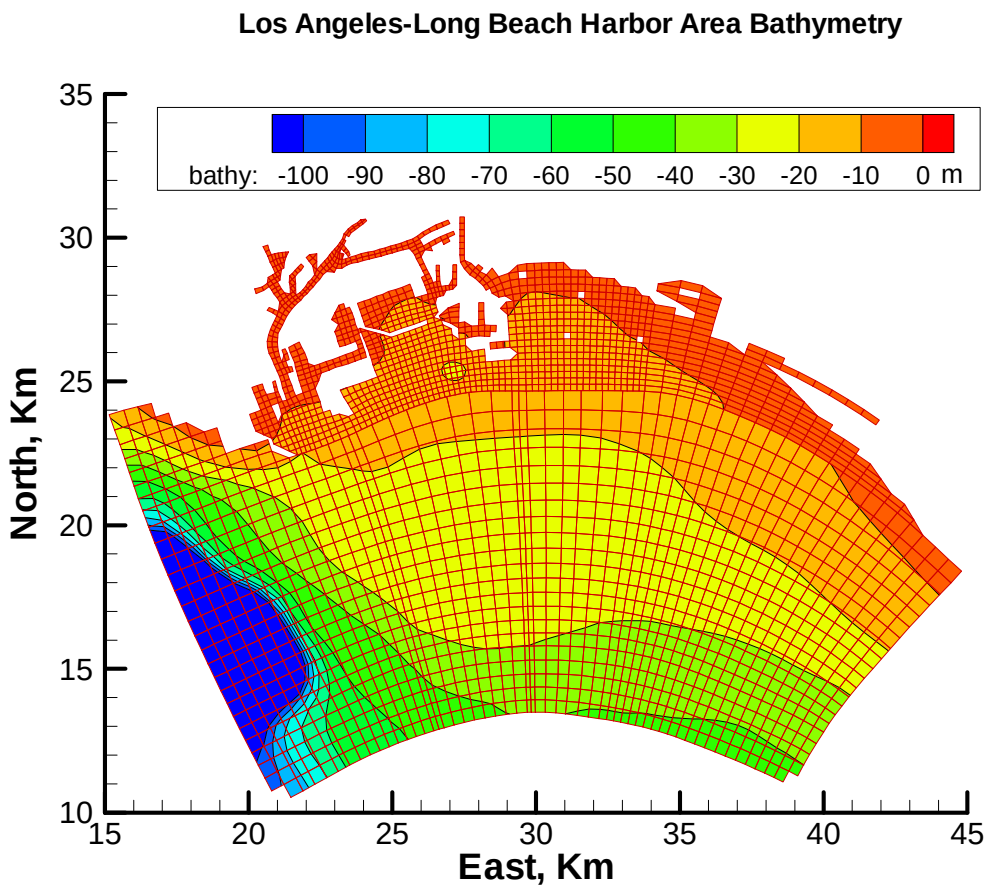

Note: Elevation in meters relative to local mean sea level.

Figure 2. Los Angeles-Long Beach Harbor area bathymetry

4.4. Open Boundary Hydrodynamic Forcing

Circulation in the greater harbor system is forced by water surface elevation and transport along the grid boundaries in San Pedro Bay. The hydrodynamic boundary condition used along the three open boundaries is a radiation separation condition of the form

$$\zeta - \frac{\mathbf{n} \cdot \mathbf{u} H}{\sqrt{gH}} = 2\zeta_R \qquad (1)$$

where ζ is the water surface elevation relative to a sea-level data, **n** is the outward normal vector to the boundary, **u** is the horizontal barotropic velocity vector, H is the water depth, and ζ_R is the equivalent progressive wave amplitude.

Along the open boundaries, the water surface elevation is composed of periodic tidal components and a transient or low frequency component in the sub-tidal frequency spectrum. The equivalent incoming wave boundary condition (1) was specified as the sum of a low frequency component and harmonic components, described by equation (2):

$$\zeta_R = \zeta_{LF} + \sum_{m=1}^{M} \left(\zeta_{RCm} \cos(\omega_m t) + \zeta_{RSm} \sin(\omega_m t) \right) \qquad (2)$$

where *M* is the number of tidal constituents, ζ_{RCm} and ζ_{RSm} are cosine and sine amplitudes at frequency ω_m. Six harmonics constituents (M2, S2, N2, K1, O1, and P1) were used. Since observational data were not available along the open boundaries, the tidal frequency components of the incoming wave open boundary condition were estimated by an optimization based inverse procedure to obtain a best fit prediction of water surface elevation and current meter observations within the model domain shown in Figure 3.

4.5. Salinity and Temperature Open Boundary Conditions

Salinity and temperature open boundary conditions were specified as spatially constant and temporally varying along the open boundary. The salinity boundary condition was based on fitting monitoring data to a seasonally varying function with an adjustment factor to account for higher salinities in San Pedro Bay. The adjustment factor was calibrated. The temperature boundary condition was based on fitting the Palos Verde Shelf station A8 CTD record (SAIC, 2004) to a seasonally varying function.

4.6. Wind and Atmospheric Forcing

Wind speed and direction and atmospheric thermal conditions including air temperature, relative humidity, rainfall, solar short wave radiation, and cloud cover data were obtained from the NOAA National Climate Data Center for Los Angeles International Airport (LAX). These data were supplemented by California Irrigation Management Information System observational data for Long Beach and Santa Monica and NOAA National Data Buoy Center observational data for off shore stations 46025 and 46086. The resulting model wind forcing is a spatially variable weighted average taking into account regional topographic conditions, while the atmospheric thermal forcing is spatially uniform and based on a composite of the various data sets. The NOAA Ports observational system for Los Angeles and Long Beach Harbors began providing wind speed and direction data for seven stations in May 2005. Since these data spanned only 25 percent of the 2003-2005 simulation and did not cover the high freshwater inflow events of January 2003 and December 2004 to February 2005, they were not used in the current model configuration. In addition, during the period of May

2005 to December 2005, there were no salinity data to evaluate whether these data would improve model performance. However they should be considered for use in potential update model configurations if the simulation intervals are expanded into 2006 and beyond (when additional observational data may be available to further evaluate model performance).

4.7. Fresh Water Inflow

Fresh water inflow along the boundaries of the model domain is introduced for Dominguez Channel, the Los Angeles River, and the San Gabriel River. For these three sources, inflow data provided by the Los Angeles County Department of Public Works or from LSPC models (Tetra Tech, 2006) can be used. Terminal Island Treatment Plant Discharges, provided by the City of Los Angeles, were introduced into the interior model grid cell at the corresponding diffuser location. Non-point source freshwater inflows corresponding to 67 local near shore watersheds were provided by the LSPC watershed model (Tetra Tech, 2006).

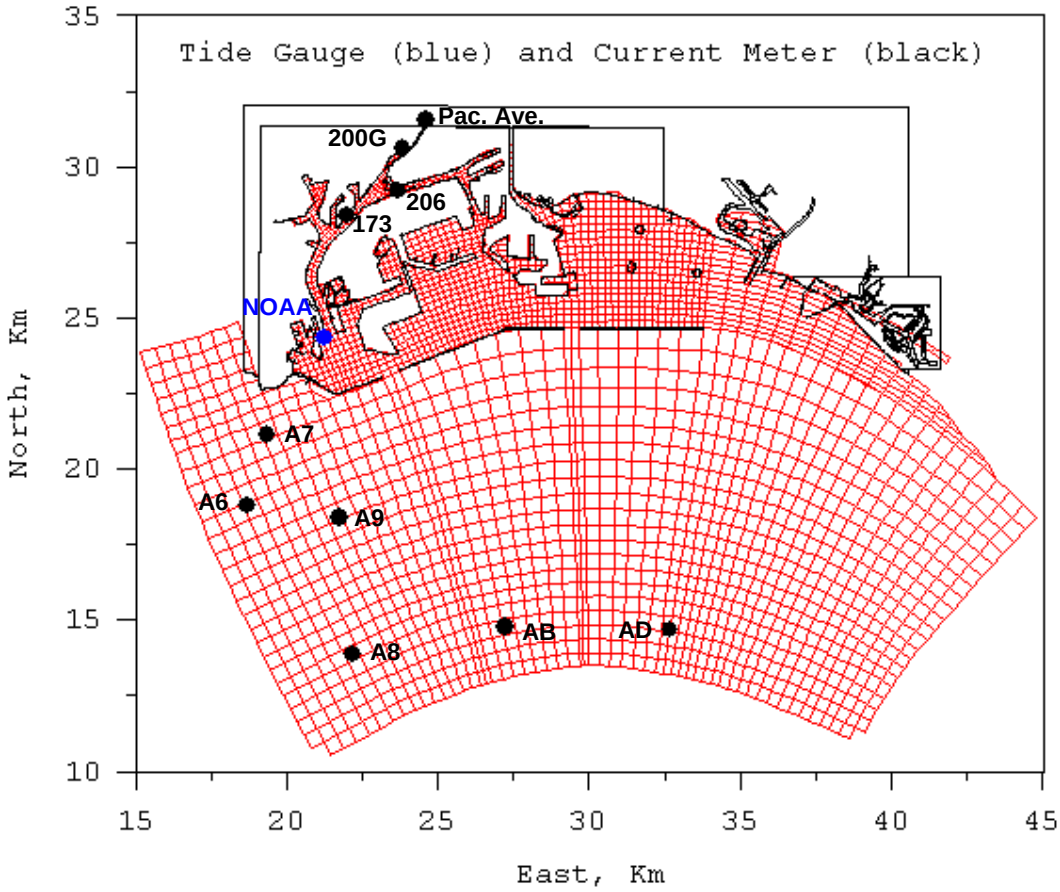

Figure 3. Location of Tide Gauge (blue) and Current Meters (black)

5. Hydrodynamic Calibration

Hydrodynamic model calibration involved the adjustment of open boundary forcing, bottom roughness, and bottom elevations to obtain a general best agreement between model predictions and observations of water surface elevation and horizontal currents. Quantitative evaluation of the hydrodynamic calibration is based on comparison of observed and model predicted harmonic amplitudes and phases of tidal water surface elevation and currents and time series error analysis of observed and low frequency water surface elevation. The following subsections summarize the steps followed in the calibration process.

5.1. Tidal Frequency Water Surface Elevation

Tidal frequency water surface elevation calibration is based on comparison of observed and model predicted tidal constituent amplitudes and phases at the NOAA Los Angeles Harbor tide gauge shown in Figure 3 and water surface elevation records at four Los Angeles inner harbor current meter stations also shown in Figure 3. Tables 3 through 7 summarize the comparisons for these five locations. For the NOAA gauge (Table 3) four of the six constituents have normalized amplitude errors less than 1 percent (0.01). The normalized amplitude error for the N2 constituent is approximately 10 percent, but is acceptable because the N2 constituent is of secondary importance. Absolute phase error for the dominant M2 constituent is just over 1 minute. Agreement between observed and predicted constituent amplitudes and phases is reasonably good for inner harbor stations 206B (Table 4) and 173 (Table 5), which also indicate that there is little change in amplitude and phase throughout the system consistent with previous model study findings. For station 200G (Table 6), the harmonic analysis of the data essentially failed and model predictions are tabulated to support the conclusion of marginal amplitude and phase variability. For the Pacific Avenue station in Dominguez Channel (Table 7), the amplitude and phase errors are large for all constituents. The failure of harmonic analysis to resolve the data at station 200G (Table 6) and the disagreement at Pacific Avenue (Table 7) is likely due to a large number of default entries in the data records. As will be shown in section 5.3, model comparison with current meter data at these two stations is more reasonable.

5.2. Low Frequency Water Surface Elevation

Low frequency or sub-tidal water surface elevation in the greater harbors responds to low-frequency sea level variability in San Pedro Bay with negligible amplitude and phase variation. Figure 4 shows a comparison of model predicted and observed low frequency sea level at the Los Angeles Harbor NOAA Tide Gauge. Time series error analyses for the observed and predicted low frequency

sea level are summarized in Table 8. These, and other, model performance measures are described in Appendix B.

Table 3. Water Surface Elevation Tidal Constituents Comparison at NOAA Gauge

Tidal Constituent	Observed Amplitude (meters)	Modeled Amplitude (meters)	Amplitude Error (|Observed-Modeled|/Observed)	Observed Phase (seconds)	Modeled Phase (seconds)	Phase Error (Seconds)
M2	0.503	0.505	0.004	27434	27498	64
S2	0.203	0.202	0.005	31335	31149	186
N2	0.119	0.119	0.000	31824	31657	167
K1	0.371	0.364	0.019	19854	19095	759
O1	0.246	0.240	0.024	7829	7082	747
P1	0.107	0.102	0.047	22894	26560	3666

Table 4. Water Surface Elevation Tidal Constituents Comparison at 206B Gauge

Tidal Constituent	Observed Amplitude (meters)	Modeled Amplitude (meters)	Amplitude Error (|Observed-Modeled|/Observed)	Observed Phase (seconds)	Modeled Phase (seconds)	Phase Error (Seconds)
M2	0.500	0.508	0.016	27273	27489	216
S2	0.219	0.204	0.068	31102	31123	21
N2	0.120	0.119	0.008	31436	31664	228
K1	0.380	0.366	0.037	18958	19214	256
O1	0.254	0.241	0.051	8891	7136	1755
P1	0.102	0.103	0.010	22507	26241	3734

Table 5. Water Surface Elevation Tidal Constituents Comparison at 173 (Data File Borx) Gauge

Tidal Constituent	Observed Amplitude (meters)	Modeled Amplitude (meters)	Amplitude Error (|Observed-Modeled|/Observed)	Observed Phase (seconds)	Modeled Phase (seconds)	Phase Error (Seconds)
M2	0.575	0.508	0.116	27065	27502	437
S2	0.250	0.203	0.188	31921	31127	794
N2	0.135	0.119	0.118	32390	31667	723
K1	0.400	0.366	0.085	18089	19217	1128
O1	0.303	0.241	0.204	9299	7136	2163
P1	0.086	0.103	0.197	23452	26229	2777

Table 6. Water Surface Elevation Tidal Constituents Comparison at 200G (Data file Barg) Gauge

Tidal Constituent	Observed Amplitude (meters)	Modeled Amplitude (meters)	Amplitude Error (|Observed-Modeled|/Observed)	Observed Phase (seconds)	Modeled Phase (seconds)	Phase Error (Seconds)
M2	0.163	0.508		21967	27503	
S2	0.614	0.204		19966	31129	
N2	0.070	0.119		33352	31670	
K1	0.664	0.366		30625	19217	
O1	0.160	0.241		12668	7138	
P1	0.809	0.103		25720	26251	

Table 7. Water Surface Elevation Tidal Constituents Comparison at DC Pacific Avenue Gauge

Tidal Constituent	Observed Amplitude (meters)	Modeled Amplitude (meters)	Amplitude Error (|Observed-Modeled|/Observed)	Observed Phase (seconds)	Modeled Phase (seconds)	Phase Error (Seconds)
M2	0.897	0.510	0.431	39765	27705	12060
S2	0.378	0.204	0.460	18710	31333	12623
N2	0.245	0.119	0.510	44224	31909	12315
K1	0.361	0.370	0.025	39878	19428	20450
O1	0.225	0.242	0.076	30302	7349	22953
P1	0.148	0.102	0.310	45411	26159	19252

Table 8. Instantaneous and Low Frequency Water Surface Elevation Statistical Comparison at NOAA Gauge

Statistical Measure	Instantaneous	Low Frequency
Mean Error (meters)	0.001	0.001
Absolute Mean Error (meters)	0.122	0.003
Maximum Absolute Error (meters)	0.670	0.047
RMS Error (meters)	0.168	0.004
RMS Error/RMS Observed	0.324	0.058
Linear Regression Intercept (meters)	0.001	0.001
Linear Regression Slope	0.959	0.993
Correlation Coefficient	0.986	0.997
Skill (0 to 1, 1 being perfect)	0.973	0.999

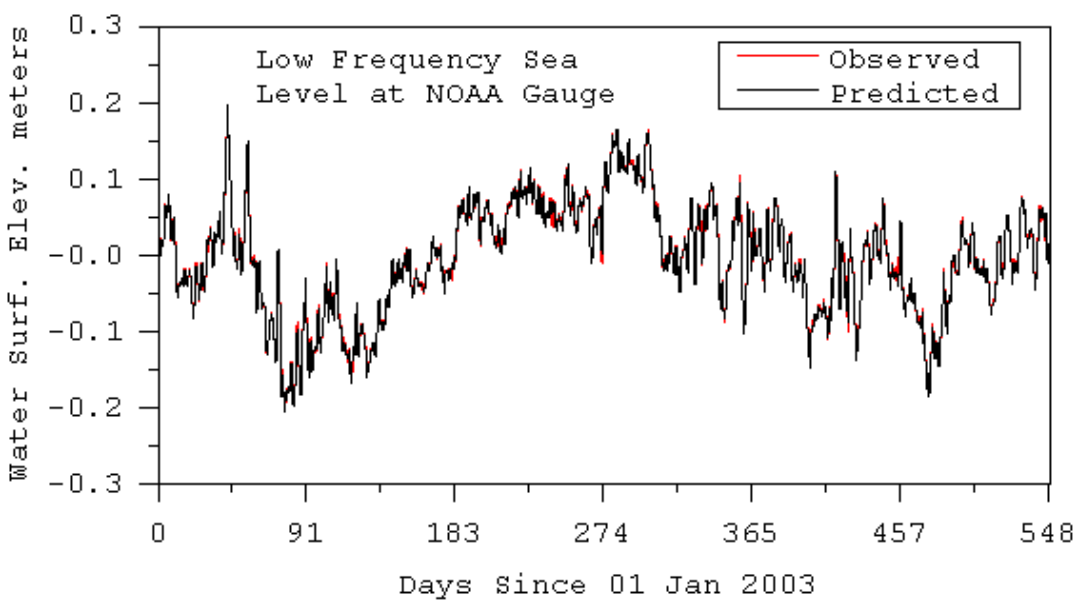

Figure 4. Low frequency sea level comparison at NOAA tide gauge in Los Angels Harbor

5.3. Tidal Frequency Currents

Table 9 through Table 14 summarize the comparison of horizontal tidal current major axis amplitudes, phases, and orientation angles at six Palos Verde Shelf current meter locations for the six primary tidal constituents. The locations correspond to the six current meter locations outside the breakwater shown in Figure 3. Although absolute quantitative agreement between the observations and model predictions is poor, the qualitative agreement is reasonable in that current magnitudes are similar and phases are consistent. Predicted major axis orientations are generally good having angular errors of less than 20 degrees.

Tables 15 through 20 summarize the comparison of horizontal tidal current major axis amplitudes, phases, and orientation angles at the four Los Angeles Inner Harbor current meter locations shown in Figure 3. Tidal currents are weak at the 173, 200G, and 206B stations and on the order of 2 cm/sec or less for all constituents. However, the model predicted major axis amplitudes and phases compare reasonably well at these three stations and directions. The Pacific Avenue station in Dominguez Channel has much stronger currents and the model predicted major axis amplitudes, phase, and directions compare well with the observations. The strong agreement between model predicted currents at the Pacific Avenue station tends to support the conclusion that water surface elevation observations at this station are compromised.

Table 9. Horizontal Current M2 Major Axis Amplitude, Orientation and Phase Comparison at Palo Verde Shelf Current Meter Stations

Station	Observed Major Amplitude (m/s)	Modeled Major Amplitude (m/s)	Observed Phase (seconds)	Modeled Phase (seconds)	Observed Angle (degrees CCW from East)	Modeled Angle (degrees CCW from East)
PV A6	0.053	0.023	9126	8091	160	170
PV A7	0.096	0.047	10840	9709	179	180
PV A8	0.047	0.060	5084	4326	145	152
PV A9	0.069	0.059	7843	9190	171	15 (195)
PV AB	0.053	0.077	2731	5080	141	161
PV AD	0.052	0.050	21788	3125	126	117

Table 10. Horizontal Current S2 Major Axis Amplitude, Orientation and Phase Comparison at Palo Verde Shelf Current Meter Stations

Station	Observed Major Amplitude (m/s)	Modeled Major Amplitude (m/s)	Observed Phase (seconds)	Modeled Phase (seconds)	Observed Angle (degrees CCW from East)	Modeled Angle (degrees CCW from East)
PV A6	0.027	0.014	17329	17372	175	178
PV A7	0.050	0.028	18703	17986	2	0
PV A8	0.024	0.031	13561	14130	131	155
PV A9	0.032	0.033	16132	17200	174	15 (195)
PV AB	0.028	0.043	10211	14209	151	169
PV AD	0.021	0.022	7372	12358	136	127

Table 11. Horizontal Current N2 Major Axis Amplitude, Orientation and Phase Comparison at Palo Verde Shelf Current Meter Stations

Station	Observed Major Amplitude (m/s)	Modeled Major Amplitude (m/s)	Observed Phase (seconds)	Modeled Phase (seconds)	Observed Angle (degrees CCW from East)	Modeled Angle (degrees CCW from East)
PV A6	0.012	0.007	14608	12120	166	166
PV A7	0.025	0.013	14521	13794	0 (180)	179
PV A8	0.009	0.017	8373	8419	121	155
PV A9	0.016	0.015	12077	13427	152	15
PV AB	0.012	0.021	6201	9430	145	162
PV AD	0.012	0.013	827	8026	105	112

Table 12. Horizontal Current K1 Major Axis Amplitude, Orientation and Phase Comparison at Palo Verde Shelf Current Meter Stations

Station	Observed Major Amplitude (m/s)	Modeled Major Amplitude (m/s)	Observed Phase (seconds)	Modeled Phase (seconds)	Observed Angle (degrees CCW from East)	Modeled Angle (degrees CCW from East)
PV A6	0.034	0.024	4924	7573	129	82
PV A7	0.048	0.031	42864	32391	162	4 (184)
PV A8	0.032	0.056	2027	11750	104	152
PV A9	0.046	0.056	2086	29650	131	17
PV AB	0.036	0.058	39852	19312	125	154
PV AD	0.031	0.043	42692	42053	141	21

Table 13. Horizontal Current O1 Major Axis Amplitude, Orientation and Phase Comparison at Palo Verde Shelf Current Meter Stations

Station	Observed Major Amplitude (m/s)	Modeled Major Amplitude (m/s)	Observed Phase (seconds)	Modeled Phase (seconds)	Observed Angle (degrees CCW from East)	Modeled Angle (degrees CCW from East)
PV A6	0.026	0.019	37240	40430	143	74
PV A7	0.034	0.022	38133	22097	170	3 (183)
PV A8	0.014	0.036	39197	91780	110	154
PV A9	0.025	0.040	36670	17039	149	16
PV AB	0.018	0.039	34854	6872	138	152
PV AD	0.017	0.027	33163	26160	140	0 (180)

Table 14. Horizontal Current P1 Major Axis Amplitude, Orientation and Phase Comparison at Palo Verde Shelf Current Meter Stations

Station	Observed Major Amplitude (m/s)	Modeled Major Amplitude (m/s)	Observed Phase (seconds)	Modeled Phase (seconds)	Observed Angle (degrees CCW from East)	Modeled Angle (degrees CCW from East)
PV A6	0.006	0.007	6472	15643	116	77
PV A7	0.005	0.009	3839	39296	112	0 (180)
PV A8	0.008	0.015	42175	19610	134	153
PV A9	0.007	0.015	41014	36314	39	16
PV AB	0.010	0.017	39484	26896	51	153
PV AD	0.010	0.012	1007	3990	99	13

Table 15. Horizontal Current M2 Major Axis Amplitude, Orientation and Phase Comparison at Los Angeles Inner Harbor Current Meter Stations

Station	Observed Major Amplitude (m/s)	Modeled Major Amplitude (m/s)	Observed Phase (seconds)	Modeled Phase (seconds)	Observed Angle (degrees CCW from East)	Modeled Angle (degrees CCW from East)
206 B	0.021	0.017	19382	21780	1	14
200G	0.023	0.019	15881	14407	57	29
173	0.020	0.026	10989	12645	59	53
DC PA	0.365	0.317	17542	17306	64	60

Table 16. Horizontal Current S2 Major Axis Amplitude, Orientation and Phase Comparison at Los Angeles Inner Harbor Current Meter Stations

Station	Observed Major Amplitude (m/s)	Modeled Major Amplitude (m/s)	Observed Phase (seconds)	Modeled Phase (seconds)	Observed Angle (degrees CCW from East)	Modeled Angle (degrees CCW from East)
206 B	0.005	0.007	2543	6861	4	14
200G	0.010	0.008	20890	17170	54	26
173	0.008	0.014	19476	16920	60	53
DC PA	0.156	0.119	21958	21340	64	60

Table 17. Horizontal Current N2 Major Axis Amplitude, Orientation and Phase Comparison at Los Angeles Inner Harbor Current Meter Stations

Station	Observed Major Amplitude (m/s)	Modeled Major Amplitude (m/s)	Observed Phase (seconds)	Modeled Phase (seconds)	Observed Angle (degrees CCW from East)	Modeled Angle (degrees CCW from East)
206 B	0.005	0.004	21792	25047	7	14
200G	0.004	0.004	22337	18580	54	26
173	0.005	0.006	15018	16930	62	53
DC PA	0.082	0.072	22027	21350	64	60

Table 18. Horizontal Current K1 Major Axis Amplitude, Orientation and Phase Comparison at Los Angeles Inner Harbor Current Meter Stations

Station	Observed Major Amplitude (m/s)	Modeled Major Amplitude (m/s)	Observed Phase (seconds)	Modeled Phase (seconds)	Observed Angle (degrees CCW from East)	Modeled Angle (degrees CCW from East)
206B	0.008	0.004	42848	27923	1	14
200G	0.008	0.005	468	24060	61	29
173	0.002	0.014	1353	38330	62	52
DC PA	0.138	0.125	41512	40890	64	60

Table 19. Horizontal Current O1 Major Axis Amplitude, Orientation and Phase Comparison at Los Angeles Inner Harbor Current Meter Stations

Station	Observed Major Amplitude (m/s)	Modeled Major Amplitude (m/s)	Observed Phase (seconds)	Modeled Phase (seconds)	Observed Angle (degrees CCW from East)	Modeled Angle (degrees CCW from East)
206B	0.007	0.004	27528	39638	-2	14
200G	0.004	0.006	32331	9203	66	26
173	0.002	0.006	38429	20710	60	53
DC PA	0.086	0.075	32783	31020	63	60

Table 20. Horizontal Current P1 Major Axis Amplitude, Orientation and Phase Comparison at Los Angeles Inner Harbor Current Meter Stations

Station	Observed Major Amplitude (m/s)	Modeled Major Amplitude (m/s)	Observed Phase (seconds)	Modeled Phase (seconds)	Observed Angle (degrees CCW from East)	Modeled Angle (degrees CCW from East)
206B	0.005	0.005	15789	24410	-4	14
200G	0.003	0.001	3300	8369	54	26
173	0.003	0.007	28868	37500	65	53
DC PA	0.004	0.025	2950	3126	61	60

6. Transport Calibration

Transport calibration involves the quantitative comparison of model predicted and observed concentrations of dissolved and suspended material in the water column. For freshwater influenced estuarine and coastal waterbodies, salinity transport calibration provides an additional level of confidence in model predictive

ability, particularly in the absence of extensive current meter observations. Model prediction of temperature is generally more sensitivity to wind and atmospheric thermal forcing rather than hydrodynamic transport, the exception being situations that have large thermal loads from power plants. In the absence of significant salinity variability, simulation of other tracers, including dye, is also an important means of transport calibration. This section presents the results of model calibration for salinity. Temperature simulation is typically not conducted for modeling applications directed at simulating sediment and contaminant transport and fate, unless temperature stratification and thermal buoyancy induced current contribute significantly to transport processes. Evaluation of temperature observations in the greater harbors systems indicates that this is not the case and temperature is not simulated. Model configuration and calibration for sediment and adsorptive contaminant transport calibration are presented in sections 7 and 8, respectively.

6.1. Salinity Calibration

Salinity calibration involves the adjustment of salinity open boundary conditions and possibly freshwater inflows if there is significant uncertainty associated with the inflows. Although there are approximately120 salinity monitoring stations, only 20 of those stations, whose locations are shown in Figure 5, have significant salinity variability (when the salinity is significantly less than the 32 to 33 ppt level characteristic of the greater harbors system). Bight 03 event stations in San Pedro Bay (Figure 6) did not show salinity variations significant enough for comparison with model predictions. Figure 7 shows a scatter plot comparing predicted and observed data for the 20 station locations shown in Figure 5. The surface and bottom notation corresponds to averages over the upper and lower halves of the water column. The data comparison points correspond to seven sampling times (Julian Days 16, 44, and 72 of 2003, Julian Day 351 of 2004, and Julian Days 13, 55, and 68 of 2005), three of which (44 of 2003 and 13 and 55 of 2005) correspond to depressed observed salinity. Predicted salinities over the lower half of the water column agree reasonably well with observations although there are a number of stations where the model under predicts salinity. Predicted salinities for the upper half of the water column agree reasonably well at many stations (Figure 7) although the model under predicts surface salinity at the same locations where it under predicts bottom salinity, as illustrated by the close proximity of similar station numbers in Figure 8.

Due to the extreme scatter of the data, lumped error statistics are not particularly meaningful. The salinity response of the model is better represented by time series plots of continuous model simulations of salinity observations at the twenty stations. These plots are presented in Figures A-1 through A-20 of Appendix A. Although point wise agreement is not always good, the model does represent the general response to the high freshwater inflow events represented by the observations. The model tends to under predict observed stratification. There

are a number of possible causes for the salinity under prediction and the under prediction of stratification. Under prediction of stratification might result from too much vertical mixing, which can influence the dynamics of the freshwater plume from the Los Angeles River during storm events. During significant storm events, the freshwater inflows should exit through the gate opening in the breakwater. However, if the dynamics of the freshwater plume are impacted by excessive vertical mixing in the model, the low salinity water could enter into the sampling area (rather than taking the intended path through the gate in the breakwater).

Vertical mixing in the model is predicted by a robust and widely accepted turbulence model having universal parameters. Adjustment of these parameters to force a fit to a spatially and temporally limited observational data, set such as that being discussed here is not considered acceptable. As previously noted, these are the only observations of salinity response to freshwater inflow events in the other regions of the harbor. A more extensive set of observations having a wider spatial coverage over multiple events would be necessary to quantify the dynamics of the freshwater transport and diagnose the cause of the present under prediction. The settling dynamics of particulate matter carrying contaminates can result in contaminant transport patterns different from fresh water making model performance extrapolations speculative.

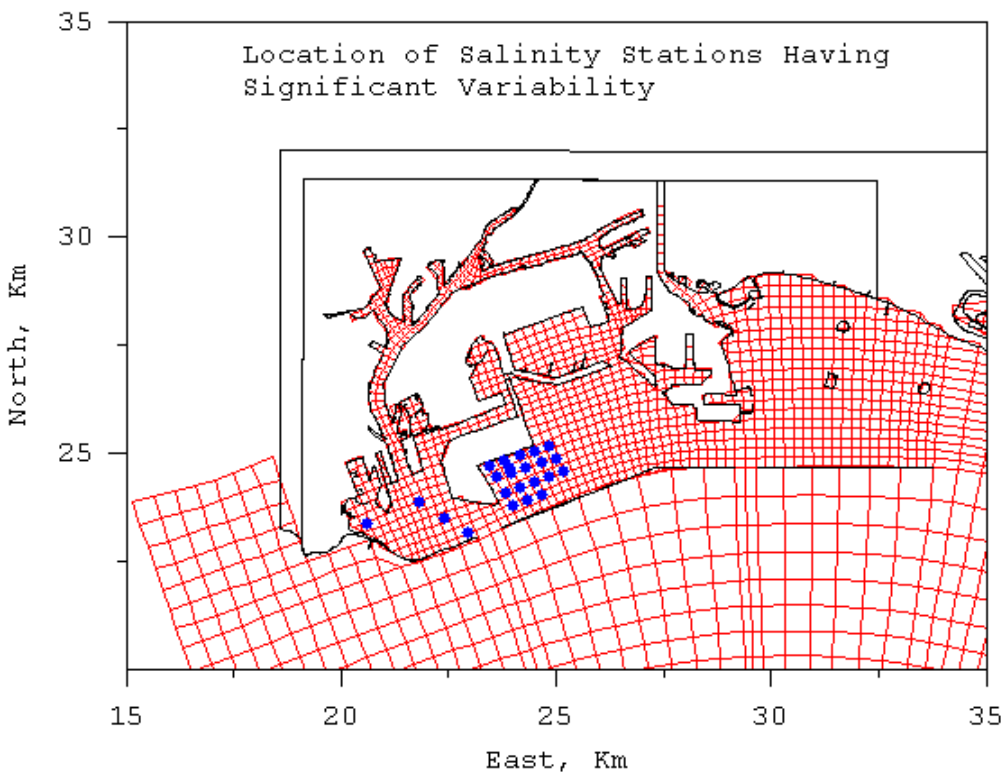

Note: Stations illustrated are where the salinity during the simulation period is significantly less than the 32 to 33 ppt level characteristic of the greater harbors system.

Figure 5. Location of salinity stations having significant variability

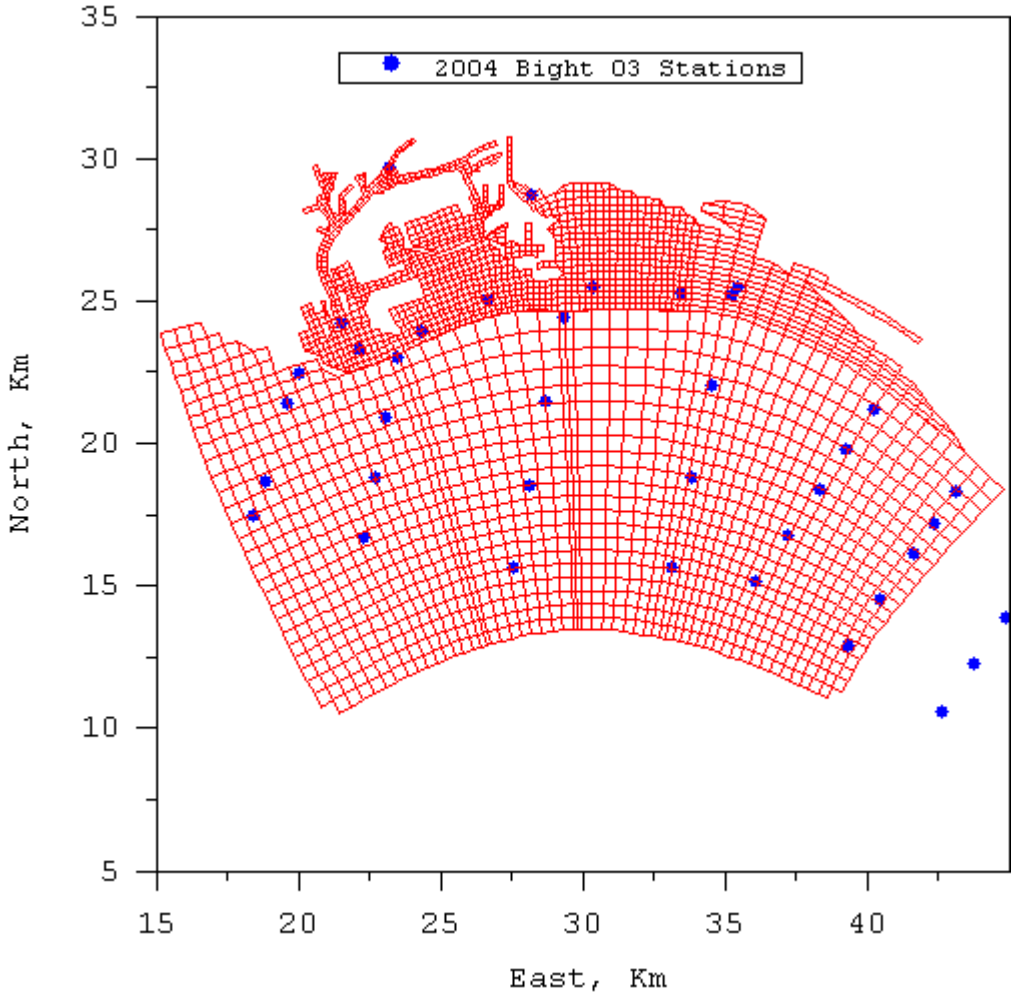

Figure 6. Location of Bight 03 salinity sampling stations

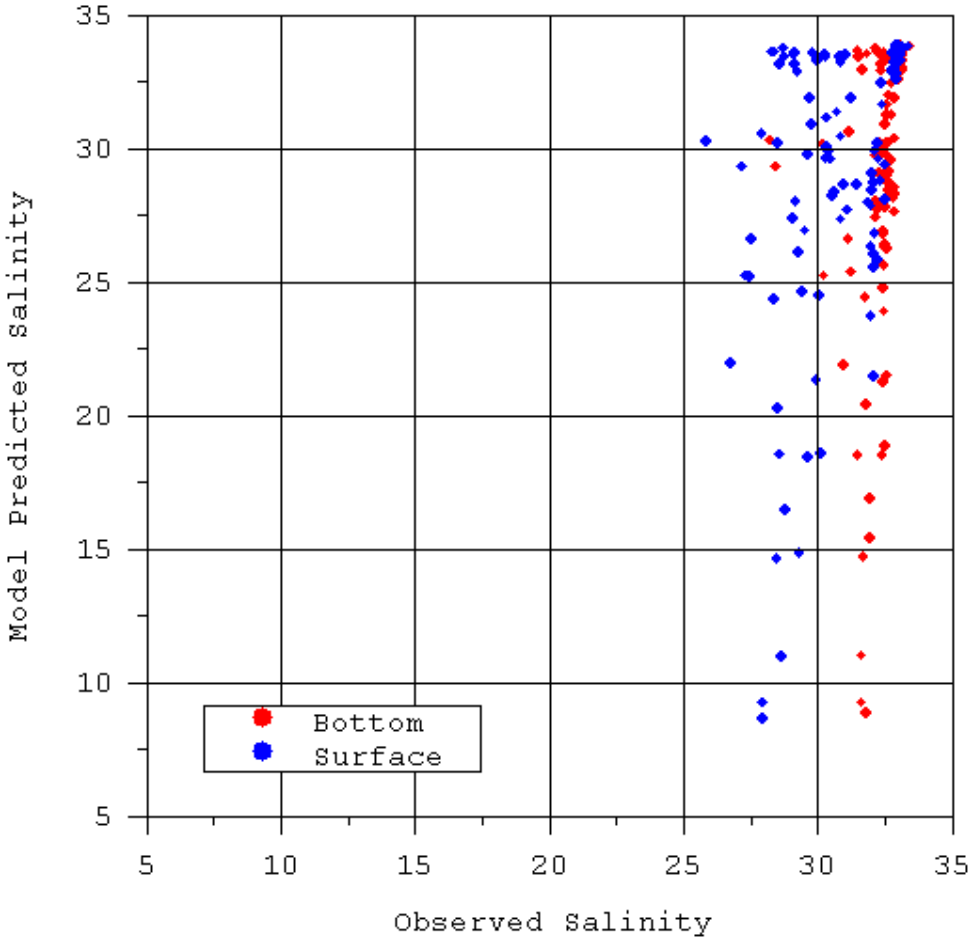

Figure 7. Comparison of predicted and observed salinity at 20 stations during seven monitoring times over upper (surface) and lower (bottom) fractions of the water column

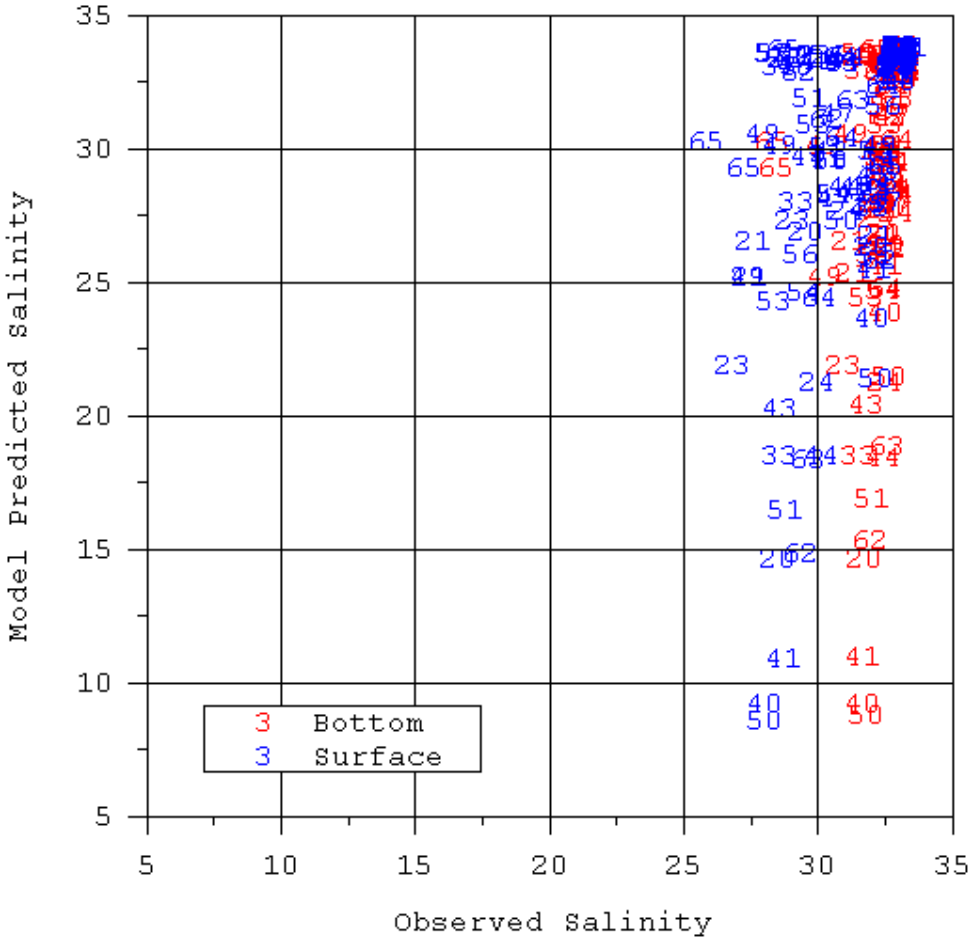

Figure 8. Station numbers associated with the comparison of predicted and observed salinity at 20 stations during seven monitoring times over upper (surface) and lower (bottom) fractions of the water column

7. Sediment and Contaminant Transport Model Configuration

This section describes the configuration of the EFDC based greater harbors model for the simulation of sediment and adsorptive contaminant transport simulation. Sediment and contaminant transport formulations in the EFDC model are documented by Tetra Tech (2007). Both fine, cohesive behaving sediment and noncohesive sand are simulated. Particulate organic material is assumed to be associated with the fine sediment class. Contaminants modeled include three metals; copper, lead, and zinc and three organics; DDT, PAH, and PCB. Two-phase equilibrium partitioning is used to represent adsorption of the metals and organics to the fine sediment class. The EFDC model simulates transport and fate in both the water column and sediment bed. Water column transport includes advection, diffusion, and settling for sediment and sediment adsorbed contaminates. The sediment bed is represented by multiple layers with internal

transport of contaminants by pore water advection and diffusion. Sediment and water is exchanged between the water column and bed by deposition and erosion, with corresponding exchange of adsorbed and dissolved contaminants. Dissolved phase contaminants are also exchanged by diffusion between bed pore water and the overlying water column. The following subsections describe specific aspects of model configuration including: establishment of spatially varying initial conditions in the sediment bed, specification of sediment erosion potential, specification of contaminant partition coefficients, and external loadings and boundary conditions.

7.1. Sediment Bed Initial Conditions

Inter-annual scale simulation of sediment adsorbed contaminants requires establishment of sediment bed initial conditions to the highest possible level of accuracy because the bed can be a significant source and/or sink of contaminants with respect to the water column as well as a reservoir for exposure and subsequent transport up the aquatic food chain. In contrast to water column initial conditions that wash out or rapidly respond to external sources and open boundary conditions, bed initial conditions are persistent with changes in bed sediment composition and contamination levels occurring slowly at annual scales and longer. Initial conditions are required for both sediments and contaminants. Sediment initial conditions influence both sediment transport dynamics and the phase distribution and mobility of contaminants in the bed. Required model initial conditions include sediment size class fractional distribution and a measure of water content such as porosity or void ratio. Organic material composition as specified by particulate or total organic carbon (POC or TOC) is also desirable.

Numerous studies in the greater harbors system have collected sediment bed physical data. However the data sets are quite heterogeneous in that they include near surface samples, composite cores, and depth varying sub-cores having data ranging from fraction of fine sediment to detailed grain size distributions. To achieve the widest spatial coverage, approximately 200 data points were selected, which are distributed among the datasets described in Table 2. Data inside the breakwaters prior to 1998 were excluded while all data outside the break water were used. Grain size information was reduced to two classes, fines composed of silt and clay, and sand and coarser particles, using 0.063 mm as the class size boundary. Water content measures were all converted to porosity. Figure 9 shows the location of 200 data sites having bed sediment size information, while Figure 10 shows a zoom of the most recent sub-set of these data.

Since many of the sites had no information on water content as defined by porosity, correlations between porosity and fine sediment fractions were developed using sites having data for both (Figure 11). The average of these two correlations was used to estimate porosity at sites having no data. Due to

lack of quantitative data in San Pedro Bay, sediment composition near the open boundaries was assumed to be 25 percent fine with a porosity of 0.5. The fine sediment fraction and porosity data including assumed values along the open boundaries in San Pedro Bay were interpolated to the model grid (Figure 1) using a Laplacian scheme which is equivalent to bi-linear interpolation with the exception that interpolation over land is prohibited. Figures 12 and 13 show the bed initial conditions for fine sediment fraction and porosity. The sediment bed was also configured to initially have 4 layers, each 20 cm thick. Sediment size class fractions, porosity, and contaminant concentrations are assumed uniform over the depth of the sediment bed at each horizontal location.

The procedure for establishing initial conditions for contaminants in the sediment bed follows that for sediment physical properties. To again achieve the widest spatial coverage, approximately 250 to 300 data points were selected for each contaminant, which are distributed among the datasets shown in Table 2. Data inside the breakwaters prior to 2000 were excluded while all data outside the breakwater were used. Figure 14 shows the location of all contaminant bed concentration data sites, while Figure 15 shows the location of sites recently sampled in fall 2006. The bed data for sites shown in Figure 15 were used to initialize metals and organics concentrations, while the overlying water data at these stations were used for calibration of sediment and contaminant transport. Since data in San Pedro Bay were extremely limited, bed solid phase concentrations near the open boundaries were estimated to be 10, 10, and 50 mg/kg for copper, lead, and zinc, and 0.01, 0.1, and 0.01 mg/kg for DDT, PAH, and PCB. Figures 16 through 21 show the spatial distribution of total sediment-normalized bed initial conditions for six contaminants using logarithmic concentration scales. For clarification of the logarithmic concentration scales, the log of the pollutant-specific sediment quality guidelines are identified in the figure captions as well as on the concentration legends.

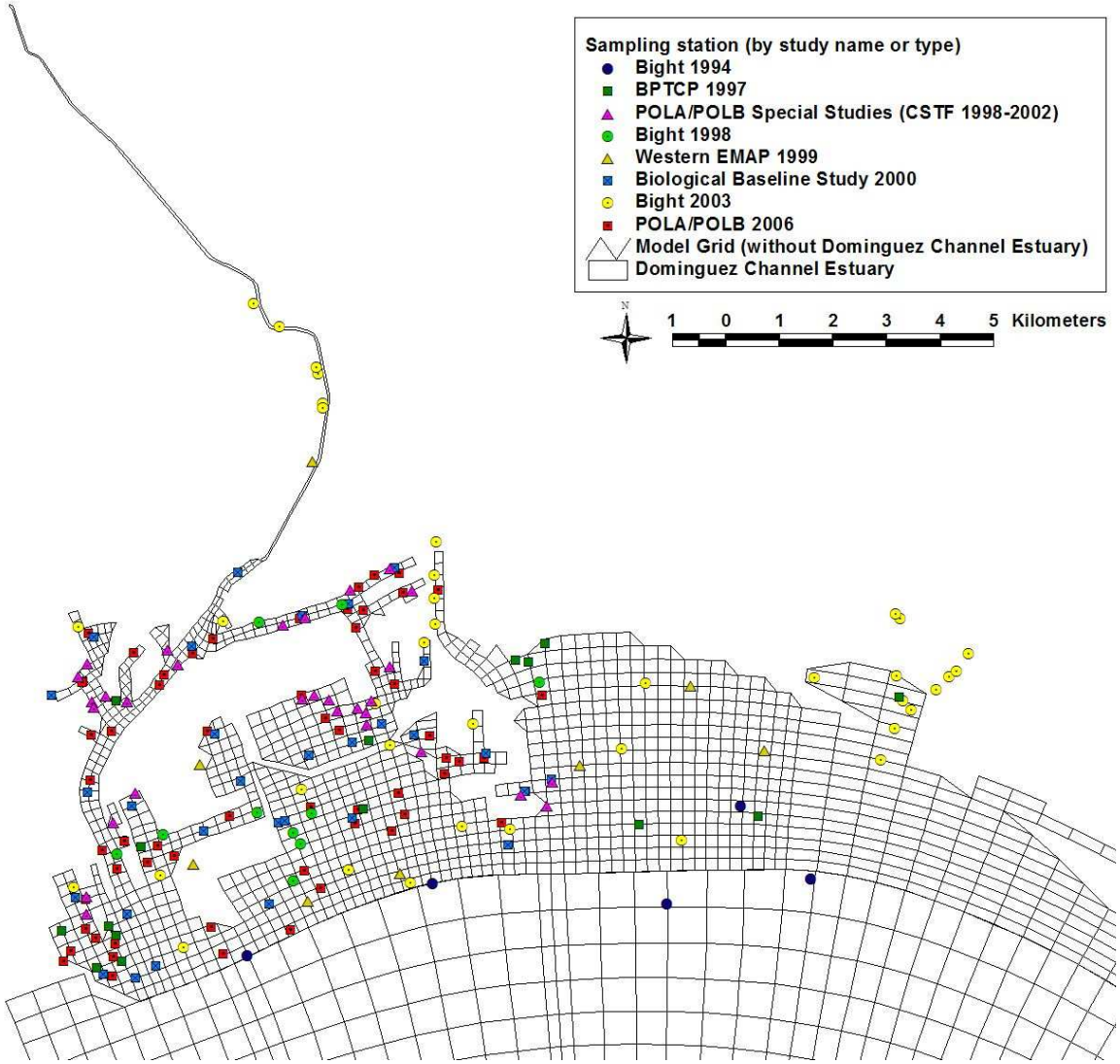

Figure 9. Location of 200 data sites used to initialize sediment bed physical properties

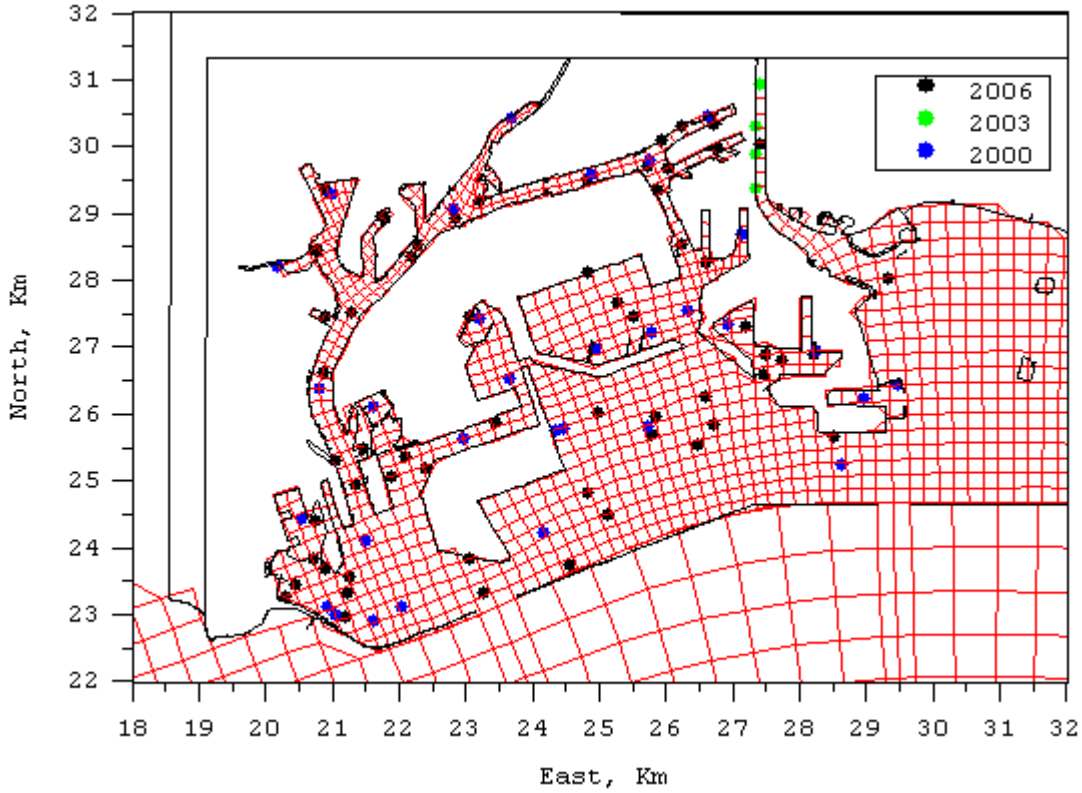

Note: 2006 data points refer to the POLA/POLB fall 2006 sampling; Bight 03 samples are represented by the 2003 points; 2000 data points refer to the POLA/POLB Biological Baseline Study conducted in 2000.

Figure 10. Most recent sediment bed physical data sites inside the breakwater

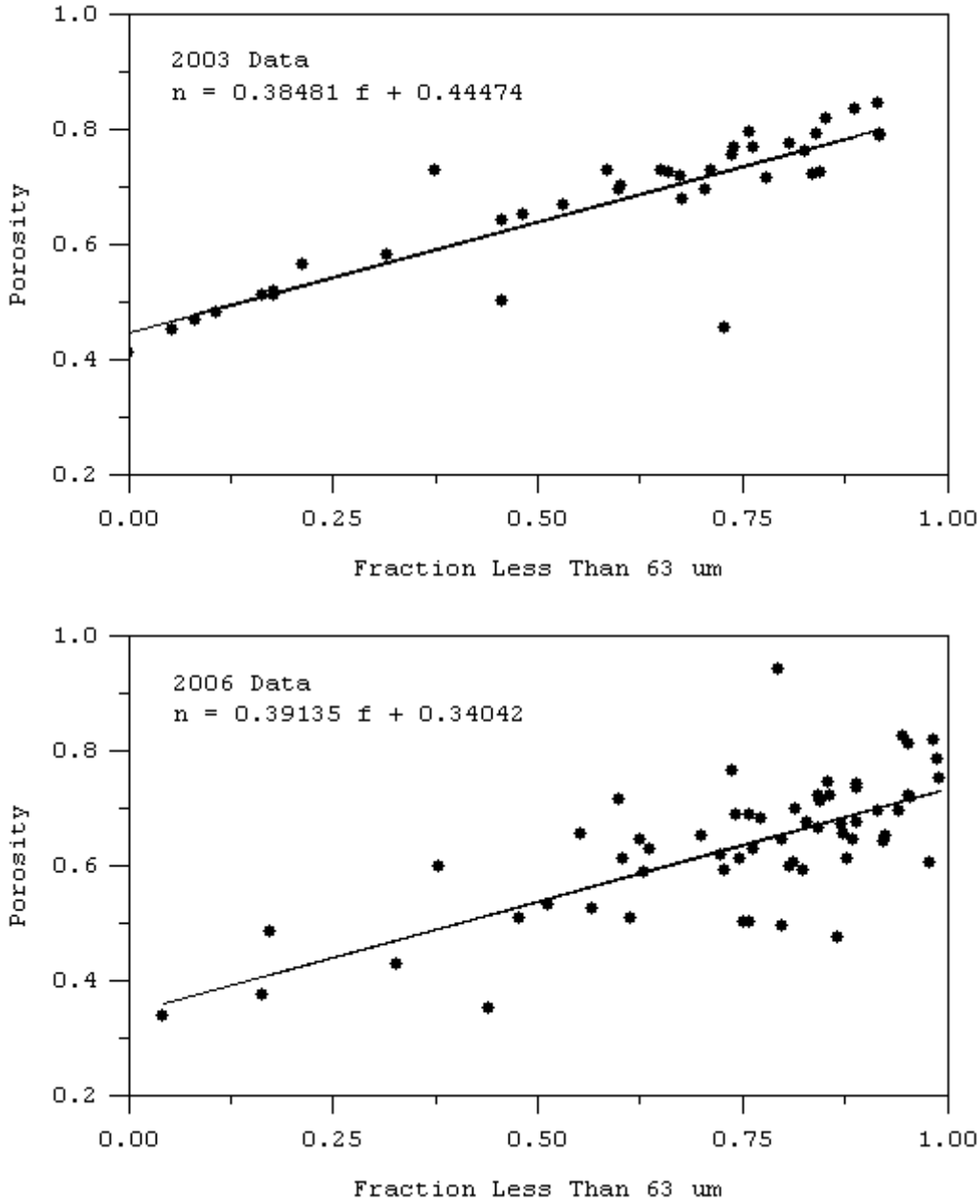

Figure 11. Porosity as a function of fine sediment fraction

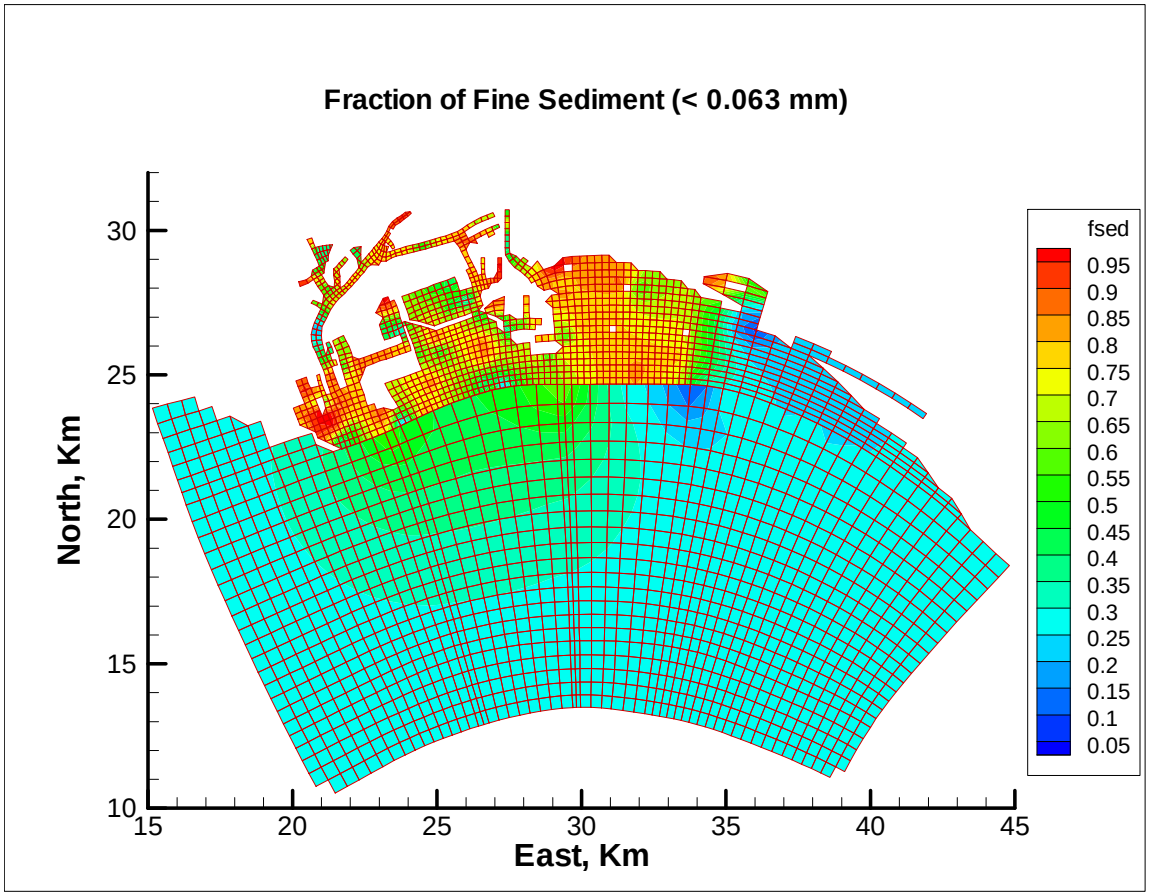

Figure 12. Fraction of fine sediment (< 0.063 mm) in the sediment bed used for model initialization

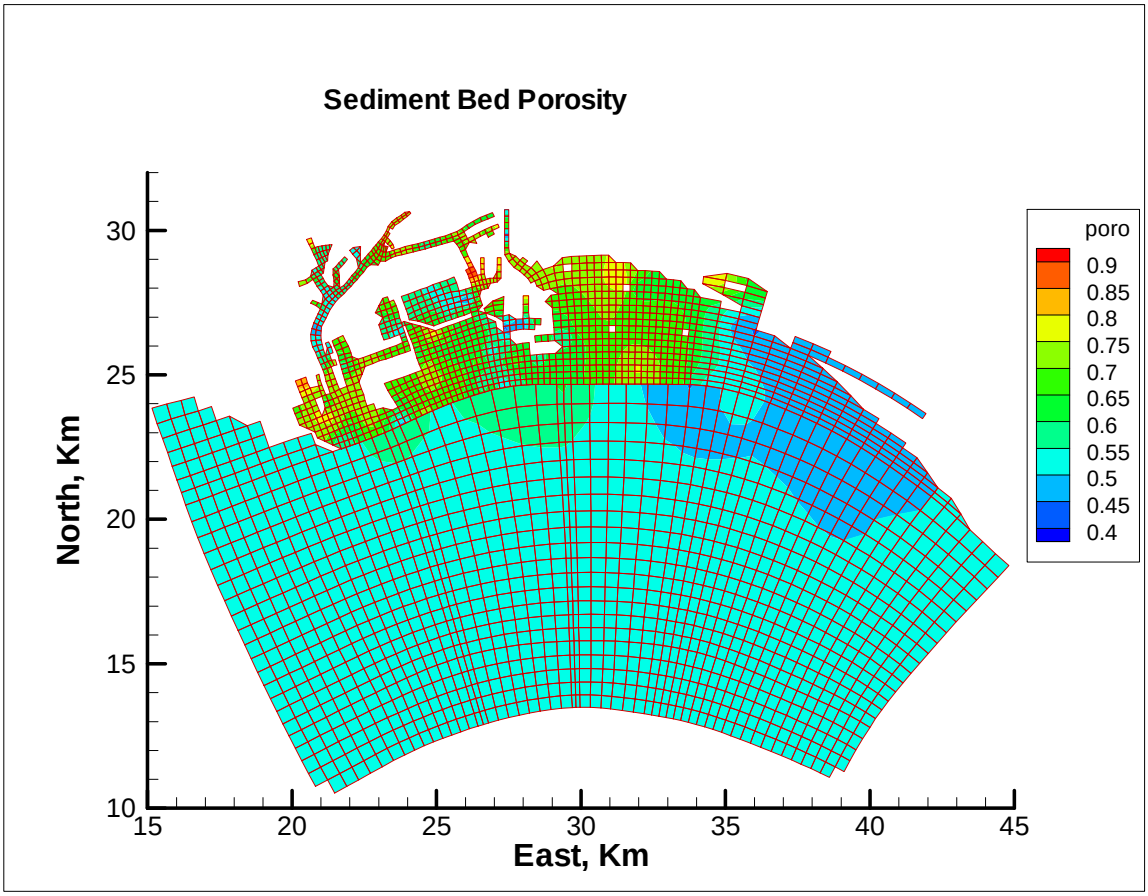

Figure 13. Sediment bed porosity used for model initialization

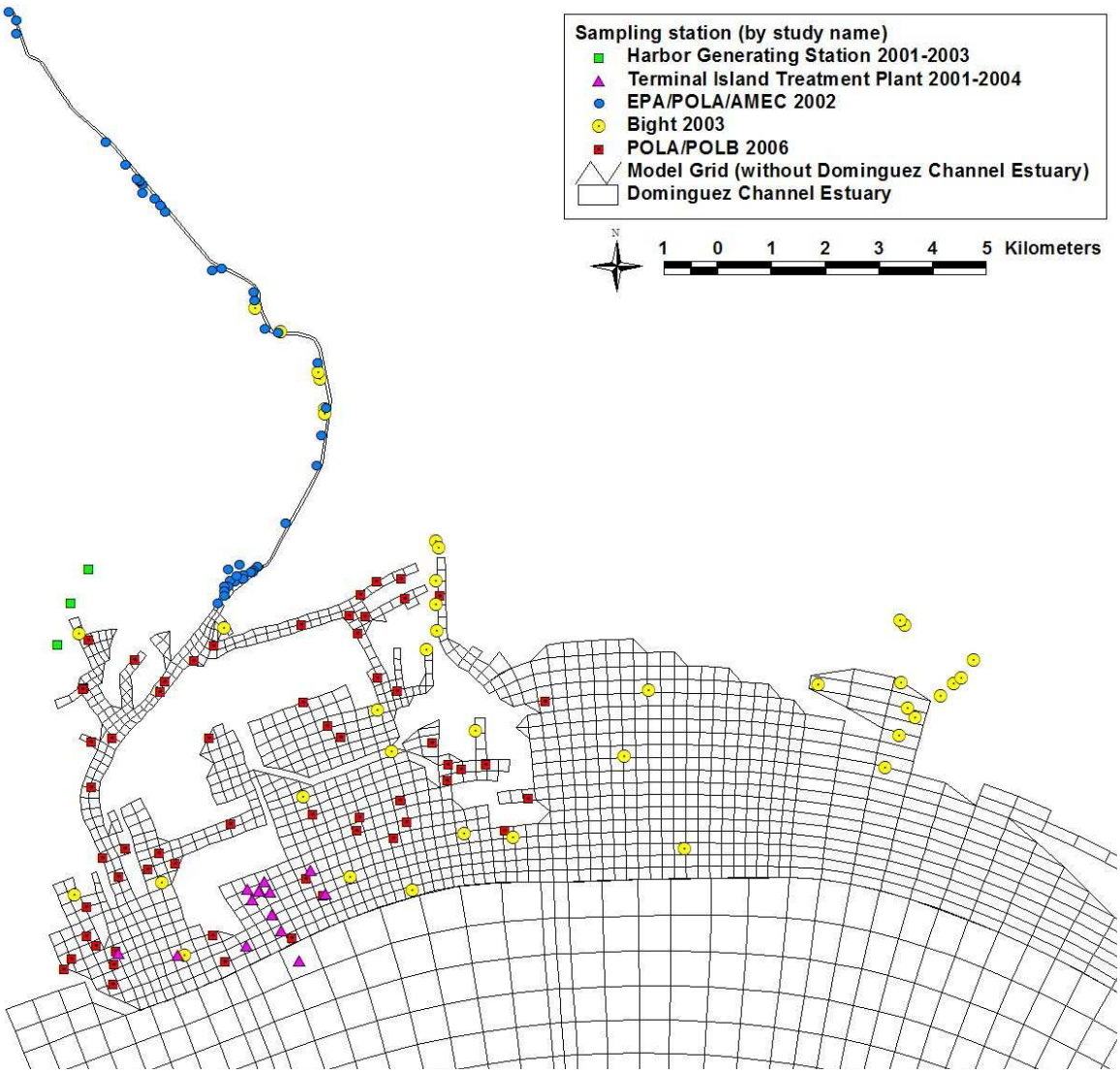

Figure 14. All sites used to initialize sediment bed metals, and organics concentrations

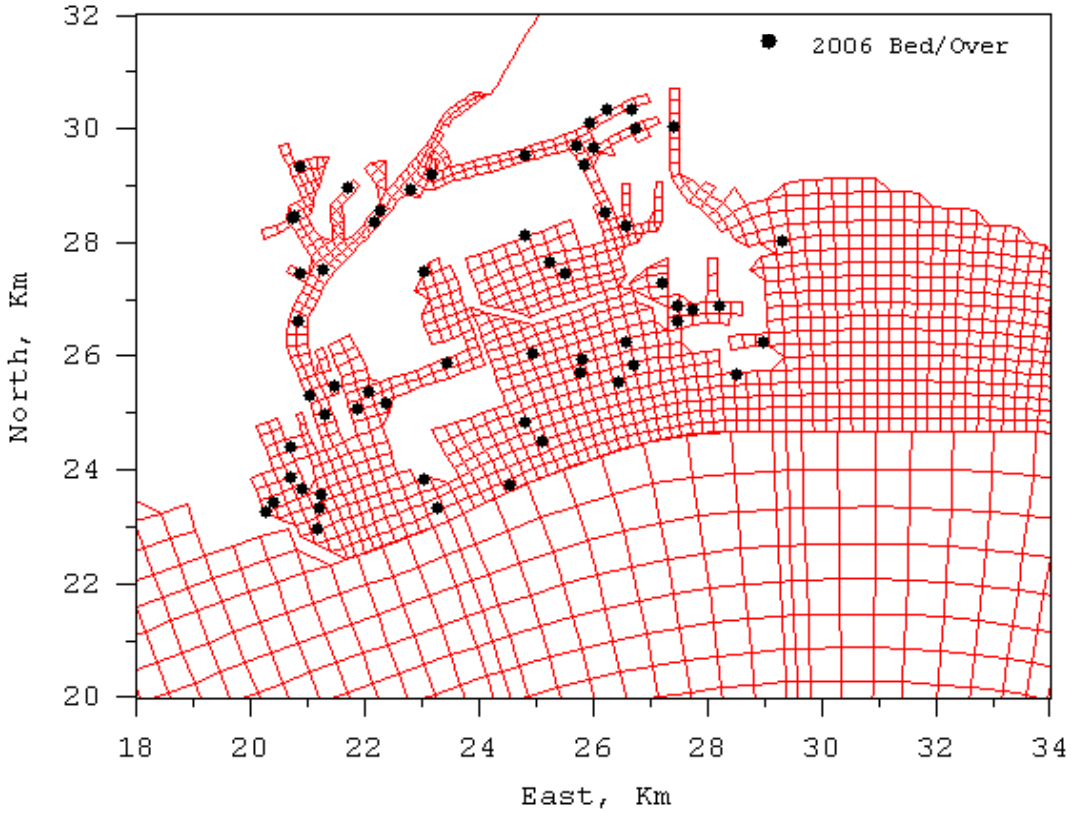

Note: These stations are the recently sampled locations in the greater harbors used for model configuration and calibration (POLA/POLB 2006). They are a subset of the stations presented in Figure 14. Bed data used to initialize sediment, metals, and organics concentrations. Overlying water data used for sediment and contaminant transport calibration.

Figure 15. Fall 2006 bed and overlying water column sample sites

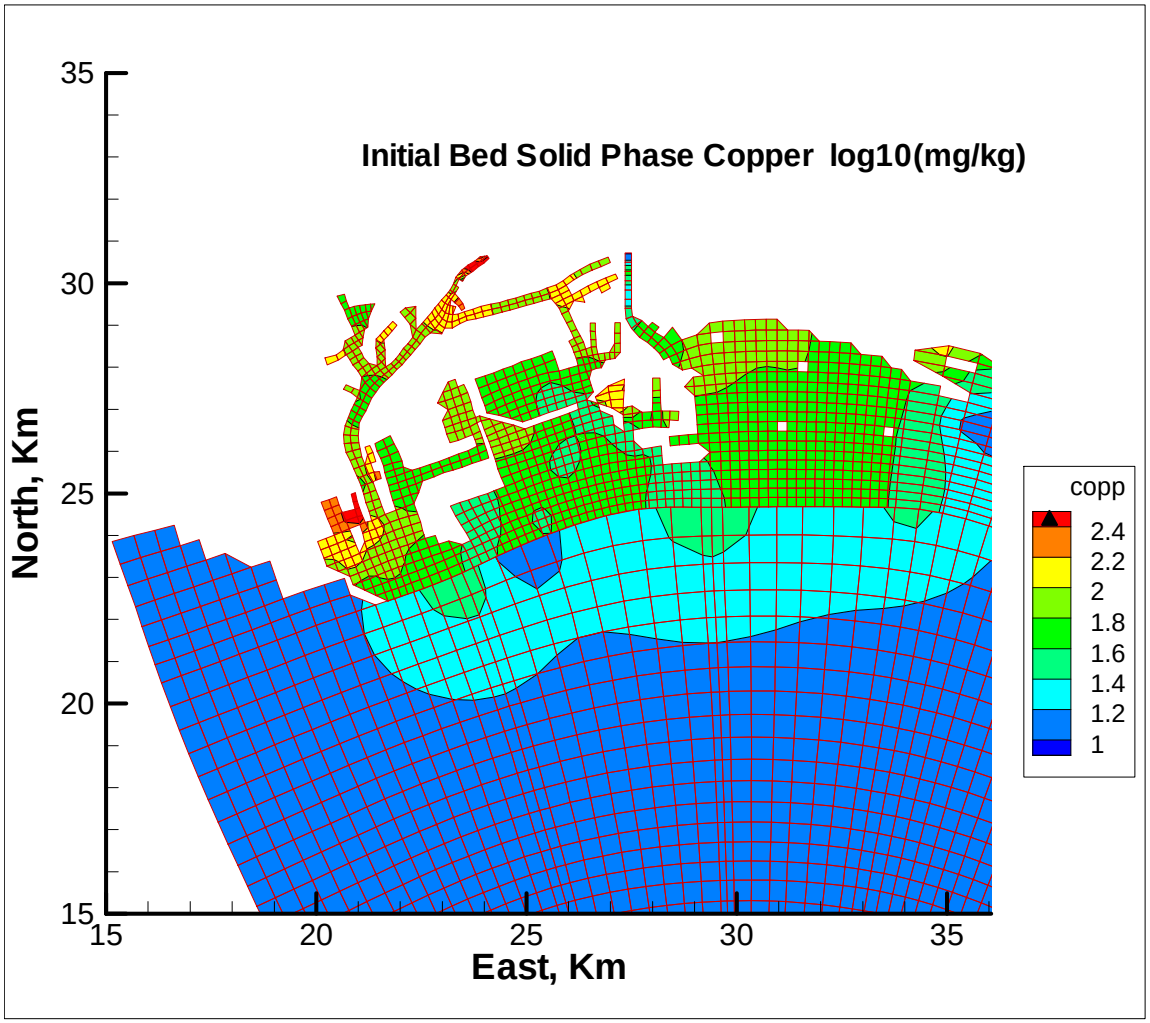

Note: Copper sediment quality guideline is 270 ppm (or mg/kg dry weight). Log(270) = 2.4 (represented by a black triangle in the concentration legend).

Figure 16. Initial bed solid phase copper concentration

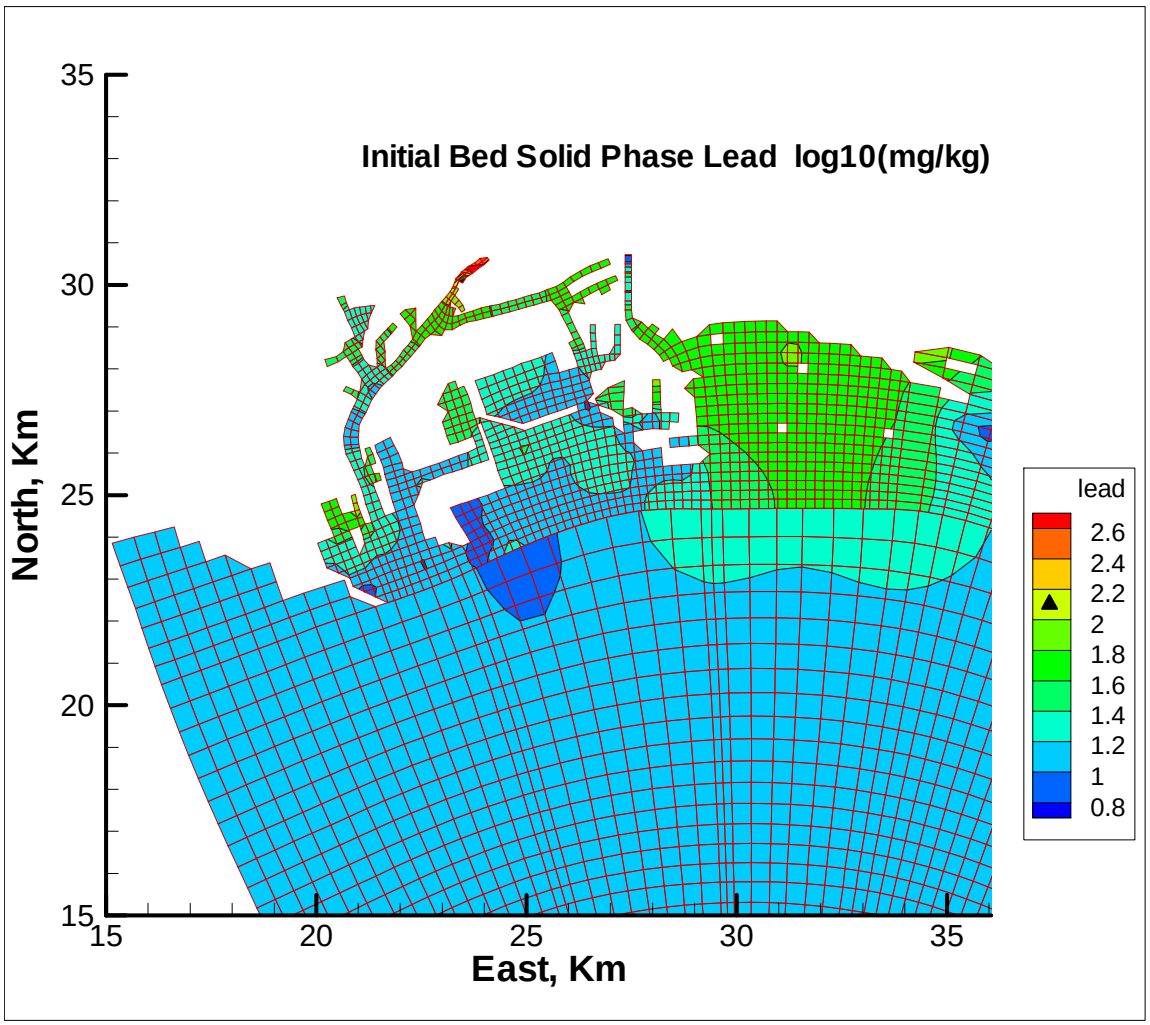

Note: Lead sediment quality guideline is 112 ppm (or mg/kg dry weight). Log(112) = 2.1 (represented by a black triangle in the concentration legend).

Figure 17. Initial bed solid phase lead concentration

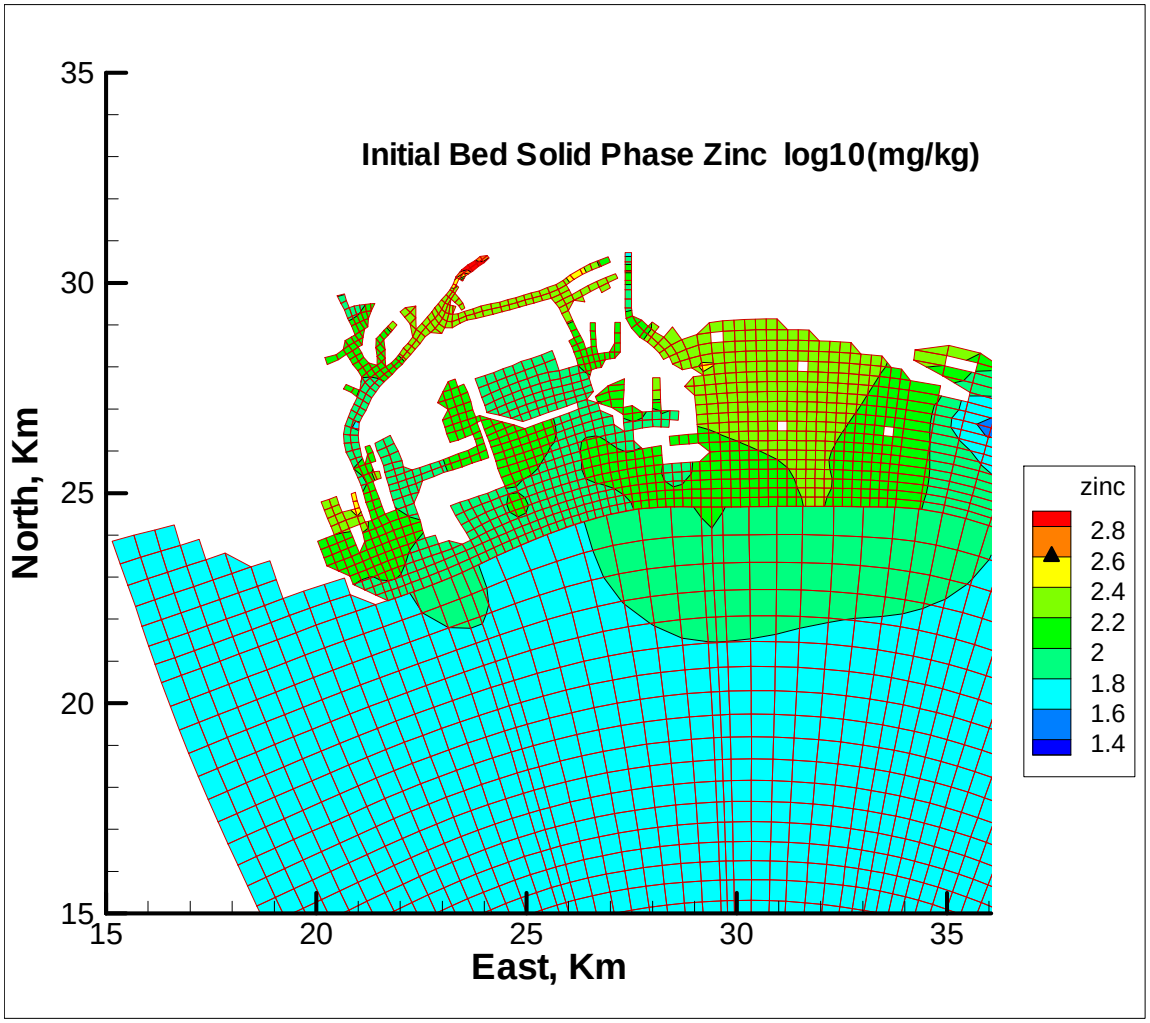

Note: Zinc sediment quality guideline is 410 ppm (or mg/kg dry weight). Log(410) = 2.6 (represented by a black triangle in the concentration legend).

Figure 18. Initial bed phase zinc concentration

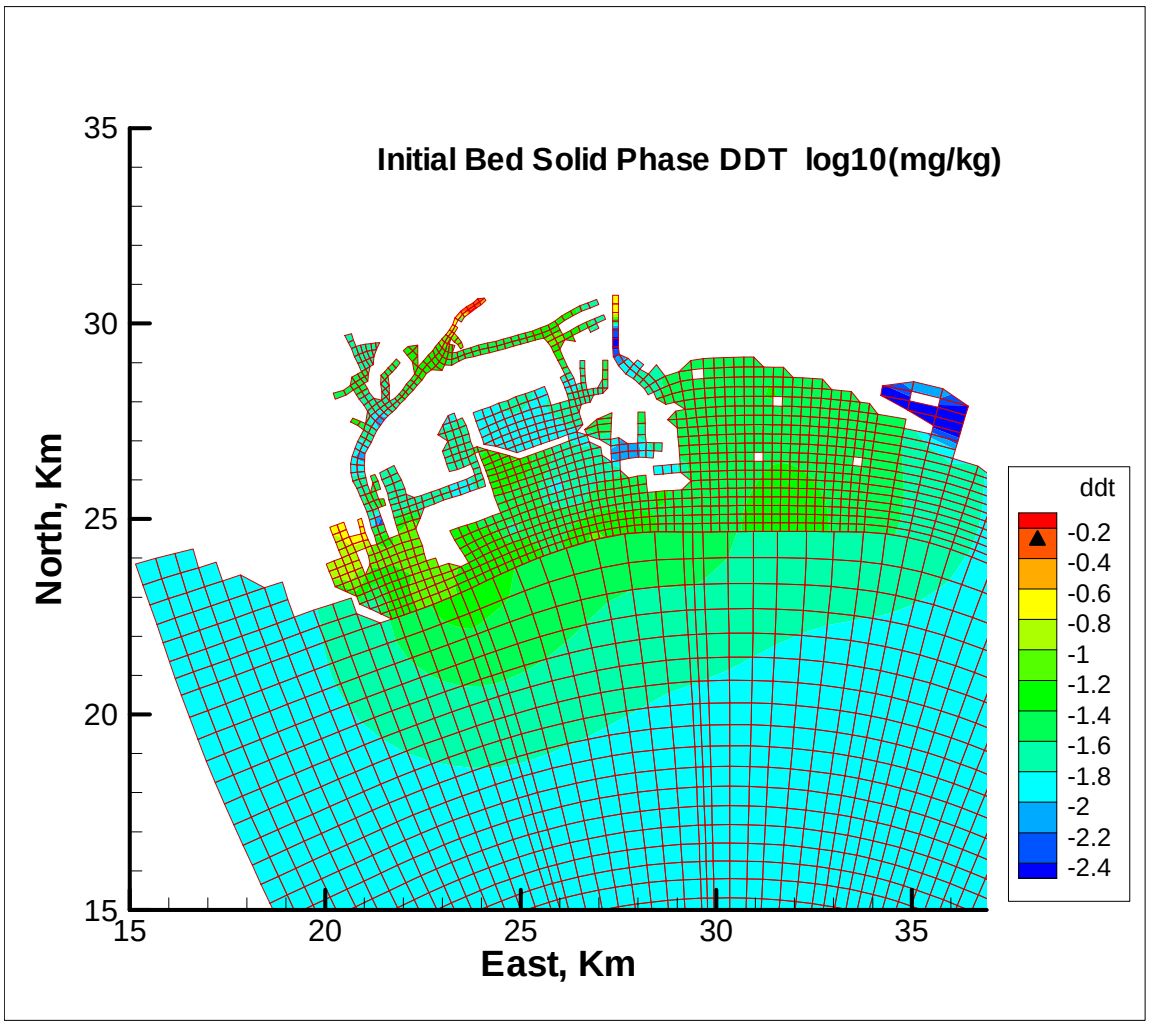

Note: DDT sediment quality guideline is 0.59 ppm (or mg/kg dry weight). Log(0.59) = -0.23 (represented by a black triangle in the concentration legend).

Figure 19. Initial bed solid phase DDT concentration

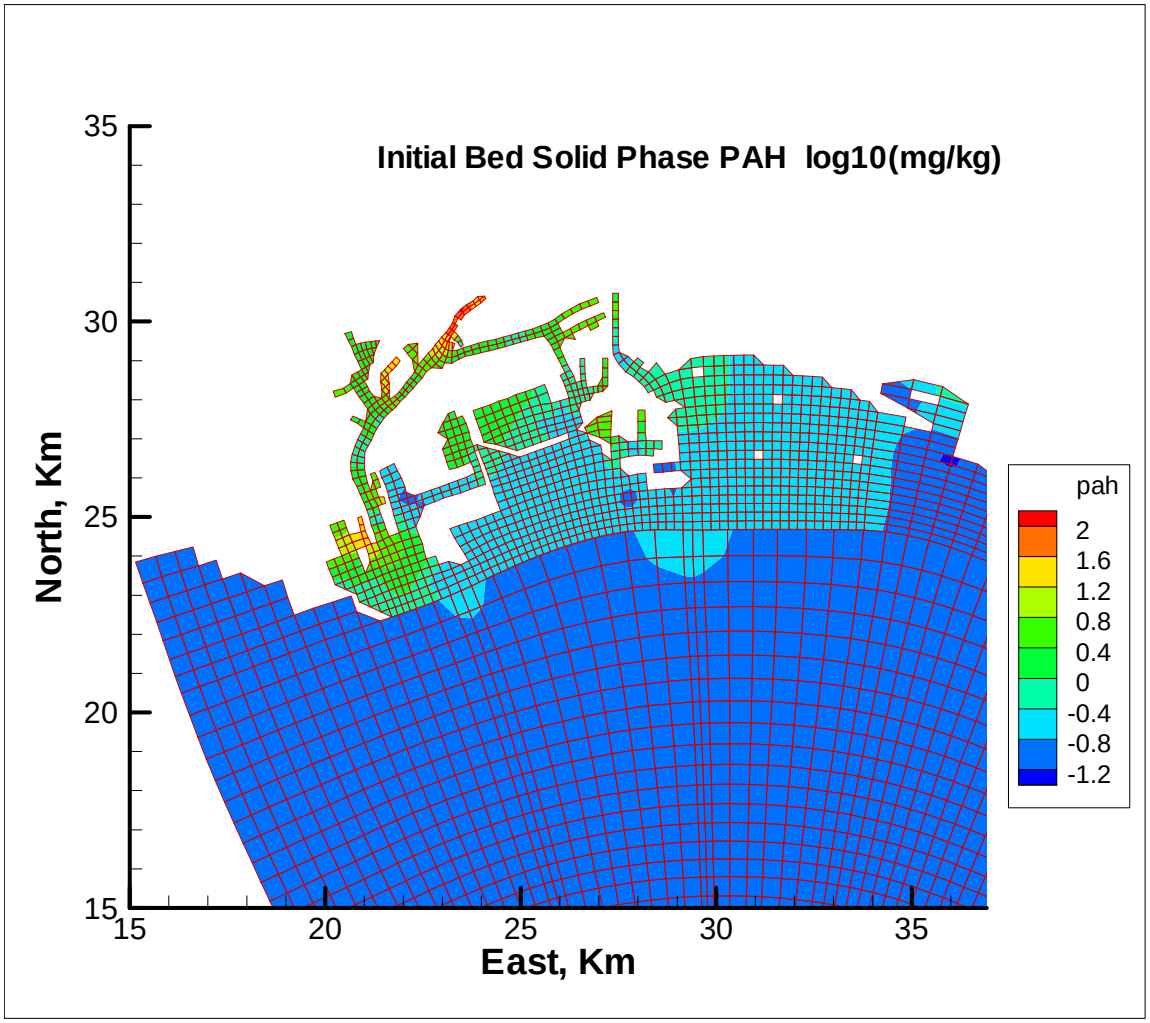

Note: Data presented are normalized to total solids.

Figure 20. Initial bed solid phase PAH concentration

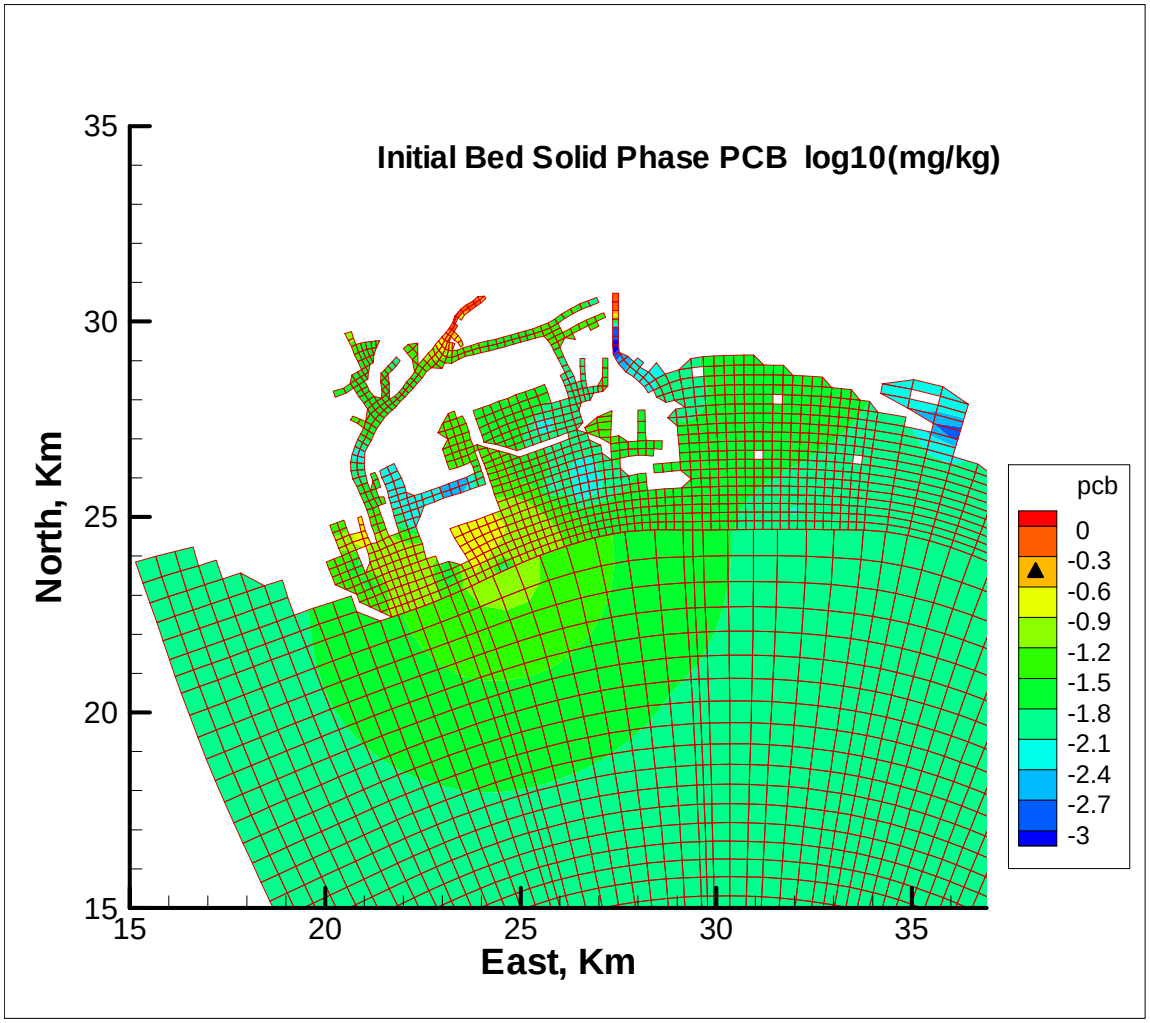

Note: PCB sediment quality guideline is 0.4 ppm (or mg/kg dry weight). Log(0.4) = -0.4 (represented by a black triangle in the concentration legend).

Figure 21. Initial bed solid phase PCB concentration

7.2. Sediment Settling, Deposition and Erosion Parameters

The sediment transport model requires specification of various sediment settling, deposition and erosion parameters. For the noncohesive sand sediment class, settling velocity is determined internally in the model based on input mean sand size. Erosion and deposition of sand associated with suspended and bed load transport is also internally parameterized in the model based on size class diameter and user choices of a number of widely accepted suspended and bed transport formulas (Tetra Tech, 2007). Available sediment bed grain size data suggest that a mean sand diameter between 0.125 and 0.250 mm would be appropriate and could be further refined during calibration.

The settling, deposition and erosion of fine cohesive-behaving silt and clay tends to be highly site specific and influenced by water ionic chemistry, organic content, sediment mineralogy and the state of bed consolidation. Site specific information requires settling column analyses and either in-situ or laboratory sediment erosion potential analyses. For environments having relatively low suspended sediment concentration, settling column analyses are not feasible and the fine sediment settling velocity is generally assigned an appropriate fresh or salt water value, in this case 0.0001 m/s, which can be adjusted during calibration as necessary.

A laboratory study of sediment erosion was conducted by Jepson et al. (1997) using intact field cores and cores reconstituted from field samples taken near Queen's Way and Queen's Gate in Long Beach Harbor. Grain size analysis of the material sampled near Queen's Gate and used to form four reconstituted cores indicated approximately 30 percent of the material to be cohesive silt and clay and the remaining 70 percent to be fine sand with a mean diameter of approximately 0.120 mm. The four reconstituted cores were allowed to consolidate for 2, 6, 20, and 60 days before their erosion potential was measured with the sedflume devise, described in Jepson et al. (1997). Consolidation of the cores allowed the degree of consolidation, represented by the void ratio, to be considered as a factor in determining erosion potential. The resulting sedflume measurements provided data to parameterize erosion as a function of applied shear stress and sediment bulk density using

$$\frac{E}{V} = \alpha \left(\frac{\tau}{V^2} \right)^{\beta} \exp\left(\frac{\gamma}{1+\varepsilon} \right) \qquad (3)$$

$$\alpha = 0.237 \quad \beta = 2.18$$

$$\gamma = -32.05$$

$$V = (\nu g)^{1/3} = 0.02\ m/s$$

for the erosion velocity, E, and

$$\frac{M}{\rho_s V} = \alpha\left(\frac{f}{1+\varepsilon}\right)\left(\frac{\tau}{V^2}\right)^{\beta}\exp\left(\frac{\gamma}{1+\varepsilon}\right) \qquad (4)$$

for the mass erosion rate M. In equations (3) and (4), ρ_s is the sediment particle density, V is a velocity scale, f is the fine fraction, τ is the kinematic shear stress, and ε is the void ratio. The coefficients α, β, and γ are based on a log-linear least squares fit of equation (3). Figure 22 compares observed erosion velocities with those predicted by equation (3).

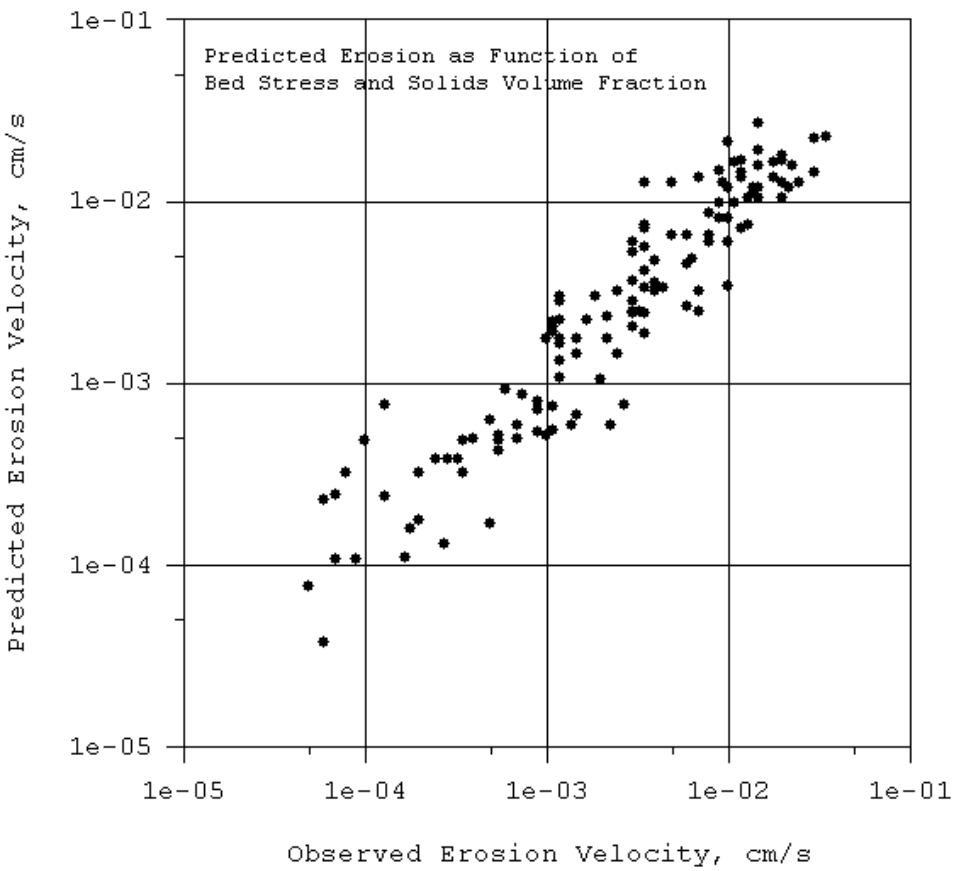

Figure 22. Erosion velocity predicted by equation (3) versus erosion velocity observed during sedflume erosion potential measurements

7.3. Equilibrium Partition Coefficients

The phase distribution of adsorptive contaminants, including metals and hydrophobic organic compounds, is an important determinant in their transport

and fate. Although arguments and evidence can be presented to question the utility of equilibrium partitioning to represent phase distribution, the equilibrium approach is accepted by US EPA for regulatory modeling studies associated with TMDL development and Remedial Investigation/Feasibility studies (RI/FS) at Superfund sites. Literature values are available for use when site specific information is not available. Site specific information, when available, is preferred to estimate equilibrium partition coefficients, in conjunction with comparison to literature values to identify unreasonable estimates. The EFDC model supports three phase equilibrium partitioning into free dissolved, complexeated or adsorbed to dissolved organic carbon, and particulate adsorbed, with further particulate phase options based on sediment size class, fraction of organic carbon and particulate organic carbon. Data available in the greater harbors system do not support three phase partitioning; therefore, the following two phase formulation was used:

$$C_d = \left(\frac{n}{n + K_p \bullet P} \right) C = dissolved \;\; per\ total\ volume \qquad (5a)$$

$$C_p = \left(\frac{P \bullet K_p}{n + K_p \bullet P} \right) C = particulate \;\; per\ total\ volume \qquad (5b)$$

$$C = contaminant\ concentration\ \ per\ total\ volume$$

$$n = porosity$$

$$P = particulate\ adsorption\ site\ concentration\ \ per\ total\ volume$$

$$K_p = \frac{C_p}{P} \bullet \frac{n}{C_d} = partition\ coefficient \qquad (5c)$$

The particulate adsorption site can be defined as the concentration of the fine sediment size class or as the concentration of particulate organic carbon (POC). The concentration of particulate organic carbon can in turn be defined as the product of a POC fraction and fine sediment concentration.

A field study in fall 2006 collected both sediment and contaminant data at approximately 60 sediment bed and overlying water sites (Figure 15). Bed data were sufficient to estimate partition coefficients using equation (5c) since both the particulate and dissolved phase contaminants were measured as total solids and organic carbon concentrations. The overlying water was sampled only for total concentration and total suspended solids. For the three metals, partition coefficients were defined in terms of fine sediment concentration. For the three organic compounds, partition coefficients were defined in terms of both the fine sediment and particulate organic carbon concentrations. Since organic carbon data were not complete for the entire sample set, a relationship between total bed solids concentration and total bed organic carbon was developed and shown in Figure 23.

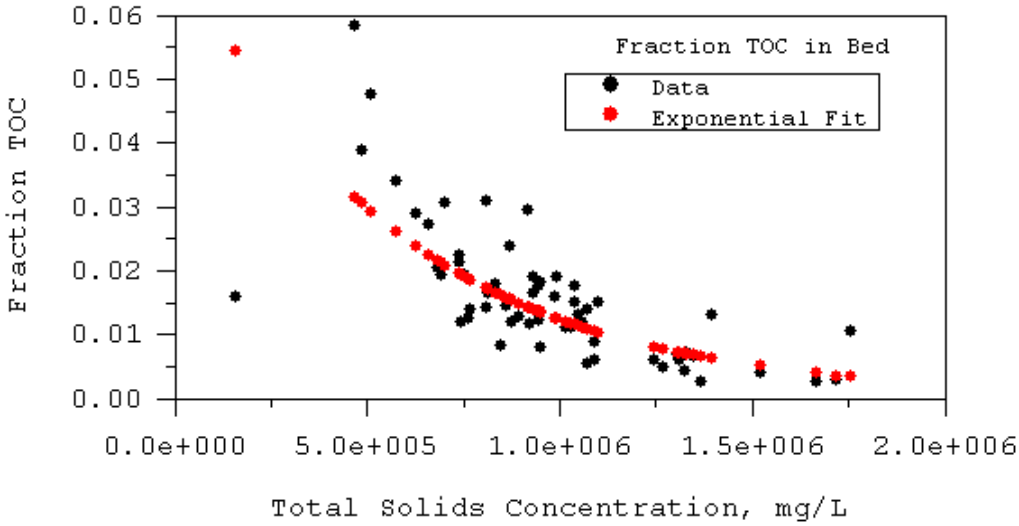

Figure 23. Total organic carbon fraction as a function of total solids concentration, based on 2006 sediment bed data

Equilibrium partition coefficients as a function of bed sediment concentration for the three metals are shown in Figure 24. Corresponding average and visual best estimates based on the 2006 sediment bed and overlying water data (Figure 15) are listed in Table 21. The visual best estimates are based on clustering and are lower than the averages by a factor of approximately two since the averages are influenced by a few large values. Both sets for values are within the literature range summarized by USEPA (2005). Water column partition coefficients for metal adsorption to dilute sediment (concentrations on the order of 1 to 100's mg/L) are typically larger than bed values. For water column sediment concentrations in the range of a few mg/L, the water column partition coefficients would be five to ten times larger than those for the bed values (USEPA, 2005). For initial metals configuration, the visual best fit bed partition coefficients (column three) were used and water column values were set to five times the bed values (column five).

Table 21. Sediment Bed and Water Column Equilibrium Partition Coefficients and Particulate to Dissolved Concentration Ratios for Metals

Contaminant	Average Bed Partition Coefficient Based on Total Solids (L/mg)[1]	Visual Best Fit Bed Partition Coefficient Based on Total Solids (L/mg)[1]	Water Column Particulate to Dissolved Concentration Ratio[2]	Estimated Water Column Partition Coefficient, 5 Times Column 3 (L/mg)[3]
Copper	0.09	0.05	0.51	0.25
Lead	0.54	0.25	7.12	1.25
Zinc	0.02	0.01	0.20	0.05

[1] Based on POLA/POLB 2006 sediment bed and overlying water data.

[2] Based on POLA 2005 and 2006 mid-water data.

[3] Calculated based on POLA/POLB 2006 sediment bed and overlying water data.

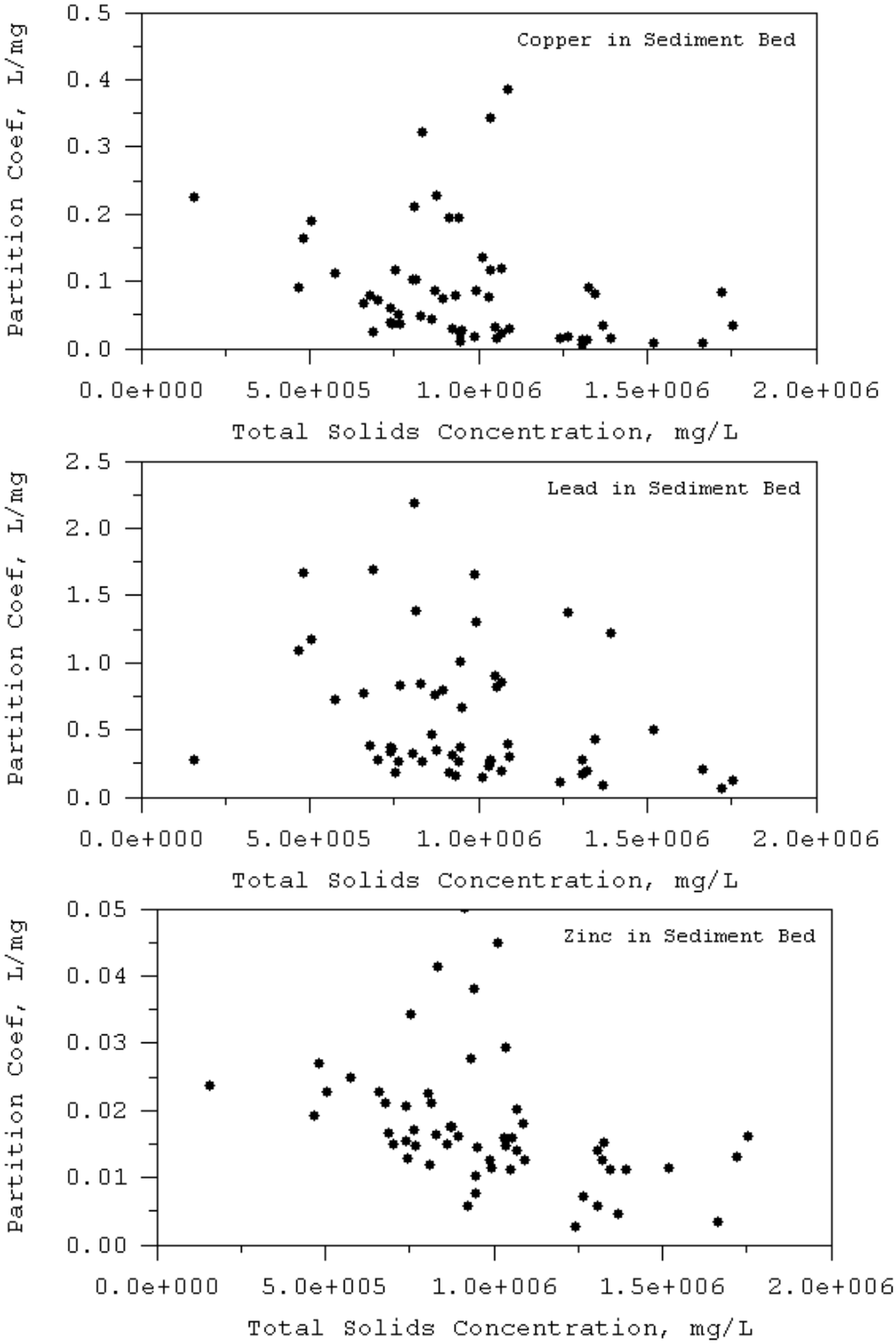

Figure 24. Equilibrium partition coefficients for copper, lead, and zinc based on bed total solids concentration.

Thomann and Mueller (1987) suggest that the product of the partition coefficient and sediment concentration, given by,

$$K_p \bullet P = \frac{C_p}{C_d} \qquad (6)$$

is approximately constant. Mid-water column metals samples collected during 2005 and 2006 (Figure 25) provide dissolved and particulate concentrations allowing the quantity defined in equation (6) to be determined. Sediment concentrations were erroneously not recorded. Figure 26 shows this product for the 2005-2006 mid-water data (Figure 25) for copper, lead, and zinc with average values tabulated in Table 21. The range of average ratios for the copper and zinc data is consistent with the value of 0.25 suggested by Thomann and Mueller (1987) while the lead value is an order of magnitude higher.

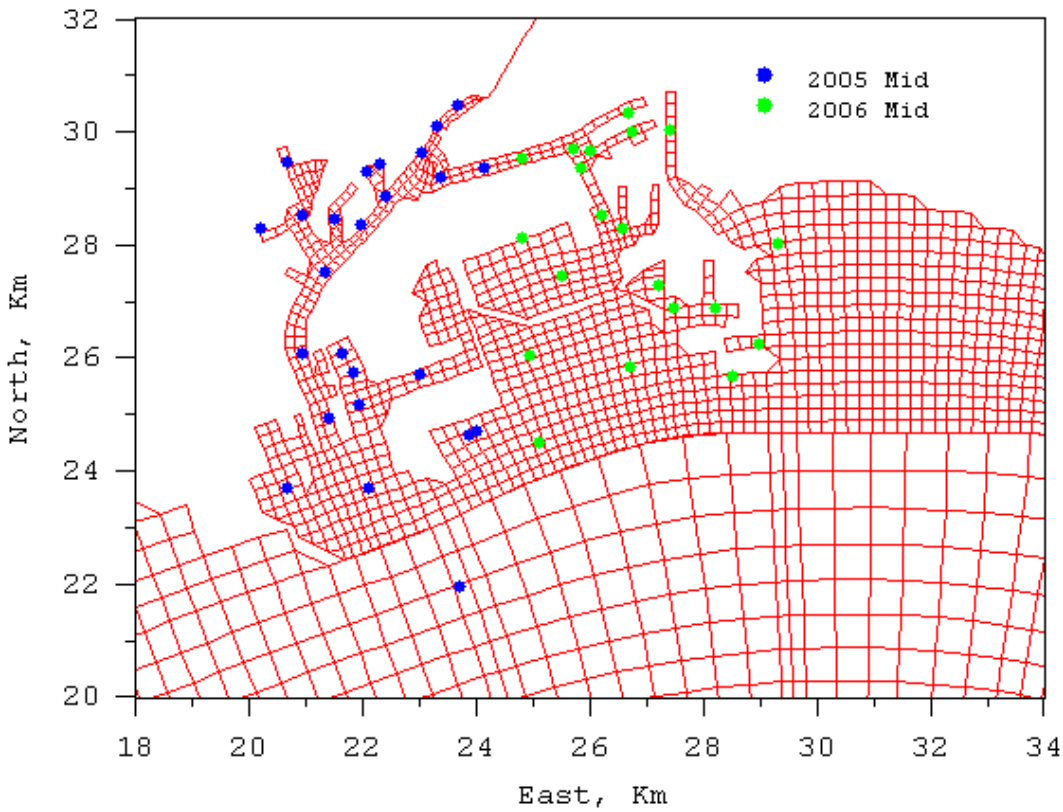

Note: 2005 data collected by POLA; 2006 data collected at POLB stations as part of 2006 POLA/POLB study.

Figure 25. Mid-water column sample sites used for metals calibration

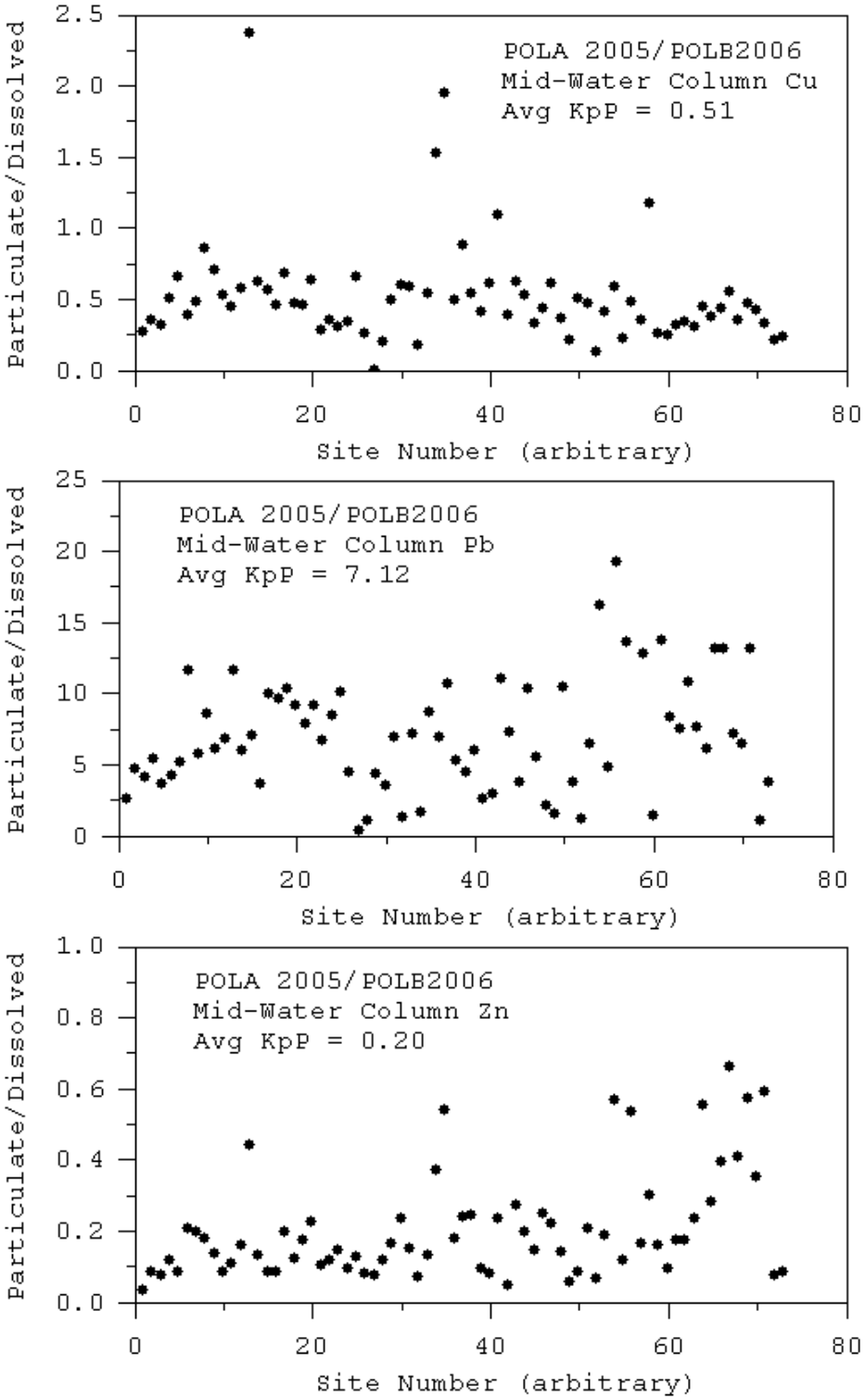

Figure 26. Particulate to dissolved concentration ratio (equal to product of partition coefficient and adsorption site particle concentration) for mid-water column metals concentrations

Subsequent to conducting the calibration and sensitivity simulations for metals, described in Chapter 8 and Appendix C, using water column partition coefficients in column 5 of Table 21, additional water column metals and sediment concentration data sets became available. These data sets include dissolved and total metals data collected during January and March 2006, and dissolved and total metals and suspended solids during January 2008 by POLA. The locations of these data sets correspond to the 2005 locations shown in Figure 25. An analysis and discussion of the significance of these additional data sets is provided in Appendix E.

Equilibrium partition coefficients based on the 2006 POLA-POLB data (Figure 15) for DDT, PAH, and PCB, as a function of bed sediment concentration and bed total organic carbon concentration, are shown in Figures 27 through 29. Table 22 summarizes approximate constant values of these equilibrium partition coefficients for the three organic contaminants based on the data shown in Figures 27 through 29. Bed solids and bed TOC based values are consistent with the ranges reported in the literature (Chapra, 1997; Chiou, 2002). Low and high range values in Table 22 are based on the range of octanol-water partition coefficients for pesticides, PAHs, and PCBs reported in Chapra (1997). For these three contaminants, organic carbon-referenced bed values should be readily utilized in the water column and can be referenced to water column solids by dividing by the ratio of TOC to total solids. A limited number of the fall 2006 overlying water sites (Figure 15) had organic carbon samples, which are shown in Figure 30. At higher sediment concentrations, the ratio is approximately 0.01, which is approximately the ratio represented by the difference in solids and TOC normalized bed values (Table 22). This suggests that the bed solids referenced partition coefficients for the three organics can also be used in the water column.

Table 22. Sediment Bed Equilibrium Partition Coefficients for Organics

Contaminant	Bed Solids Based (L/mg)[1]	Bed TOC Based (L/mg)[1]	TOC Based Low Range (L/mg)[2]	TOC Based High Range (L/mg)[2]
DDT	0.0002	0.02	0.0002	0.2
PAH	0.0004	0.04	0.01	2.0
PCB	0.0002	0.02	0.005	0.5

[1] Based on POLA-POLB 2006 sediment bed and overlying water data.

[2] Based on Chapra, 1997.

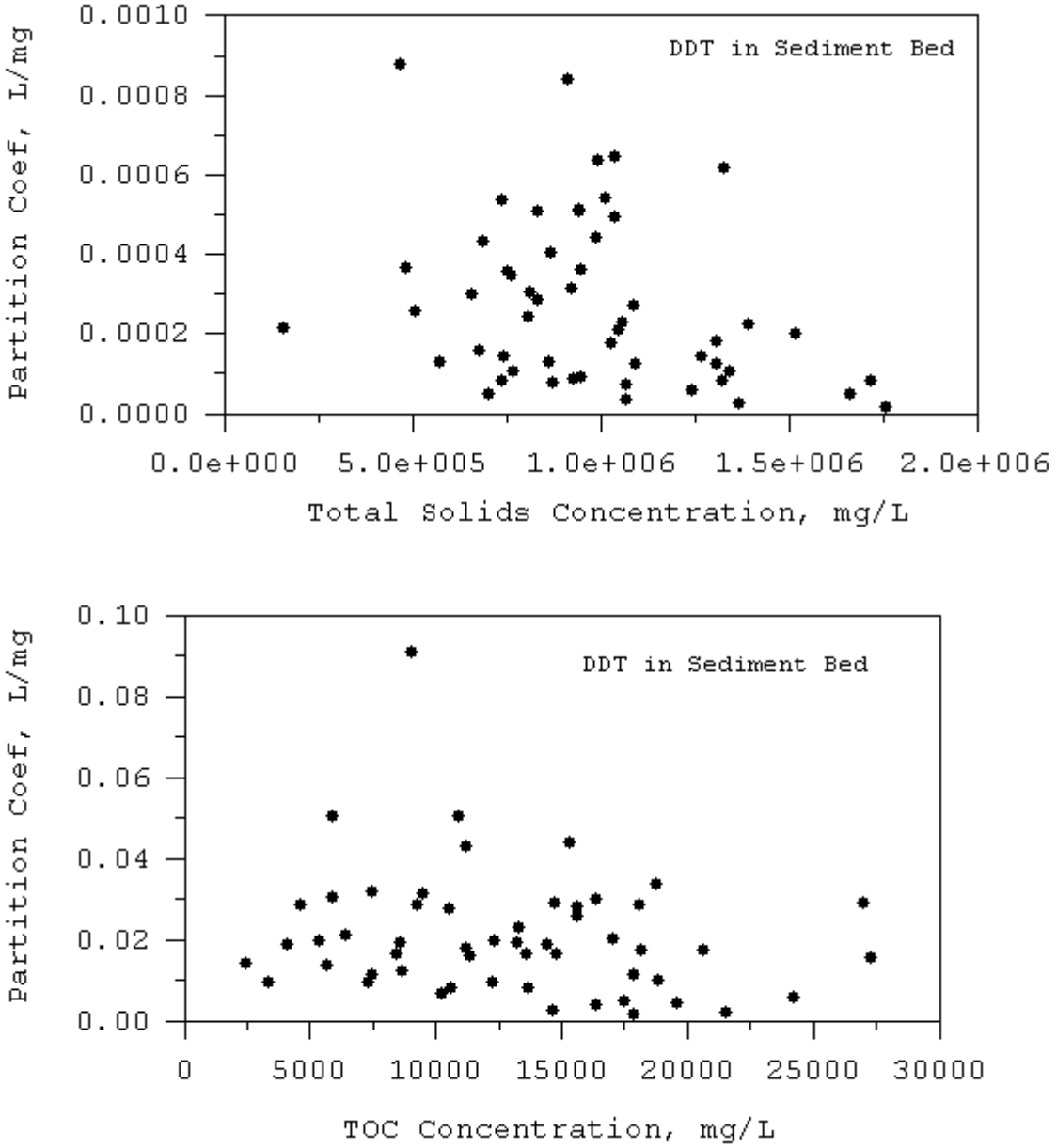

Figure 27. Equilibrium partition coefficient for DDT based on total solids (top panel) and total organic carbon (bottom panel) based on data collected in 2006

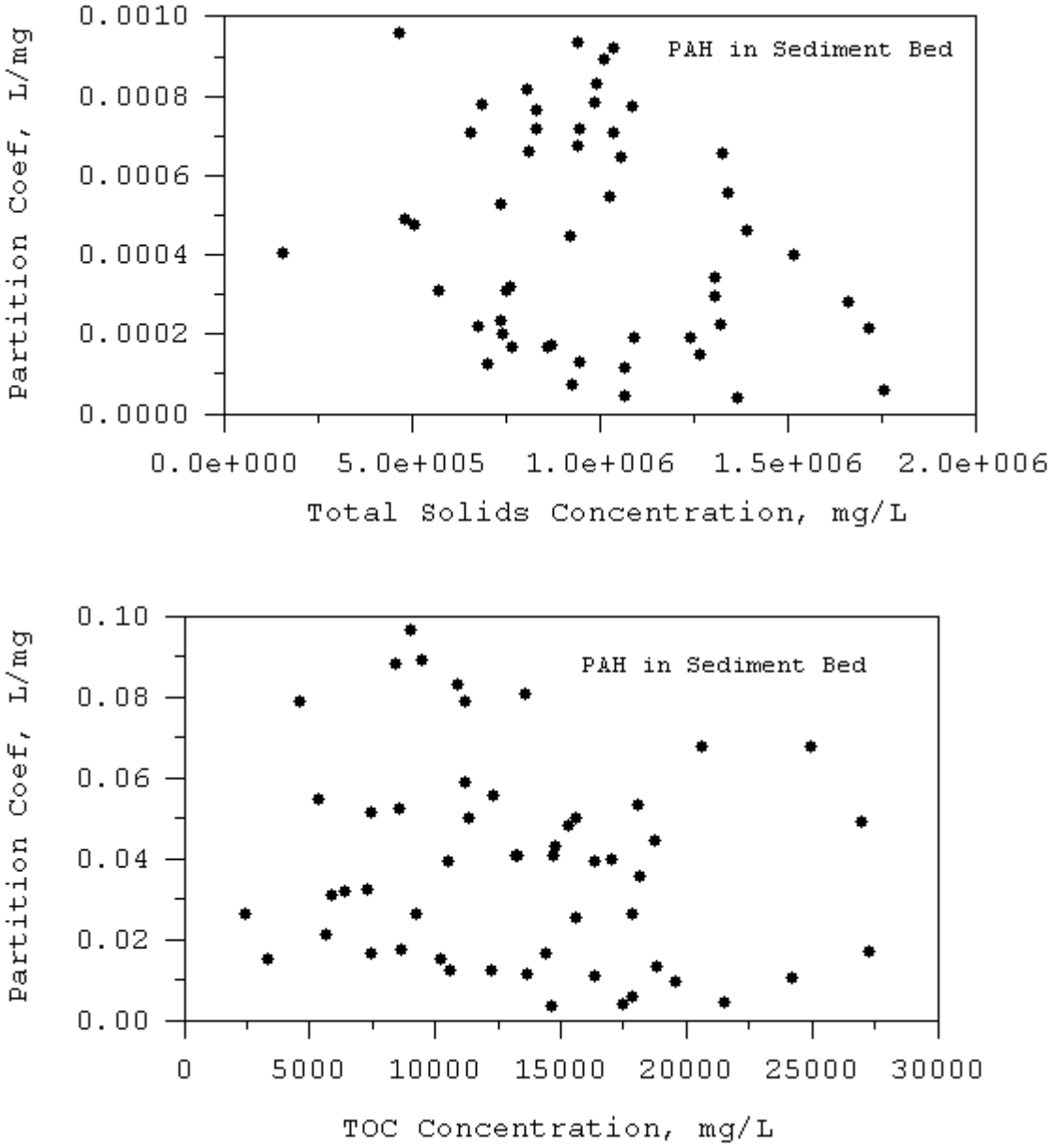

Figure 28. Equilibrium partition coefficient for PAH based on total solids (top panel) and total organic carbon (bottom panel) based on data collected in 2006

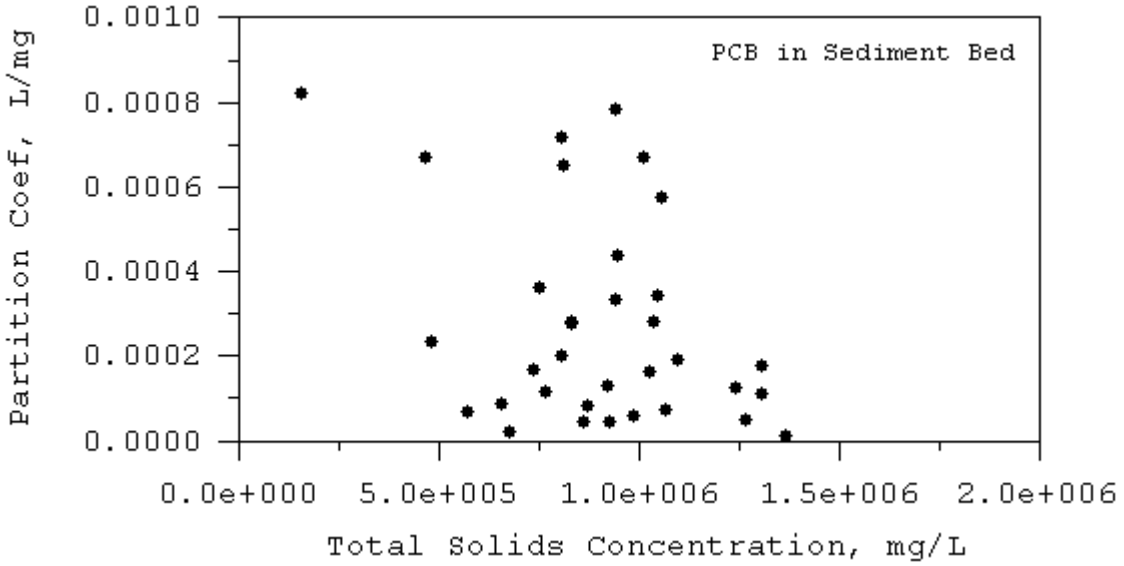

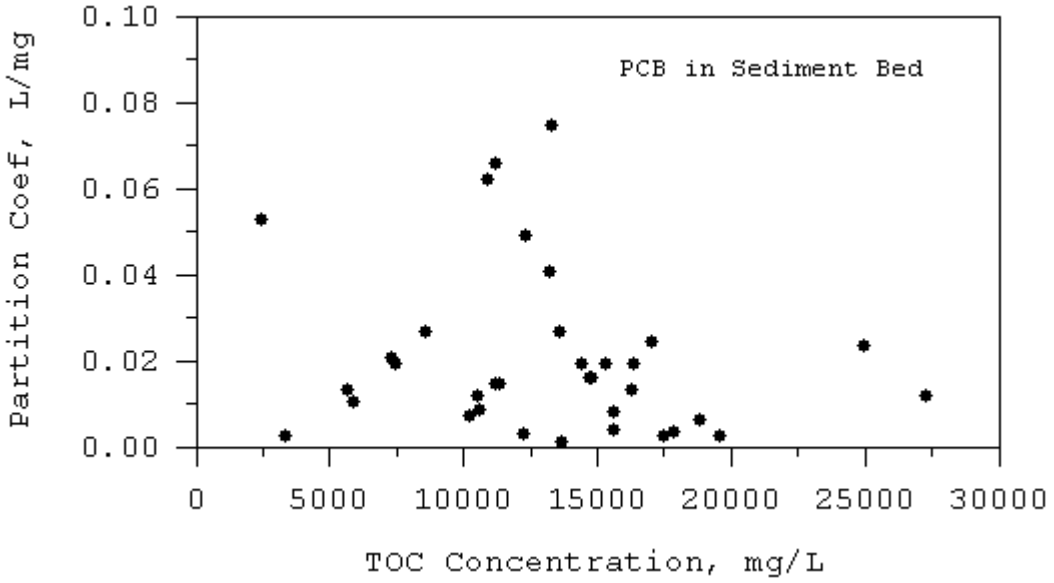

Figure 29. Equilibrium partition coefficient for PCB based on total solids (top panel) and total organic carbon (bottom panel) based on data collected in 2006

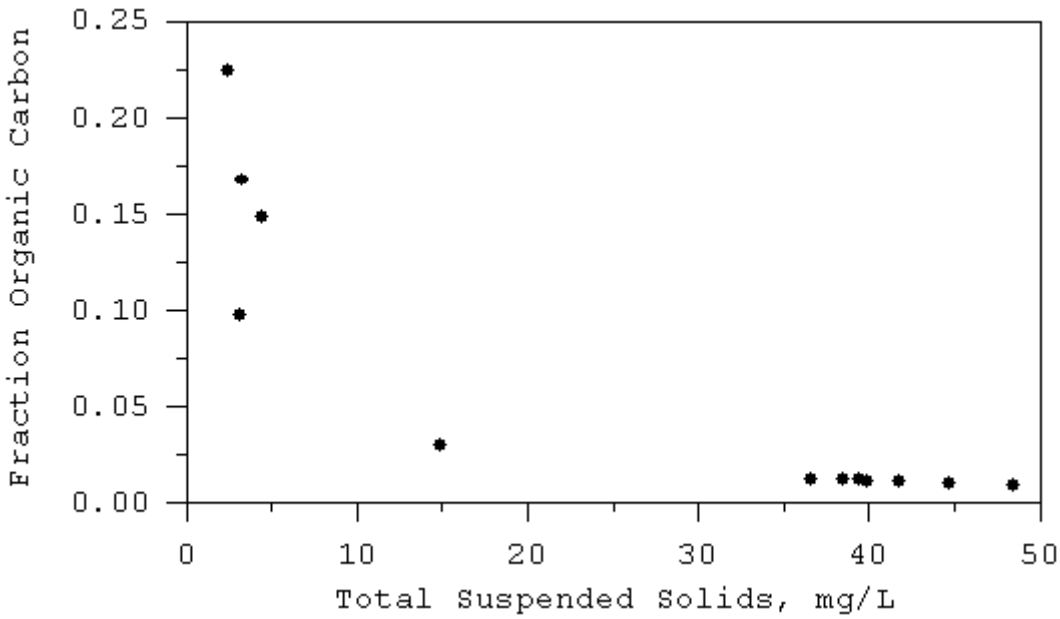

Figure 30. Fraction of organic carbon as function of total suspended solids concentration based on fall 2006 overlying water site data

7.4. External Loads and Open Boundary Conditions

External loads of sediment and contaminants are provided by the watershed model (Tetra Tech, 2006), which was used to provide point and nonpoint source inflows to the greater harbors system. Each inflow time series is assigned a corresponding time series of contaminant concentrations. Figure 31 shows an example of inflow and inflowing sediment and copper concentrations for the Los Angeles River. Loads for metals also included atmospheric dry deposition rates of 22, 14, and 160 $\mu g/m^2$-day, for copper, lead, and zinc, respectively.

Sediment and contaminant concentration must be specified on the model open boundaries in San Pedro Bay (Figure 1). Sediment concentrations on all three open boundaries were set to a value of 2.0 mg/L based on limited measurements during the Bight 03 study. Concentrations of copper, lead, and zinc were set to 0.10, 0.03, and 0.30 µg/L based on greater harbors observations during 2005 and 2006 taken near and immediately outside of the breakwater (Figure 25). Concentrations of DDT, PAH, and PCB were set to 0.25, 100.0, and 0.015 ng/L. Values for DDT and PCB were based on those reported by Zeng and Tran (2002) and Zeng, et al. (2005). Values for PAH were based on greater harbors observations during 2006 take near and immediately outside of the breakwater (Figure 25; 2006 sample locations only).

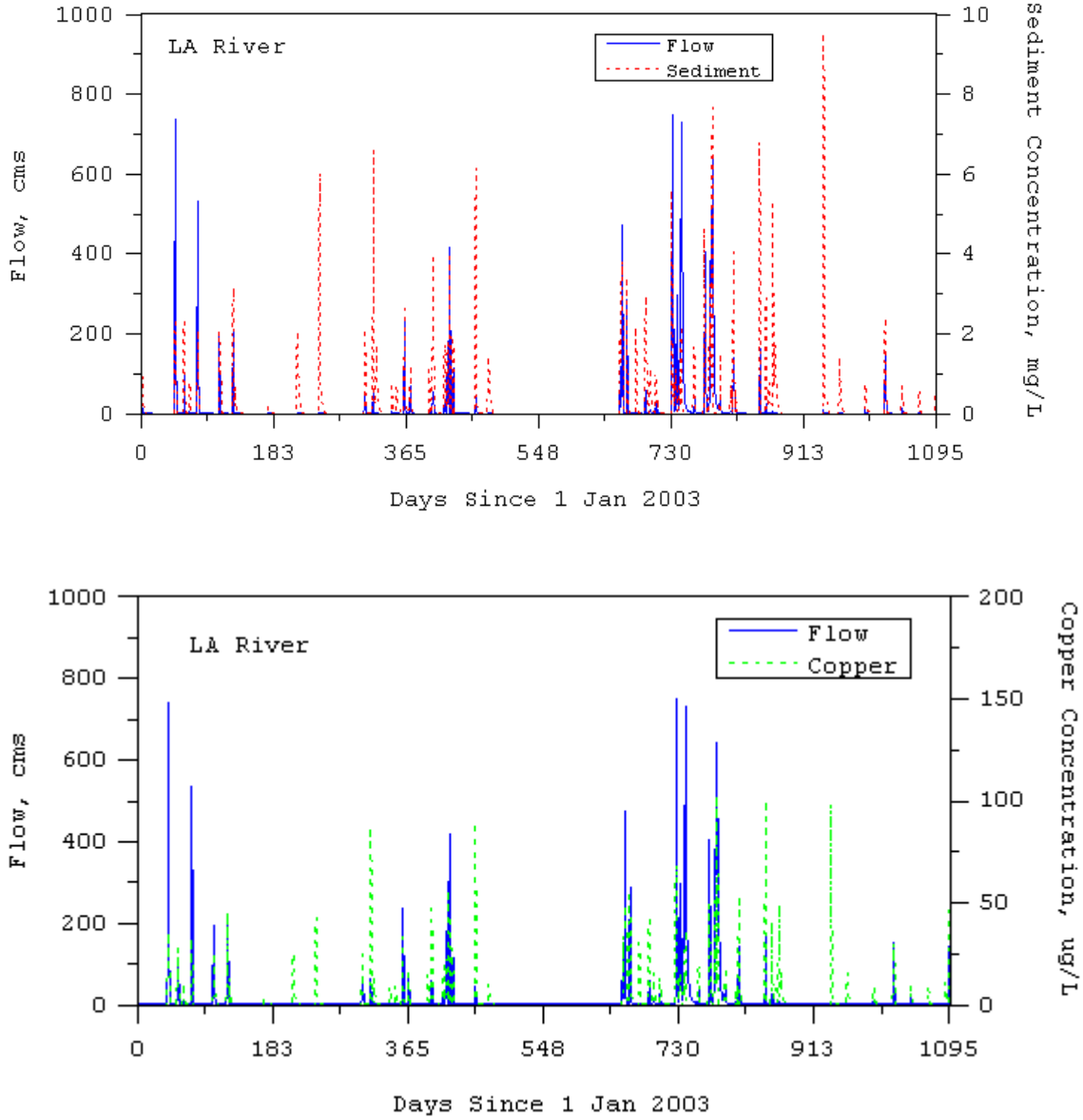

Figure 31. Examples of flow and inflowing sediment and copper concentration for the Los Angeles River

8. Sediment and Contaminant Transport Calibration

Model calibration involves the adjustment of selected model input parameters to achieve a best or targeted level of agreement between model predictions and observations. The level of agreement can be judged by combinations of qualitative methods, usually visual comparison, or quantitative methods, such as those discussed in Appendix B of this document. Subsequent validation of a calibrated model involves using the same procedures to judge the level of agreement between model predictions and a different set of observations not used for calibration. Preferably the observations used for validation should represent hydrodynamic and transport conditions different from those under which the calibration observations were obtained. In many situations, particularly when the cost of obtaining multiple observation data sets is prohibitive, calibration and validation cannot be unique activities and validation is often foregone or replaced by sensitivity analysis. Since the availability of water column sediment and contaminant data in the greater harbors precludes formal validation, sensitivity analysis was conducted (see Appendix C and Appendix D). Specifically, the dry weather sensitivity of water column sediment and contaminant concentration prediction to changes in river and watershed loads, open boundary conditions, and sediment erosion rates were analyzed (Appendix C). Long-term sensitivity was also evaluated by comparing water column and sediment bed concentration results from simulations using baseline conditions and a 50 percent reduction in river and watershed loading (Appendix D).

The observational data available for sediment and contaminant transport model calibration and validation is sparse to the extent that only a calibration effort can be undertaken. As discussed in the preceding section, observational data defining conditions in the sediment bed were used for model initialization and are not appropriate for use in calibration. Instead, the calibration approach taken in this study is to use observational data in the water column for model calibration. Observational data in the water column includes sediment and contaminant concentrations measured near the bottom of the water column during fall 2006. This data set is referred to as the overlying water observations since they were taken at the same locations as the in bed observations (Figure 15). Specifically, the data set includes total suspended sediment concentration and total concentration of the six contaminants sampled at one instance in time. Two additional water column data sets taken at mid-depth in the water column during 2005 and 2006 (Figure 25) provide observations of total and particulate concentrations of the three metals. Total suspended solids information, which would allow definition of phase distribution in these metal data sets, was not recorded. Subsequently, six of the sites sampled in 2005, were sampled for mid-water column total suspended solids in 2007. The following two sections further discuss the calibration approach and present results for sediment and contaminants.

8.1. Sediment Transport Calibration

The degree of calibration of the sediment transport model is evaluated using sediment concentrations at the 60, fall 2006 overlying water sites (Figure 15) and six of the 2005 mid-water column sites (Figure 25) which were sampled for suspended sediment concentration in fall 2007. For comparison with the instantaneous observations, taken under dry fall conditions, model predictions were averaged over a six month dry season period. Figure 32 shows the continuous model predictions at a representative site with the instantaneous observation value shown as a dashed line. Model predicted and observed sediment concentration at the 2006 overlying water sites and the 2007 mid-water column sites are shown in Figure 33. Model predicted concentrations are reasonable, however a quantitative measure of agreement would be extremely low. The average predicted values show less variation than observations, although Figure 32 shows that instantaneous predictions can vary significantly about the mean.

Calibration parameters for suspended sediment traditionally include effective diameters for noncohesive size classes, settling velocity and erosion rate for the fine cohesive size class, loading relationships, and open boundary conditions. Best estimates for all of these parameters were used for model configuration. The primary adjustment made during calibration was setting the noncohesive sediment class diameter to 0.125 mm so that excess erosion did not occur in San Pedro Bay and override the observational based boundary conditions. For the fine cohesive sediment, which represented more than 90 percent of the model predicted water column sediment, sensitivity of predictions with respect to settling velocity were conducted. Lower and higher settling velocities increased disagreement between predictions and observations at most stations. Increasing and decreasing the base cohesive sediment erosion rate coefficient (α in equation 5) resulted in similar responses using lower and higher settling velocities.

8.2. Contaminant Transport Calibration

The degree of calibration of the contaminant transport model is evaluated using contaminant concentrations at the 60, fall 2006 overlying water sites (Figure 15) and the 2005 and fall 2006 mid-water column sites (Figure 25). As previously noted, the mid-water column sites only have data for the three metals. Overlying water sites failed to provide detectable concentrations of PCB, resulting in no calibration results being presented for PCB other than confirmation that the model predicted water column PCB levels were below detection limits. As was done for the sediment comparison, contaminant concentrations were averaged over a six month dry season period for comparison with instantaneous observations taken during dry fall conditions.

Figures 34 through 36 show comparisons of model predictions and observations for total copper, lead, and zinc. The comparisons show extensive scatter, but model predicted levels are within the range of observations. For copper, the model predictions tend to be flat, on the order of 0.25 μg/L, while observations show more variability. For lead, the model predicts a larger range of concentrations than the observational data. Zinc predictions show a greater range as well as a region of flat predictions on the order of 1 μg/L. The flat prediction regions for copper and zinc have concentrations approximately three times larger than the open boundary values suggesting that they are not boundary condition driven. Predicted lead concentrations are also significantly larger than boundary conditions values. Figures 37 and 38 show comparisons of predicted and observed total concentrations of DDT and PAH. Predictions for DDT are almost constant and equal to the boundary condition value of 0.25 ng/L. Predictions for PAH show slightly more variability but are also close to the boundary condition value of 100 ng/L. Model predictions for PCB also were close to the boundary condition value of 0.015 ng/L, but are not shown since PCB levels in the samples were not detectable.

8.3. Dry Season Sensitivity Analysis

A dry season sensitivity analysis was conducted to determine the influence of open boundary concentrations, watershed loads, and sediment bed erosion rates on model predictions. These results are presented in Appendix C. Open boundary conditions, representing ambient or background concentrations in San Pedro Bay, result from much larger scale distributed sources than the greater harbors watersheds, and cannot be readily controlled with respect to a localized watershed-scale TMDL. In this respect, demonstration of low sensitivity to open boundary conditions is desirable A moderate to high sensitivity with respect to river and watershed loads indicates that these sources are primarily responsible for observed levels of contamination. In water bodies having significant existing or legacy contaminant of the sediment bed, net flux of sediment, metals, and organics from the bed to the water column due to erosion and slower diffusive flux can represent a significant source to the water column.

For the organics and, to a certain extent, zinc, the sensitivity analyses suggest that a reduction of land-derived loads may result in lower levels of water column contamination. In addition, sediment bed erosion was found to be a significant source of contamination. Pollutant load reductions may be achieved by implementation measures either individually or in combination. Such implementation measures may include, but are not limited to, reducing watershed and river inflows of contaminated sediments (but not necessarily clean sediment), localized capping or sediment removal, and gradual replacement of incoming contaminated sediment with clean sediment (to reduce contaminant

flux from the sediment bed since the new deposited cleaner sediment would lower contamination levels).

8.4. Sensitivity to Long-Term Load Reductions

To compliment the dry season sensitivity analysis and demonstrate the application of the model to investigate load allocations, two long-term simulations were conducted (Appendix D). Both simulations examined several pollutants (copper, zinc, DDT, and PAHs) and spanned a four year period from 2002 through 2005. The first (or baseline) simulation used watershed model estimated sediment and contaminant loads (i.e., the baseline conditions from the calibrated model). The second (or load reduction) simulation used sediment and contaminant loads which were reduced by 50 percent for inputs from both the rivers and near shore watersheds. The sensitivity analysis results are presented in both time series graphs and maps illustrating changes in contaminant level over the four year period.

Results for both copper and zinc indicate decreases in water column concentrations during periods of high flow, when comparing the baseline conditions with the 50 percent load reduction scenario. In addition, after the four-year period, the copper and zinc sediment bed concentrations associated with the 50 percent load reduction scenario were lower than baseline. The spatial maps of copper and zinc indicate that a 50 percent reduction of incoming loads results in a system-wide reduction in sediment bed concentrations.

Similar to the metals, DDT and PAH concentrations in the water column decrease during periods of high flow when comparing the baseline conditions with the 50 percent load reduction scenario. Sediment bed contaminant concentration behavior was more spatially varied after the four-year period for DDT; one station increased in concentration while another decreased. PAH in the sediment bed followed a pattern more similar to metals (concentrations associated with the 50 percent load reduction scenario were lower than baseline conditions). As illustrated by the maps, the spatial pattern is somewhat similar for the two organics, with the most significant changes occurring in the inner harbors and near the Los Angeles River inflow. Similar to the metals, these maps indicate that a 50 percent reduction of incoming loads results in a system-wide reduction in sediment bed DDT and PAH concentrations.

Overall, the simulations showed that water column contaminant concentrations were lower for the reduced load simulation during wet period events and that sediment bed contaminant levels were lower after the four year period for the reduced load simulation. These results suggest that the model could be used to evaluate spatially distributed and wet weather magnitude-based load reduction scenarios. Detailed discussion of the simulations are presented in Appendix D.

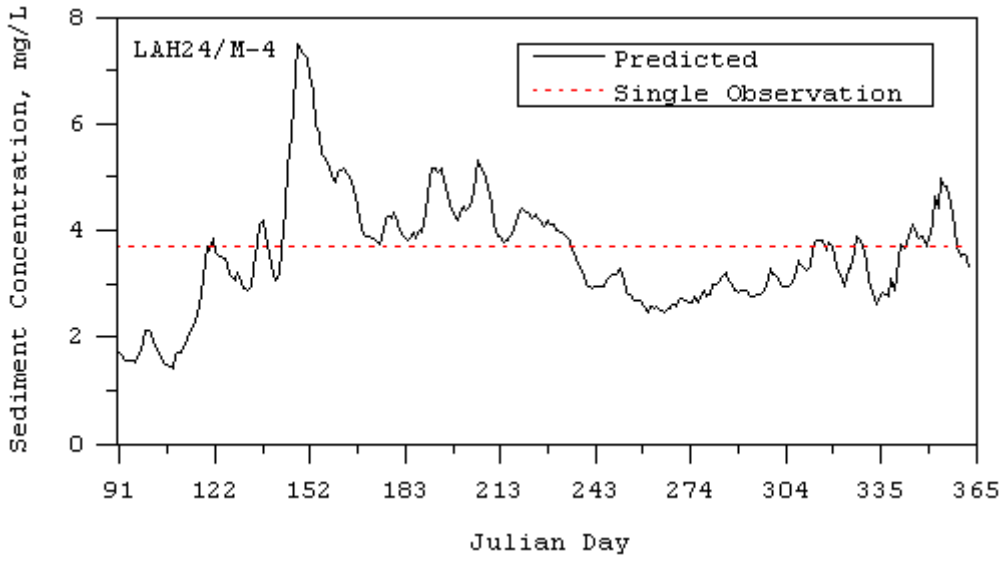

Figure 32. Comparison of model predicted and single observed sediment.

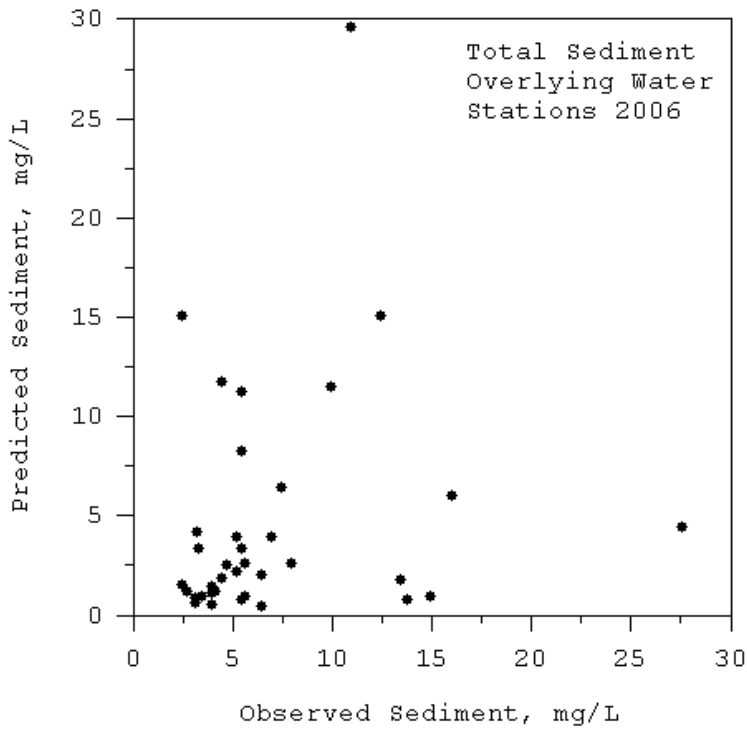

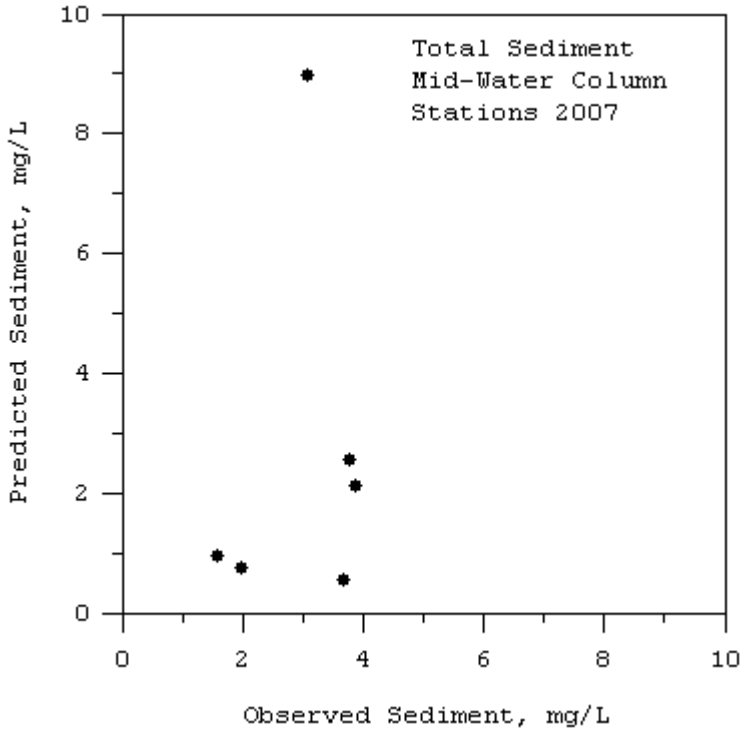

Figure 33. Comparison of model predicted and observed sediment concentration at the 2006 overlying water sites and 2007 mid-water column sites

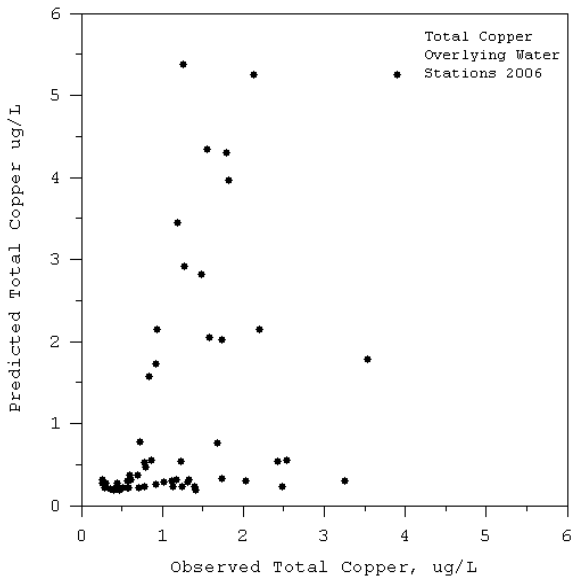

(a)

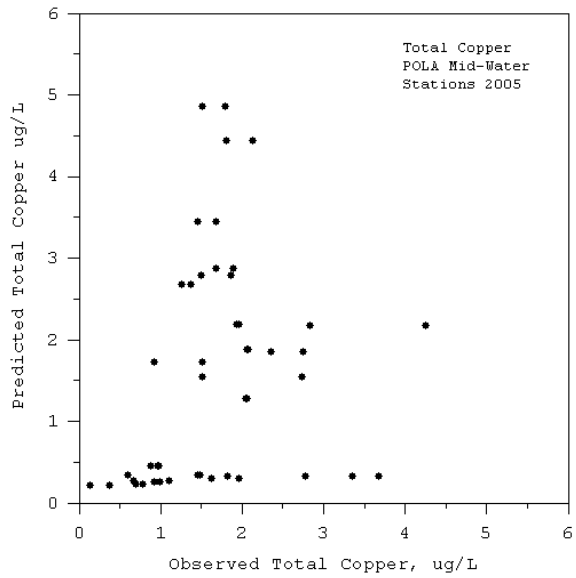

(b)

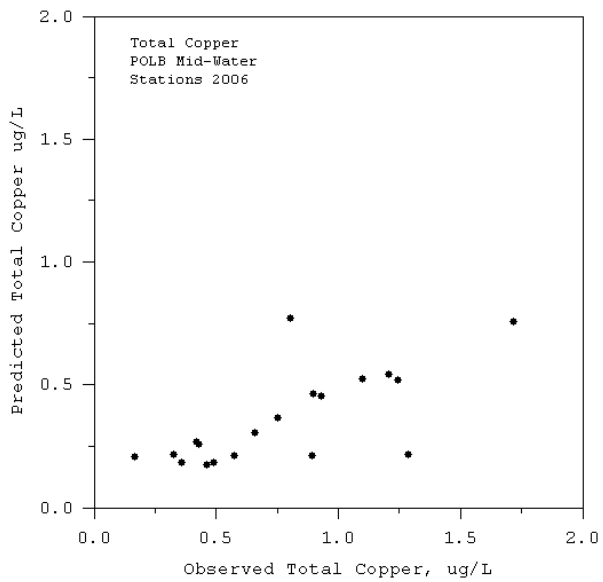

(c)

Figure 34. Comparison of model predicted and observed copper concentration at the overlying water and mid-water column sites

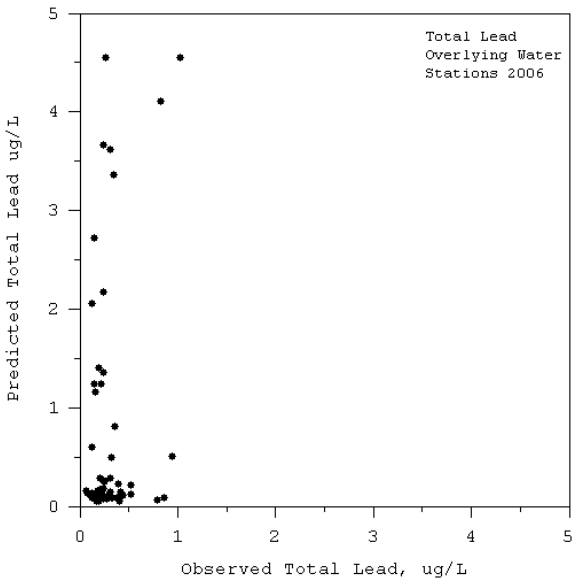

(a)

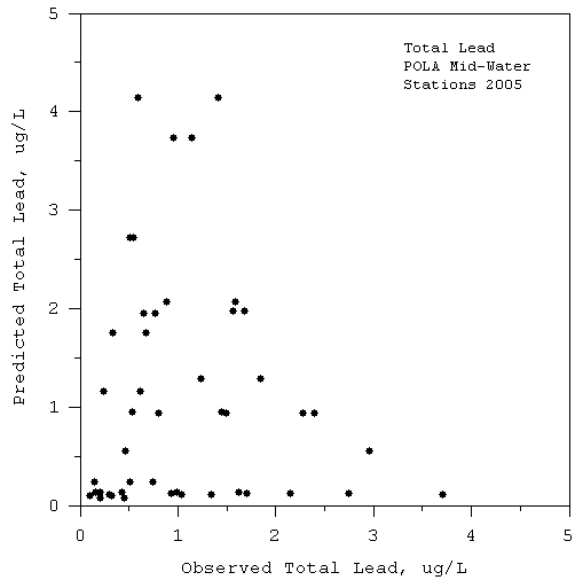

(b)

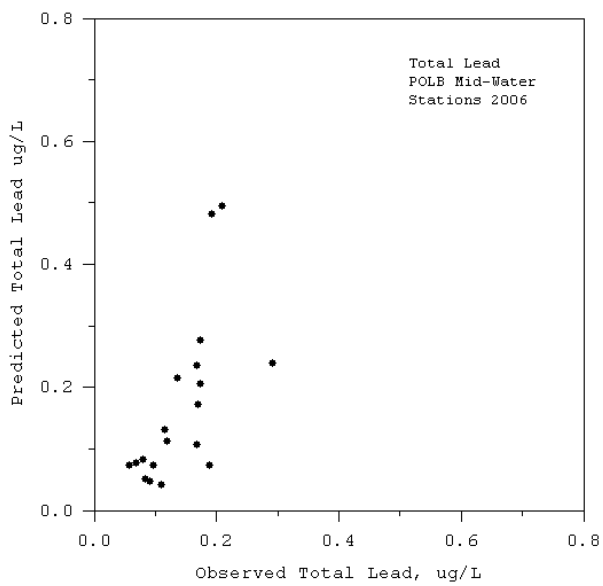

(c)

Figure 35. Comparison of model predicted and observed lead concentrations at the overlying water and mid-water column sites

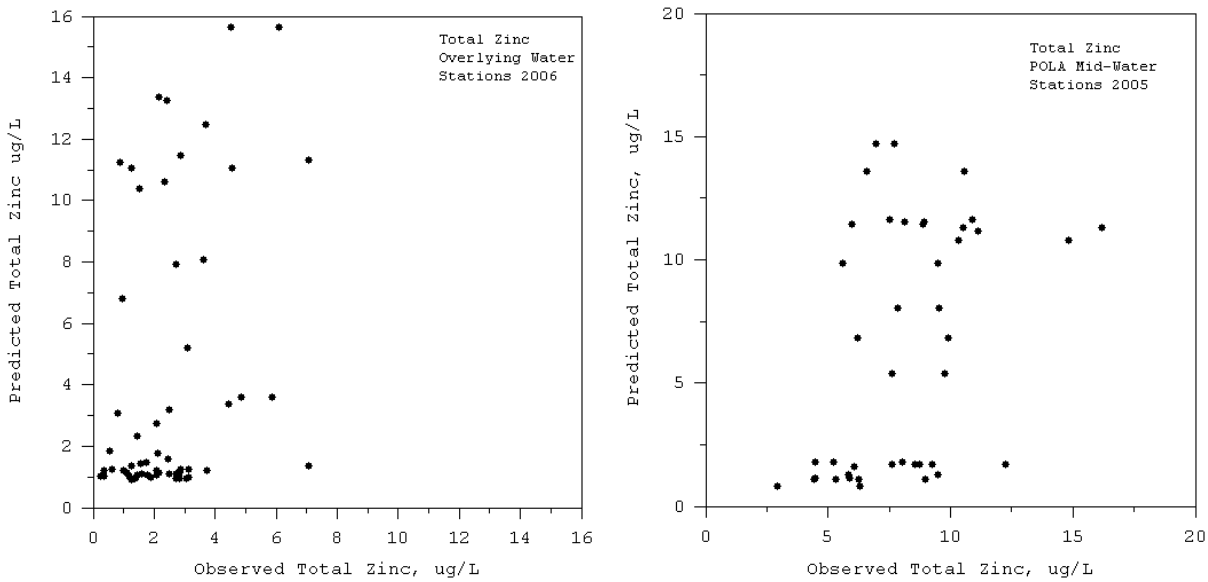

(a) (b)

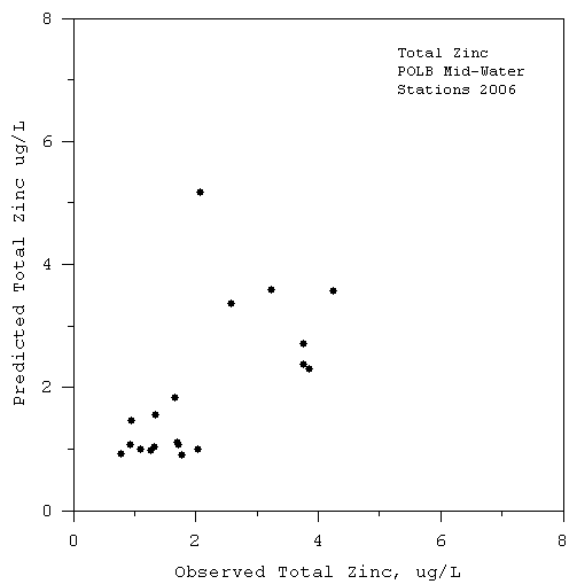

(c)

Figure 36. Comparison of model predicted and observed zinc concentration at the 2006 overlying water and mid-water column sites

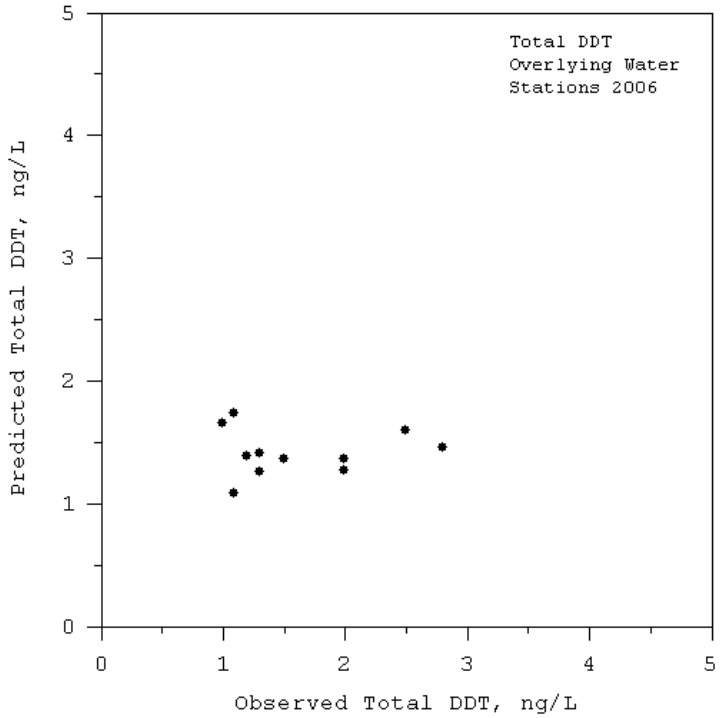

Figure 37. Comparison of model predicted and observed DDT concentration at the 2006 overlying water column sites

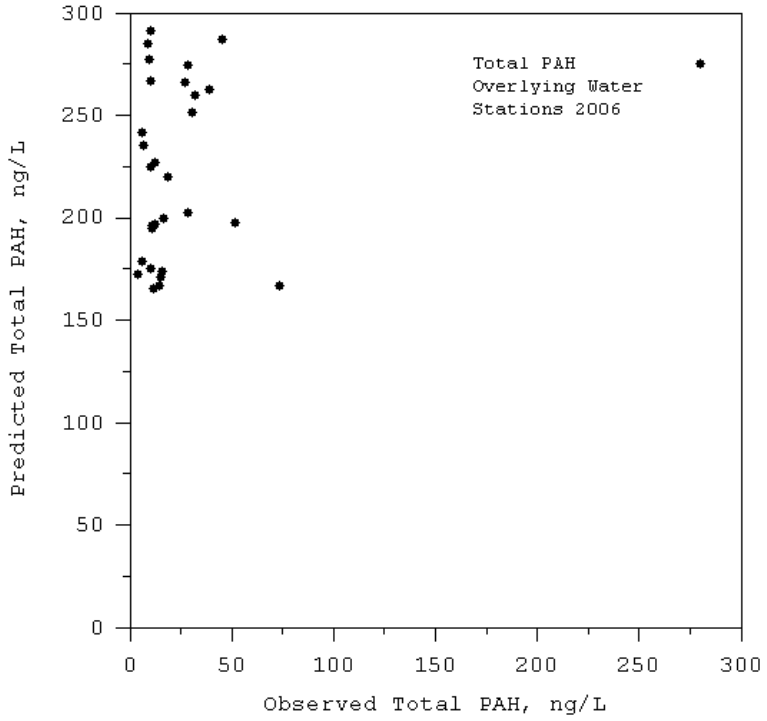

Figure 38. Comparison of model predicted and observed PAH concentration at the 2006 overlying water sites

9. Summary and Recommendations

This report summarizes the calibration of a fully coupled EFDC based hydrodynamic, sediment transport, and contaminant transport and fate model for the greater Los Angeles/Long Beach Harbors and adjacent region of San Pedro Bay. Observational data to support model configuration and calibration were reviewed and judged adequate to very adequate for model configuration. Tide gauge and current meter data were very adequate for hydrodynamic calibration and the level of calibration is consistent with other hydrodynamic modeling studies of similar scope. Due to the event-driven character of fresh water inflow into the greater harbors, salinity data sets lacked significant variability to fully evaluate salinity transport calibration as compared to studies in other estuaries and coastal harbors having continuous freshwater inflow.

Sediment and contaminant data were adequate for model configuration, which focused on establishing sediment bed initial conditions. Water column data for suspended sediment concentration are very limited and tend to constrain the level of calibration which can be achieved, although field observations during fall 2006 significantly enhanced the base of data. Water column data for metals concentration are more extensive, but metal calibration is still limited by the water column sediment transport calibration. Water column data for DDT and PAH are also limited and data for PCB indicate that levels are below detection limits. Dry weather sensitivity analyses were conducted to determine the influence of open boundary concentrations, watershed loads, and sediment bed erosion rates on water column, sediment, and contaminant concentration levels (Appendix C). Long-term sensitivity was also evaluated by comparing water column and sediment bed concentrations associated with baseline conditions and a 50 percent reduction in river and watershed loading (Appendix D). In contrast to hydrodynamic and eutrophication modeling studies in estuarine and coastal regions, extensive literature is not available for establishing what constitutes an acceptable level of calibration for sediment and contaminant transport modeling. However the calibration results presented herein demonstrate that use of available data combined with best estimates of required model parameters do yield model predictions well within the range of observations.

The EFDC based hydrodynamic, sediment transport, and contaminant transport and fate model for the greater Los Angeles/Long Beach Harbors and adjacent region of San Pedro Bay is judged suitable for use in TMDL development. The model provides a rigorous framework for contaminant response surface development with respect to the major sources including land-based loadings, net flux of legacy contaminants for the sediment bed, and open boundary driven loads. The attention given to the development of initial conditions for the sediment bed makes the modeling framework particularly useful in determining difficult to control source contributions from the sediment bed. Likewise the ease in model reconfiguration to adjust incoming contaminant levels on a sub-watershed scale will allow focused allocations to be developed.

References

Bunch, B. W., D. H. Tillman, D. J. Mark. 2000. Port of Los Angeles Pier 300 Expansion Water Quality and Hydrodynamic Study, Report ERDC/CHL TR-00-X US Army Corps of Engineers, Environmental and Coastal Hydraulics Laboratory, Vicksburg, MS.

Bunch, B. W., D. H. Tillman, D. J. Mark, 2002: Water Quality and Hydrodynamic Analysis of the Cabrillo Shallow Water Habitat. Report ERDC/CHL LR US Army Engineer District Los Angeles, Engineer Research and Development Center, Vicksburg, MS.

Bunch, B. W., D. H. Tillman, D. J. Mark, 2003: Sensitivity Analysis of Winds and Bathymetry on the Port of Los Angeles Pier 300 Expansion and Dominguez Channel Studies. Final Report ERDC/CHL LR US Army Corps of Engineers, Environmental and Coastal Hydraulics Laboratory, Vicksburg, MS.

CERC, 1990: Los Angeles and Long Beach Harbors Model Enhancement Study; Three-Dimensional Numerical Model testing of Tidal circulation. Technical Report CERC-90-16, U.S. Army Engineer Water Experiment Station, Vicksburg, MS.

Chapra, S. C., 1997: *Surface Water-Quality Modeling*. McGraw-Hill, New York, 844 pp.

Chiou, C, T., 2002: *Partition and Adsorption of Organic Contaminants in Environmental Systems*: John Wiley & Sons, Hoboken, NJ, 257 p.

Devore, J. L., 1982. *Probability and Statistics for Engineering and the Sciences*. Brooks-Cole, Monterey, CA.

Everest International Consultants, 2006. Dominguez Channel Estuary Model Study, Model Data, Calibration and Verification Report. Prepared for the Port of Los Angeles by Everest International Consultants, Long Beach, CA, 141 pp.

Hall, R. W., 1990: Los Angeles and Long Beach Harbors Model Enhancement Study; Numerical water quality model study of harbor enhancements. Technical Report EL-90-6, U.S. Army Engineer Water Experiment Station, Vicksburg, MS.

Hall, R. W., 1995: Numerical water quality study for the Los Angeles Harbor Pier 400 Project Miscellaneous Paper EL-95-1, US Army Engineer Waterways Experiment Station, Vicksburg, MS.

Hamrick, J. M., 1992: A three-dimensional environmental fluid dynamics computer code: Theoretical and computational aspects. The College of William and Mary, Virginia Institute of Marine Science, Special Report 317, 63 pp.

Hamrick, J. M., and T. S. Wu, 1997: Computational design and optimization of the EFDC/HEM3D surface water hydrodynamic and eutrophication models. *Next Generation Environmental Models and Computational Methods.* G. Delich and M. F. Wheeler, Eds., Society of Industrial and Applied Mathematics, Philadelphia, 143-156.

Jepson, R., J. Roberts, and W. Lick, 1997: Long Beach Harbor Sediment Study. A report to U. S. Army Corps of Engineers, Los Angeles District, DACW09-97-M-0068, Department of Mechanical and Environmental Engineering, University of California, Santa Barbara.

Ji, Z.-G., J. H. Hamrick, and J. Pagenkopf, 2002: Sediment and metals modeling in shallow river, *Journal of Environmental Engineering*, 128, 105-119.

King County, 1999: Water quality assessment of Elliot Bay and the Duwamish River. King County Department of Natural Resources, Seattle, WA. http://dnr.metrokc.gov/wlr/waterres/wqa/wqrep.htm

Miller, M. C., Z. Demirbilek, D. Mark and R. Hall, 1998:. Hydrodynamic and Water Quality Studies for Pier 400 Causeway Gap, Appendix 1, Letter Report submitted to the Port of Long Beach, US Army Engineer Waterways Experiment Station, Vicksburg, MS.

Park, K., A. Y. Kuo, J. Shen, and J. M. Hamrick, 1995: A three-dimensional hydrodynamic-eutrophication model (HEM3D): description of water quality and sediment processes submodels. The College of William and Mary, Virginia Institute of Marine Science. Special Report 327, 113 pp.

Preisendorfer, R. W., 1988: Principal Component Analysis in Meteorology and Oceanography. Developments in Atmospheric Science Volume 17. Elsevier, Amsterdam, pp. 429.

Science Applications International Corp., 2004: Analysis of Moored Oceanographic Data Acquired on the Palos Verdes Shelf by the LACSD During the Period from November 2000 to August 2003. Prepared for U. S. Army Corps of Engineers and U. S. Environmental Protection Agency, Region 9.

Science Applications International Corp., 2005: Data Report for the Summer 2004 Geotechnical Measurement Program Conducted on the Palos Verdes Shelf. prepared for U. S. Army Corps of Engineers and U. S. Environmental Protection Agency, Region 9.

Seabergh, W. C. and D. G. Outlaw, 1984: Los Angeles and Long Beach Harbors Model Study; Numerical analysis of tidal circulation for the 2020 Master Plan. Miscellaneous Paper CERC-84-5, U.S. Army Engineer Water Experiment Station, Vicksburg, MS.

Seabergh, W. C., 1985: Los Angeles and Long Beach Harbors Model Study; deep-draft dry bulk export terminal, Alternative No. 6: Resonant response and tidal circulation studies. Miscellaneous Paper CERC-85-8, U.S. Army Engineer Water Experiment Station, Vicksburg, MS.

Tetra Tech, Inc. 2002: VOGG: A visual orthogonal grid generation tool for hydrodynamic and water quality modeling. A report to U. S. EPA, Region 4, August 2002, 62 pp.

Tetra Tech, Inc. 2006: Watershed Model Development for Simulation of Loadings to the Los Angeles/Long Beach Harbors. Prepared for US EPA Region 9 and Los Angeles Regional Water Quality Control Board. Fairfax, VA., 64 pp.

Tetra Tech, Inc. 2007: The Environmental Fluid Dynamic Code: theory and computation, Volume 2: Sediment and contaminant transport and Fate. Fairfax, VA., 96 pp.

Thomann, R. V., 1982. Verification of water quality models. *J. Environ. Engrg. Div., ASCE*. 108, 923-940.

Thomann, R. V., and J. A. Mueller, 1987: *Principles of Surface Water Quality Modeling and Control*. Harper and Row, New York, 644 pp.

U.S. Environmental Protection Agency, 1990: Technical Guidance Manual for Performing Waste Load Allocations, Book III Estuaries, Part 2, Application of Estuarine Waste Load Allocation Models. EPA 823-R-92-003.

U.S. Environmental Protection Agency, 2005: Partition Coefficients for Metals in Surface Water, Soil, and Waste. EPA 600-R-05-074.

U. S. Environmental Protection Agency, Region 1, 2006: Link to Housatonic River PCB Superfund web page.
http://www.epa.gov/region01/ge/thesite/restofriver-reports.html

U. S. Environmental Protection Agency, Region 10, 2006: Link to Portland Harbor Superfund web page.
http://yosemite.epa.gov/R10/CLEANUP.NSF/ph/fact+sheets/$FILE/1001PH.pdf

Wang, H. V., A. Cialone and P. River, 1995: Numerical Hydrodynamic Modeling in Support of Water Quality and Ship Simulation Models in Los Angeles Harbor. Miscellaneous Paper CERC-95-1, US Army Engineer Waterways Experiment Station, CE, Vicksburg, MS.

Wool, T. A., S. R. Davie, and H. N. Rodriguez, 2003: Development of three-dimensional hydrodynamic and water quality models to support TMDL decision process for the Neuse River estuary, North Carolina. *Journal of Water Resources Planning and Management*, 129, 295-306.

Zeng, E., and K. Tran, 2002: Distribution of Chlorinated Hydrocarbons in Overlying Water , Sediment, Polychaete, and Hornyhead Turbot in the Coastal Ocean, Southern California, USA. Environmental Toxicology and Chemistry, Vol. 21, No. 8, pp. 1600–1608, 2002.

Zeng, E., D. Tsukada, D. Diehl, J. Peng, K. Schiff, J. Noblet and K. Maruya: 2005: Distribution and Mass Inventory of Total DDT in the water column Of the Southern California Bight. Environ. Sci. Technol. 39, 3347-3353

Zou, R., Carter, S., Shoemaker, L., Parker, A., and Henry, T., 2006. An integrated hydrodynamic and water quality modeling system to support nutrient TMDL development for Wissahickon Creek. *Journal of Environmental Engineering*, 132, 555-566.

Appendix A: Salinity Time Series Calibration Plots

DRAFT

November 2008

Prepared for:
USEPA Region 9
Los Angeles Regional Water Quality Control Board

Prepared by:
Tetra Tech, Inc.

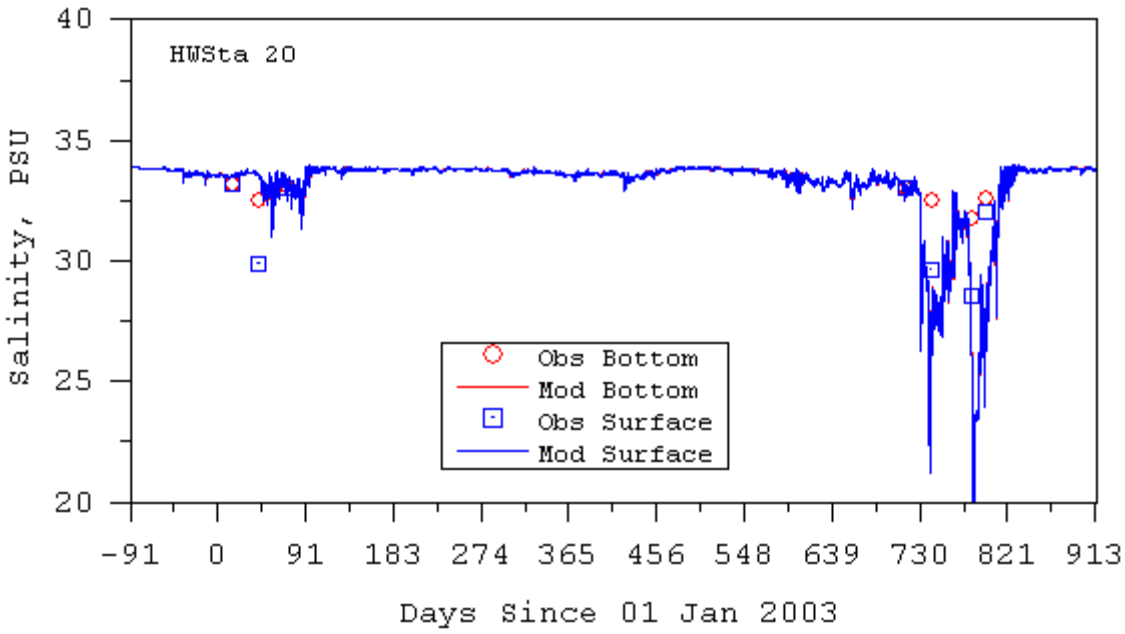

Figure A-1. Model Predicted and Observed Salinity at LAH Station 20

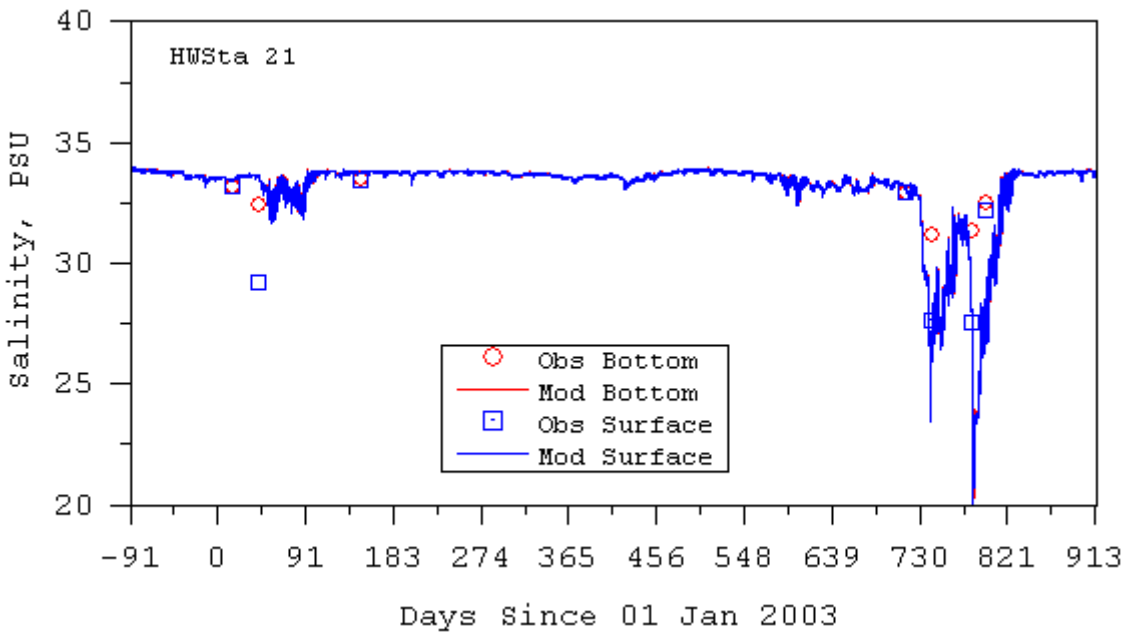

Figure A-2. Model Predicted and Observed Salinity at LAH Station 21

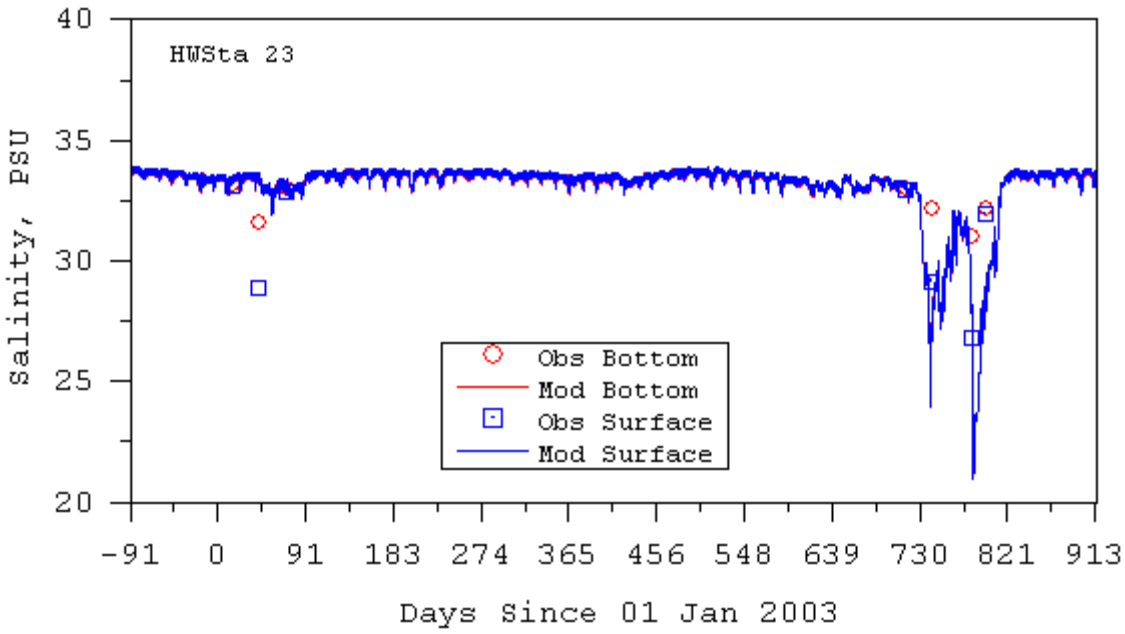

Figure A-3. Model Predicted and Observed Salinity at LAH Station 23

.

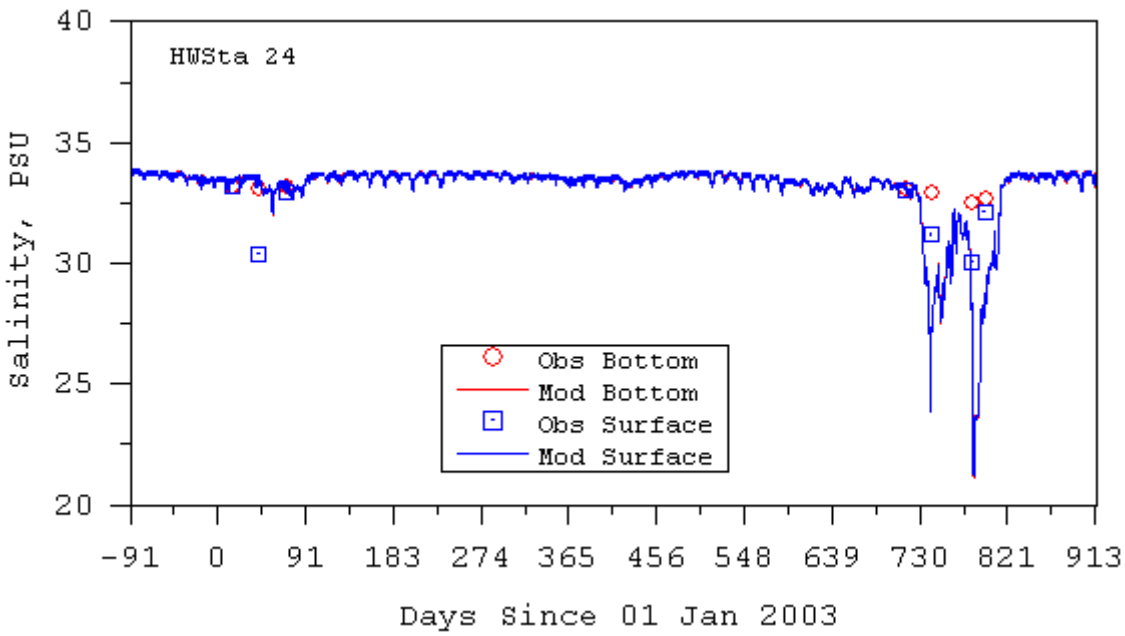

Figure A-4. Model Predicted and Observed Salinity at LAH Station 24

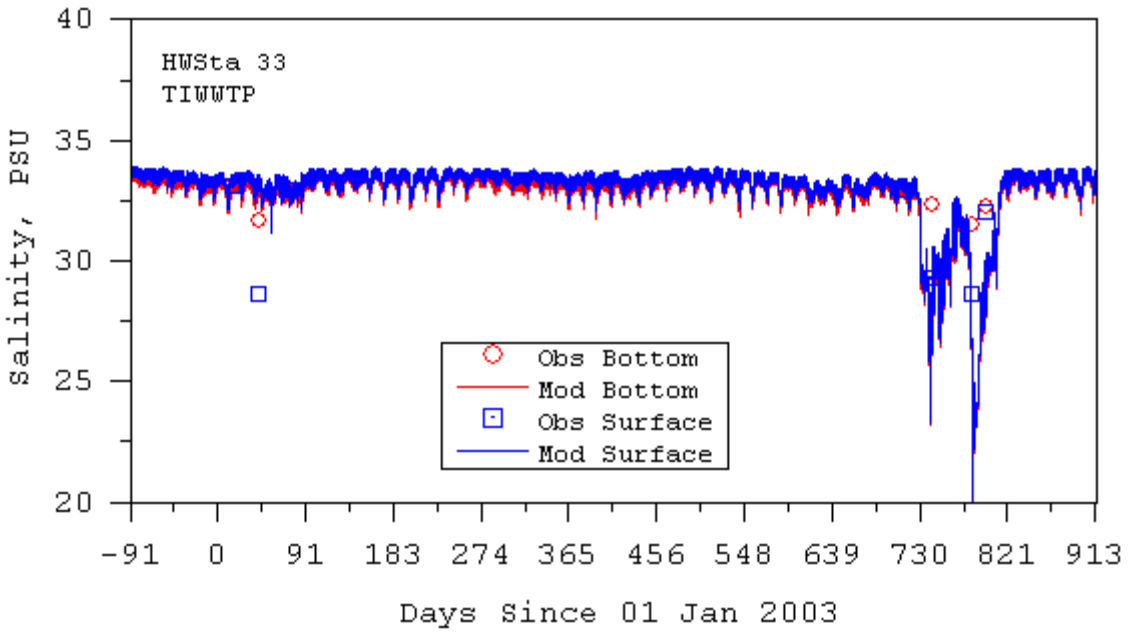

Figure A-5. Model Predicted and Observed Salinity at LAH Station 33

.

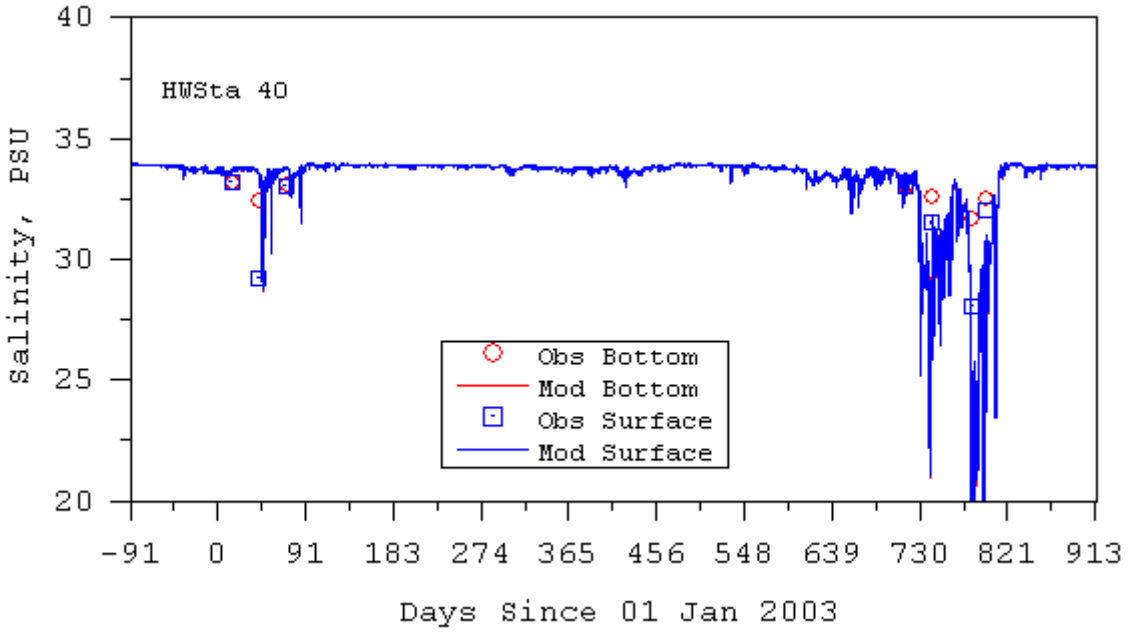

Figure A-6. Model Predicted and Observed Salinity at LAH Station 40

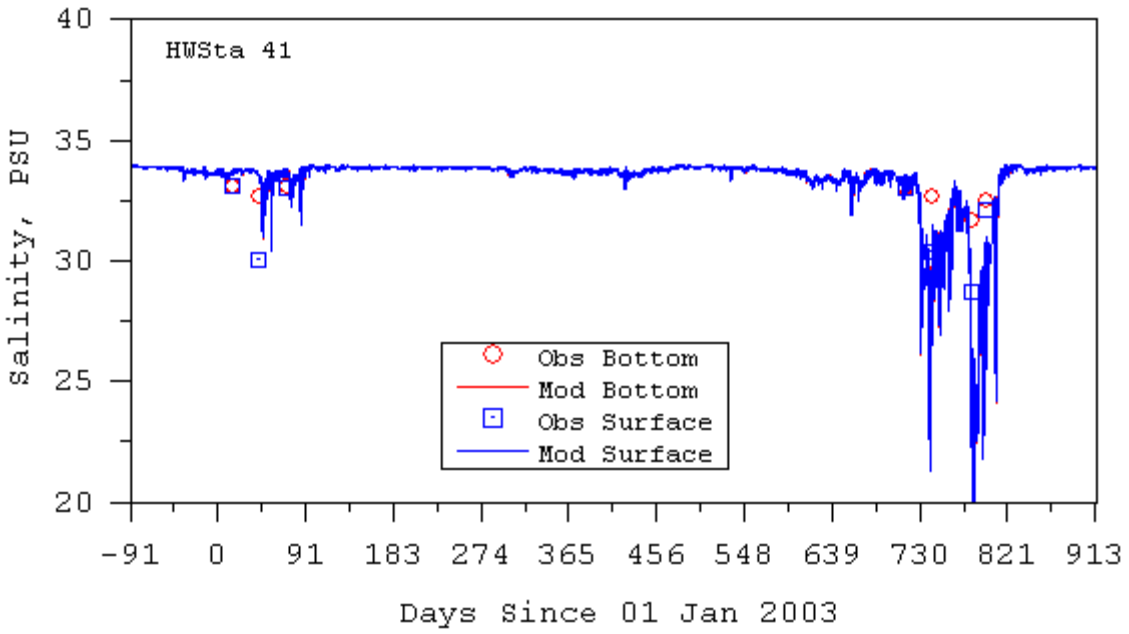

Figure A-7. Model Predicted and Observed Salinity at LAH Station 41

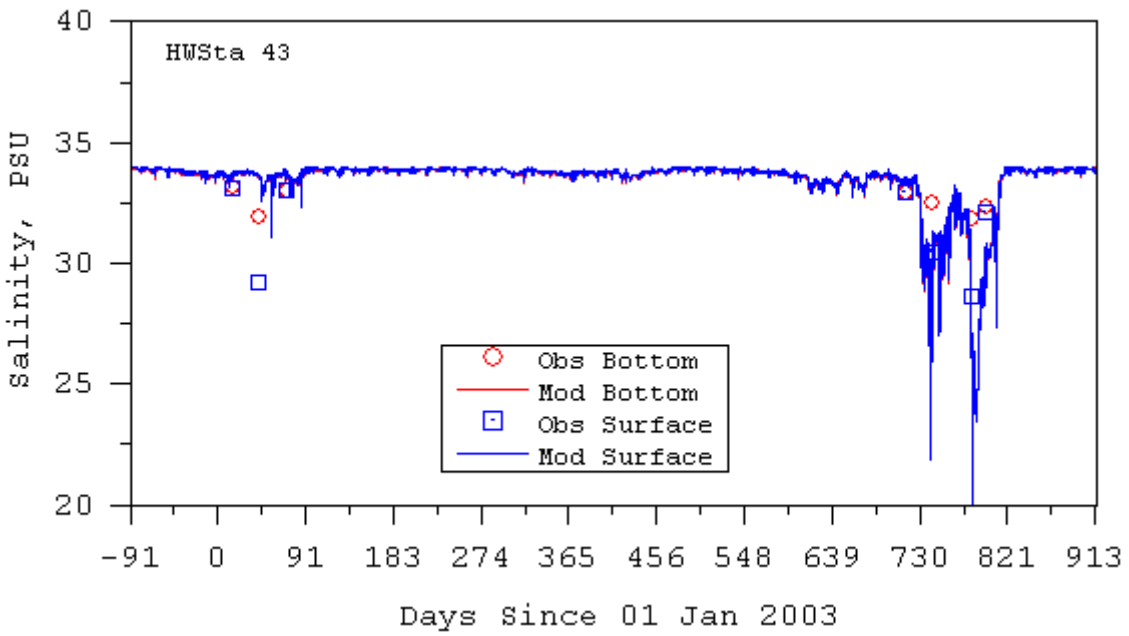

Figure A-8. Model Predicted and Observed Salinity at LAH Station 43

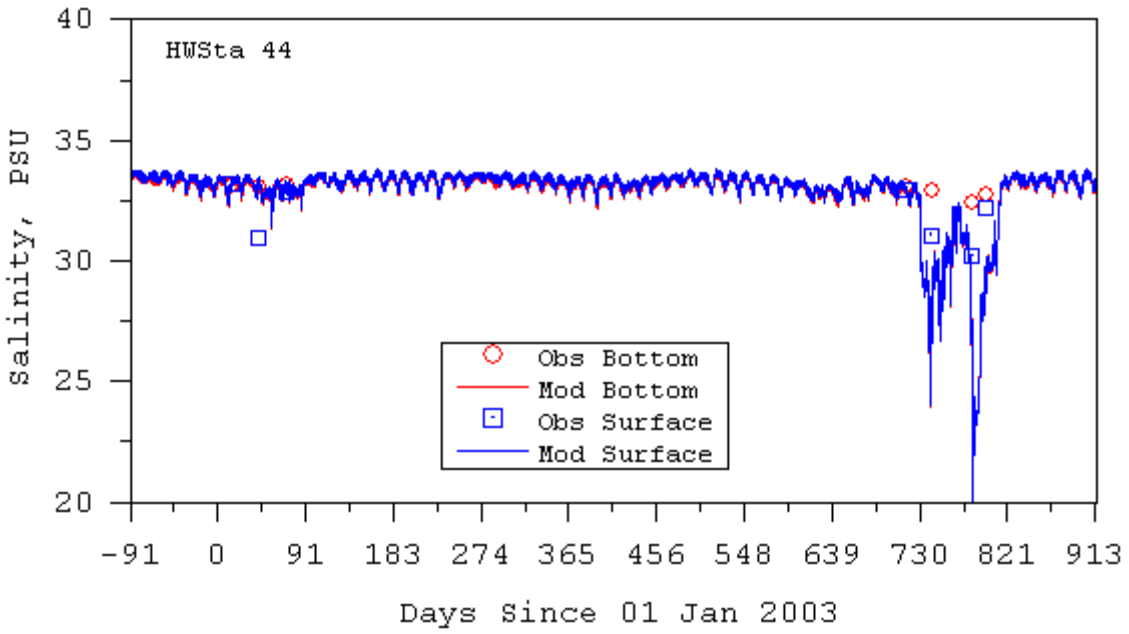

Figure A-9. Model Predicted and Observed Salinity at LAH Station 44

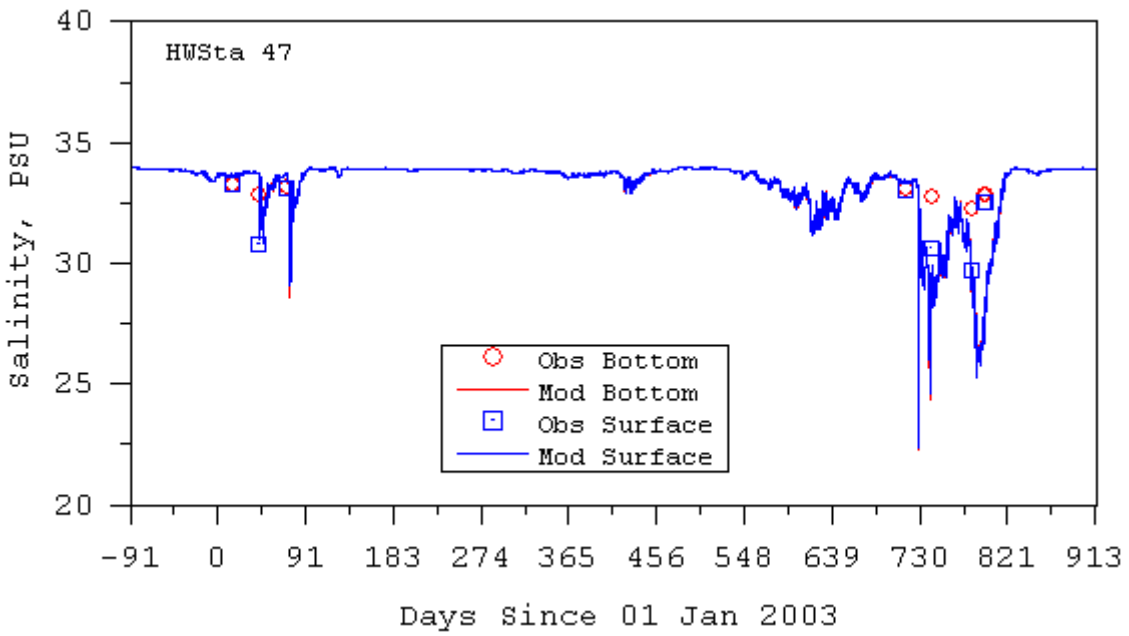

Figure A-10. Model Predicted and Observed Salinity at LAH Station 47

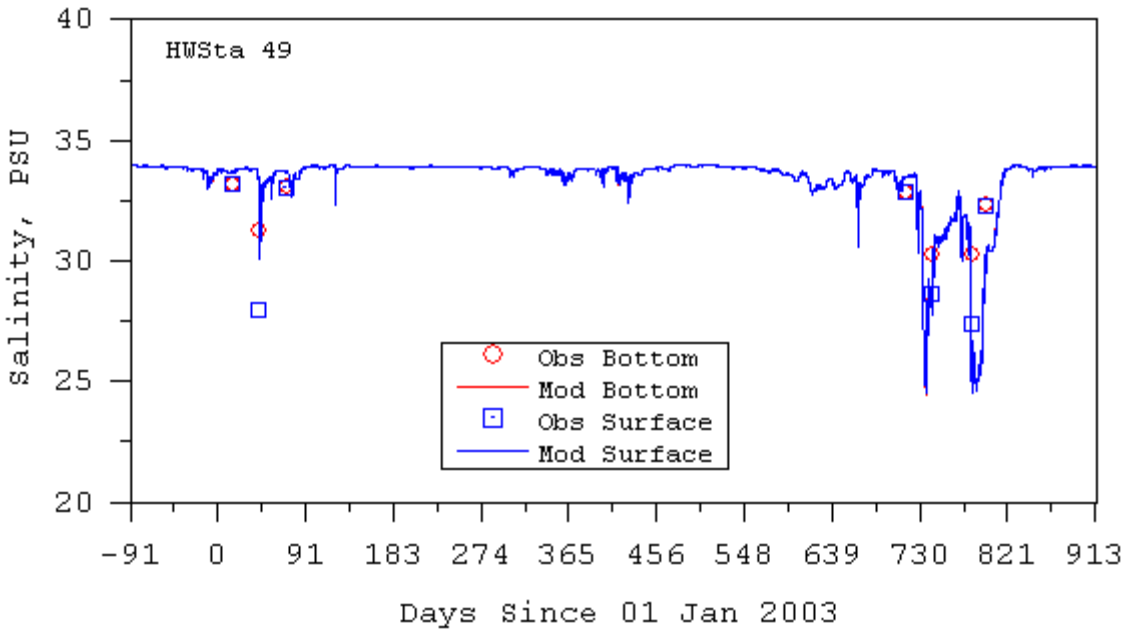

Figure A-11. Model Predicted and Observed Salinity at LAH Station 49

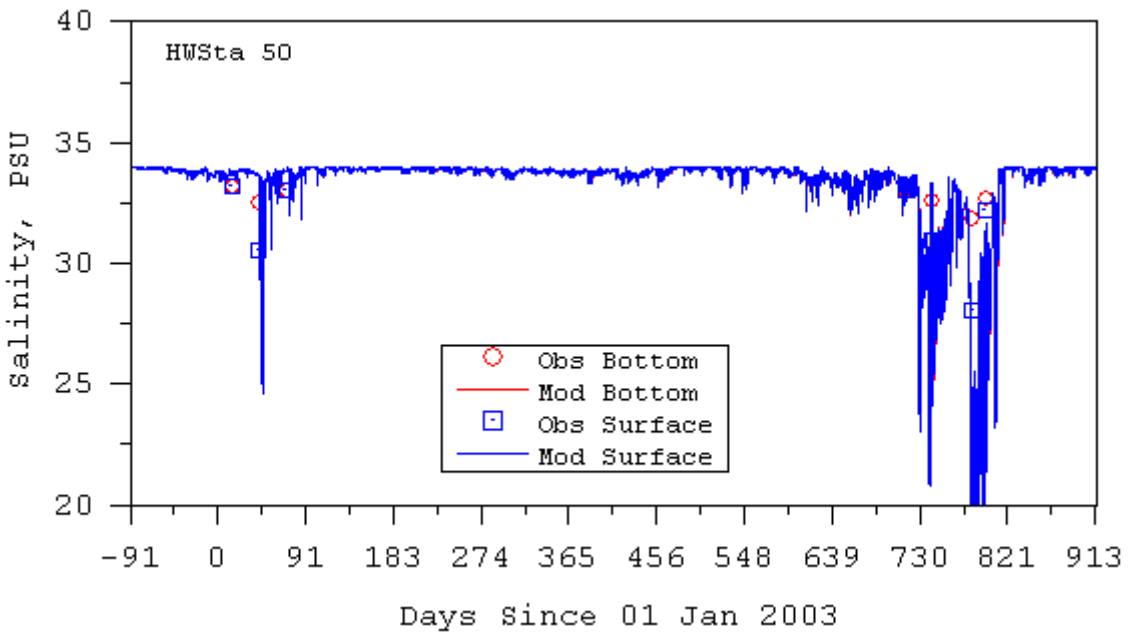

Figure A-12. Model Predicted and Observed Salinity at LAH Station 50

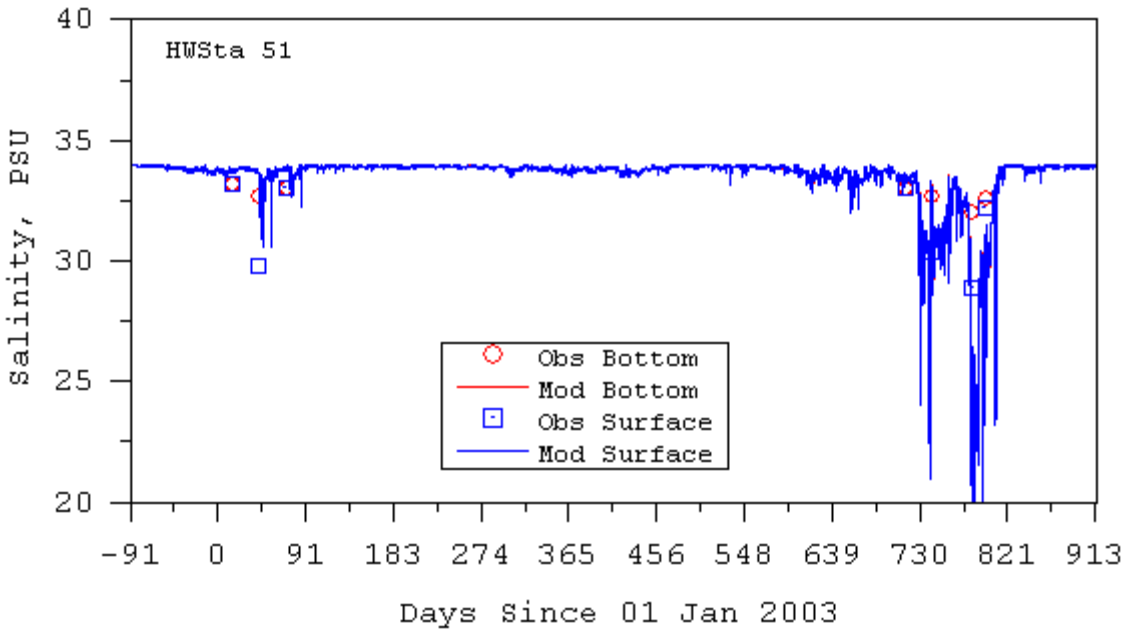

Figure A-13. Model Predicted and Observed Salinity at LAH Station 51

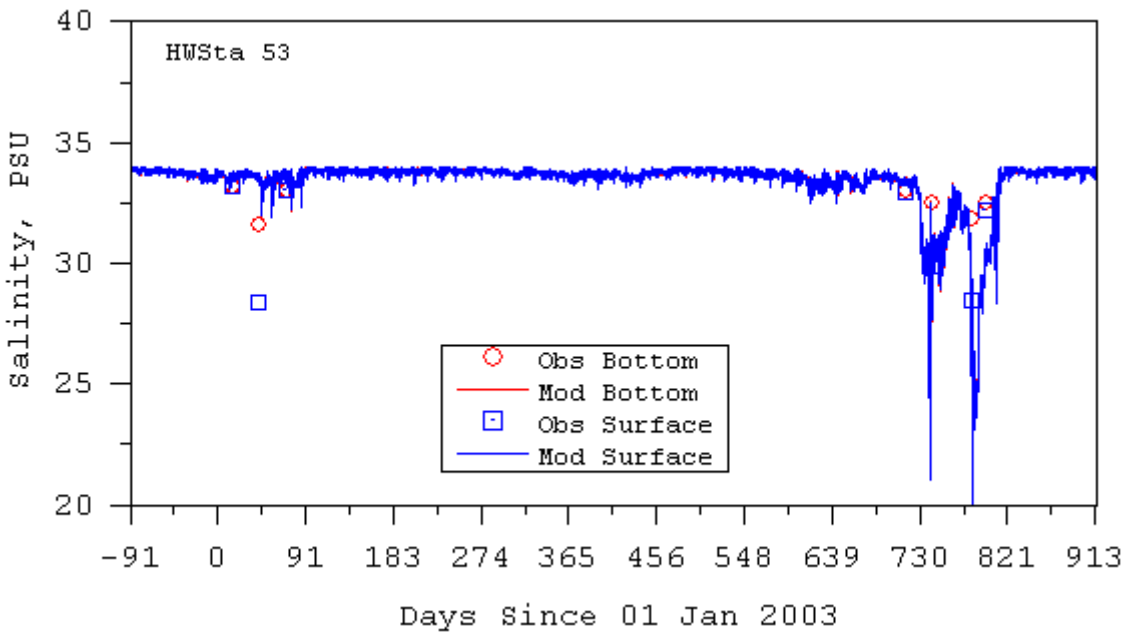

Figure A-14. Model Predicted and Observed Salinity at LAH Station 53

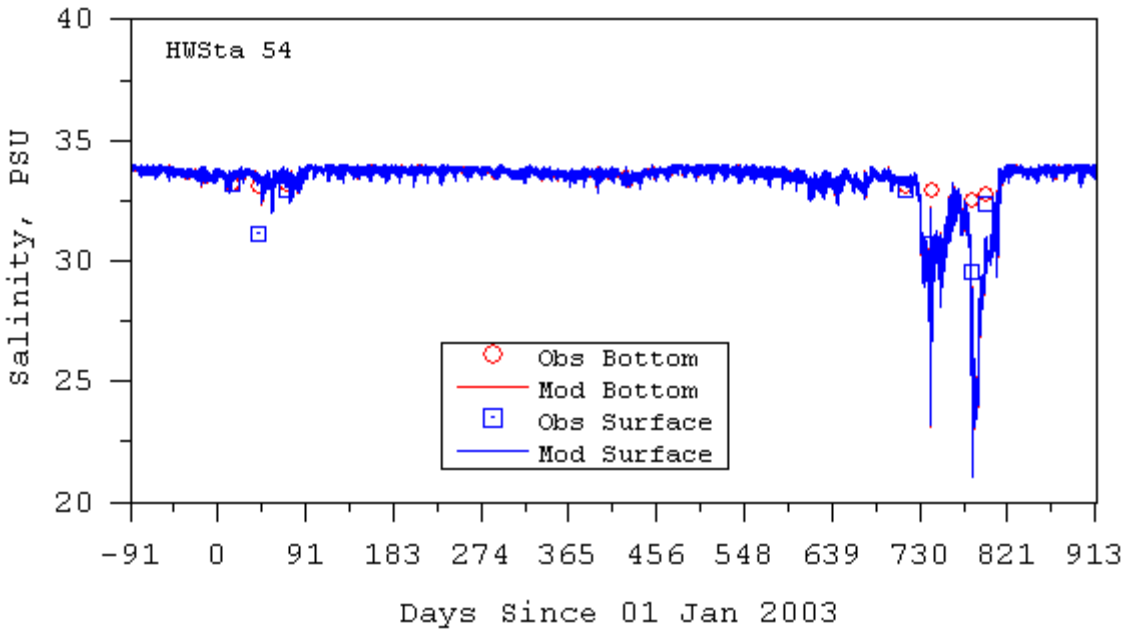

Figure A-15. Model Predicted and Observed Salinity at LAH Station 54

.

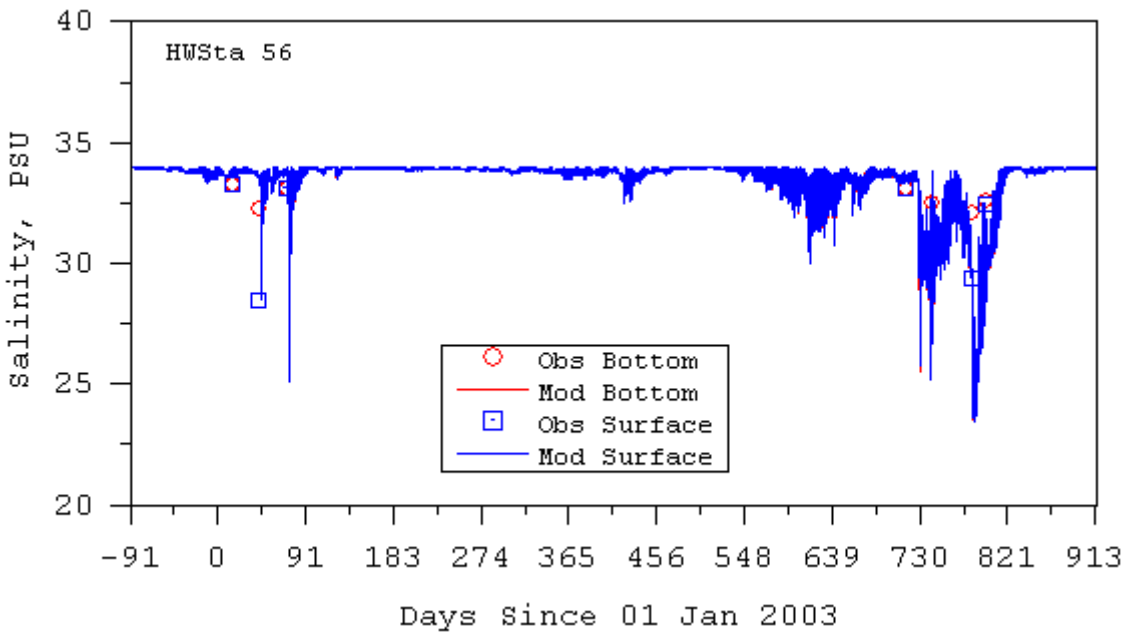

Figure A-16. Model Predicted and Observed Salinity at LAH Station 56

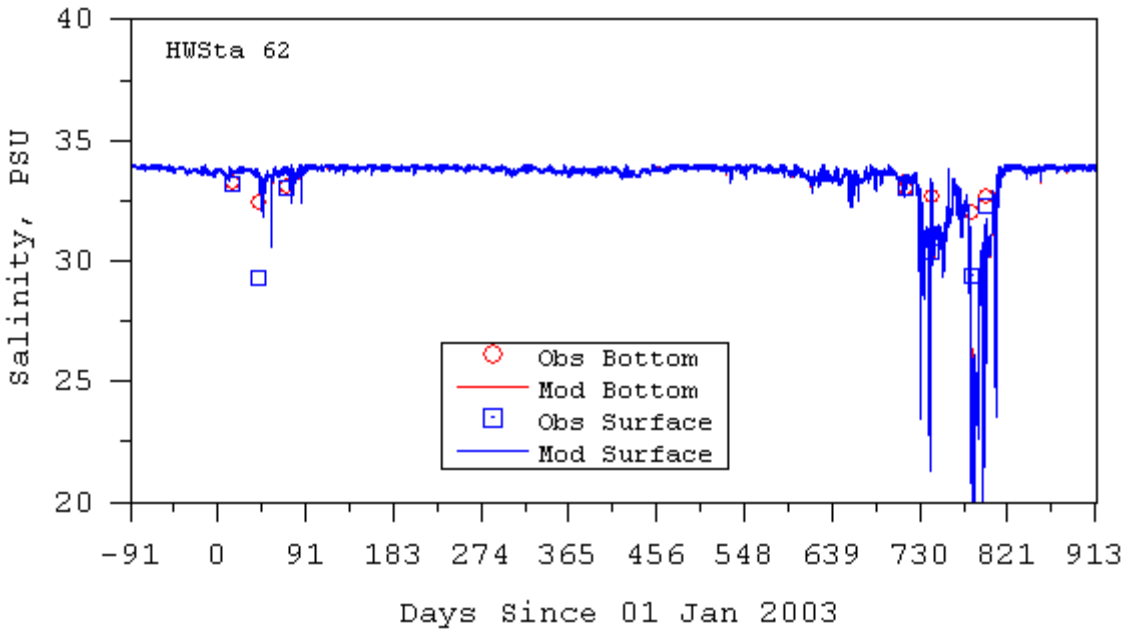

Figure A-17. Model Predicted and Observed Salinity at LAH Station 62

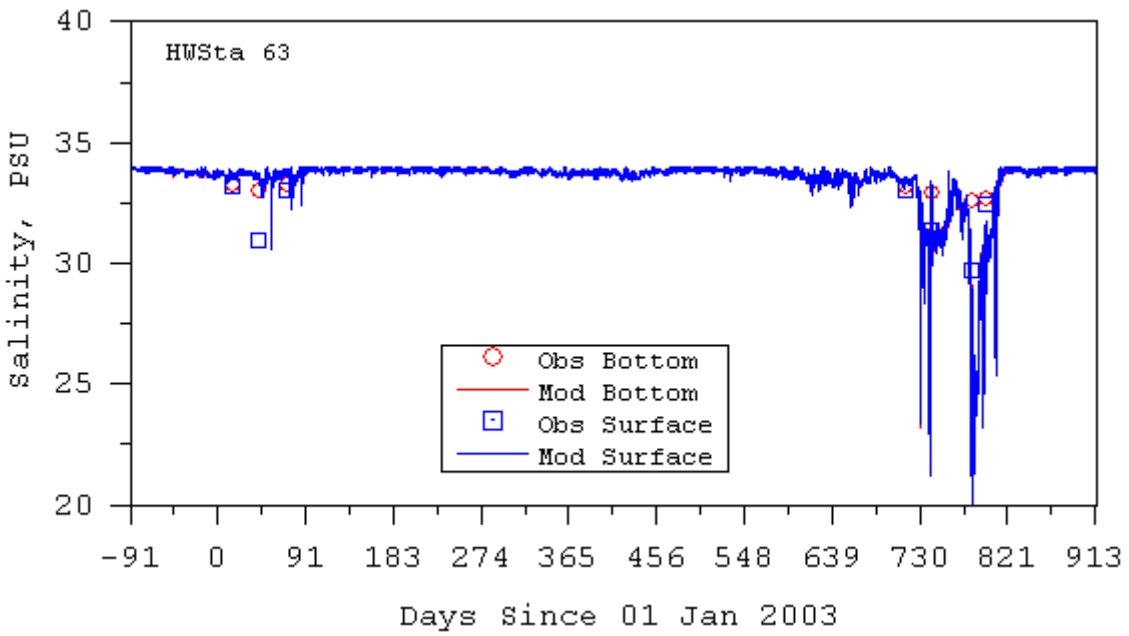

Figure A-18. Model Predicted and Observed Salinity at LAH Station 63

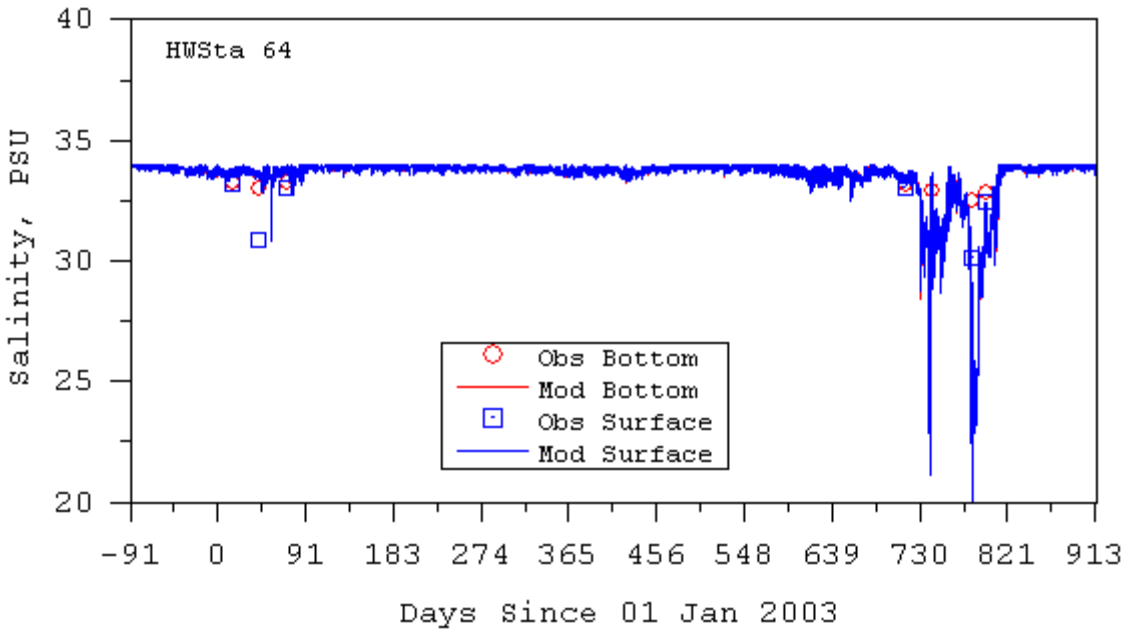

Figure A-19. Model Predicted and Observed Salinity at LAH Station 64

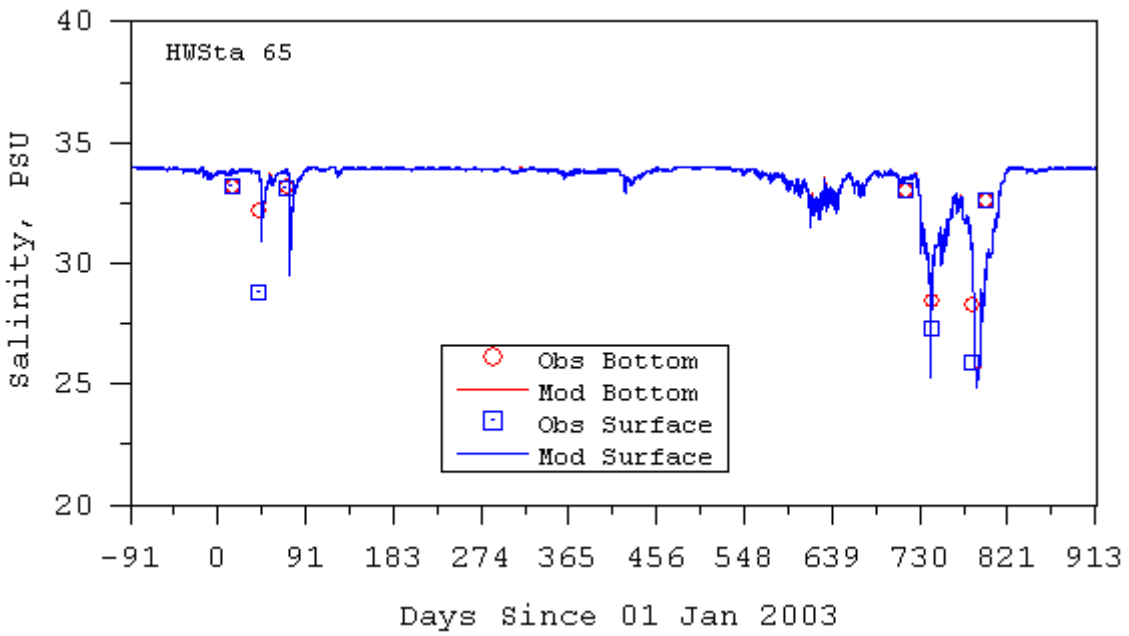

Figure A-20. Model Predicted and Observed Salinity at LAH Station 65

Appendix B: Model Performance Measures

DRAFT

November 2008

Prepared for:
USEPA Region 9
Los Angeles Regional Water Quality Control Board

Prepared by:
Tetra Tech, Inc.

To quantify the EFDC model's prediction of water surface elevation, velocity, and concentration of suspended and dissolved water scalar state variables, a number of statistical tests and time series analyses are used. This section summarizes general test and analysis procedures.

The statistical test that can be used for evaluating model predictions includes the mean error, mean absolute error, root mean square error, maximum absolute error, relative mean error and relative absolute mean error (Thomann, 1982). Letting *O* and *P* denote observed and predicted values of a quantity at *N* observation times, the mean error is defined by

$$ME = \frac{1}{N}\sum_{n=1}^{N}\left(O_n - P_n\right) \tag{B.1}$$

Positive values of the mean error indicate that the model tends to under predict the observations whereas negative values indicate that the model tends to over predict observations. The mean absolute error is defined by

$$MAE = \frac{1}{N}\sum_{n=1}^{N}\left|O_n - P_n\right| \tag{B.2}$$

Although the mean absolute error provides no indication of over prediction or under prediction, it eliminates the canceling effects of positive and negative errors and can be viewed as a more extreme measure of observation-prediction agreement. The root mean square error is defined by

$$RMSE = \sqrt{\frac{1}{N}\sum_{n=1}^{N}\left(O_n - P_n\right)^2} \tag{B.3}$$

The root mean square error can be interpreted as a weighted equivalent to the mean absolute error with larger observation-prediction differences given larger weightings. The square root operation recovers the units of the data quantities. The rms error is generally viewed as the most rigorous absolute error test. The maximum absolute error is defined by

$$MAXE = \max\left|O_n - P_n\right| \quad : n = 1, N \tag{B.4}$$

and provides information on the largest discrepancy between corresponding values of observed and predicted quantities over an interval of *N* measurements.

Relative error measures can be used to eliminate data units and to provide a measure of error relative to the magnitude of the observational data. The relative mean error and the relative mean absolute error are defined by

$$RME = \frac{\frac{1}{N}\sum_{n=1}^{N}(O_n - P_n)}{\frac{1}{N}\sum_{n=1}^{N}O_n} \tag{B.5}$$

$$MAE = \frac{\frac{1}{N}\sum_{n=1}^{N}|O_n - P_n|}{\frac{1}{N}\sum_{n=1}^{N}O_n} \tag{B.6}$$

Caution should be employed in the use of these two relative error measures, particularly when observed and predicted quantities can have small values or values that have both positive and negative signs. An alternative relative error, hereafter referred to as the relative mean square error, is

$$RSE = \frac{\sum_{n=1}^{N}\left(O^{(n)} - P^{(n)}\right)^2}{\sum_{n=1}^{N}\left(\left(O^{(n)} - \overline{O}\right)^2 + \left(P^{(n)} - \overline{O}\right)^2\right)} \tag{B.7}$$

This error measure was proposed by Willmott (1982) and Willmont *et al.* (1982) and used by Blumberg and Goodrich (1990) to analyze the prediction skill of an estuarine model. The value of *RSE* always falls between zero and unity, with an increasing value corresponding to decreasing skill of the model.

Thomann (1982) suggested the use of linear regression for comparing model predictions with observations in the context of model calibration. Following Thomann, the linear equation relating observed and predicted values of the quantity is written as

$$O = \alpha + \beta P \tag{B.8}$$

where alpha and beta are determined by

$$\alpha = \frac{1}{N}\left(\sum_{n=1}^{N}O^{(n)} - \beta\sum_{n=1}^{N}P^{(n)}\right) \tag{B.9}$$

$$\beta = \frac{\sum_{n=1}^{N}\left(O^{(n)} - O^{(avg)}\right)\left(P^{(n)} - P^{(avg)}\right)}{\sum_{n=1}^{N}\left(P^{(n)} - P^{(avg)}\right)^2} \tag{B.10}$$

(Devore, 1982). The null hypothesis for the linear regression is alpha, the intercept, equal to zero, and beta, the slope, equal to one. Also useful in the regression analysis is the correlation coefficient

$$r = \frac{N\sum_{n=1}^{N} P^{(n)}O^{(n)} - \left(\sum_{n=1}^{N} P^{(n)}\right)\left(\sum_{n=1}^{N} O^{(n)}\right)}{\sqrt{N\sum_{n=1}^{N} P^{(n)}P^{(n)} - \left(\sum_{n=1}^{N} P^{(n)}\right)^2}\sqrt{N\sum_{n=1}^{N} O^{(n)}O^{(n)} - \left(\sum_{n=1}^{N} O^{(n)}\right)^2}} \tag{B.11}$$

For a good a fit or correlation between observations and predictions, the correlation coefficient should be near one. The square of the correlation coefficient equals the fractional proportion of variation of observations explained by the regression relationship between the observations and predictions (Devore, 1982).

Time series having deterministic periodic structure can be analyzed using least squares harmonic analysis. Consider a time series of the form

$$\phi(t) = a_0 + b_0 t + \sum_{m=1}^{M} a_n \cos\left(\frac{2\pi t}{T_m}\right) + \sum_{m=1}^{M} b_n \sin\left(\frac{2\pi t}{T_m}\right) \tag{B.12}$$

composed of a constant, a_0, a linear in time term $b_0 t$, and M periodic or harmonic components having periods T_m. Note that equation B.12 can also be written in the form

$$\phi(t) = a_0 + b_0 t + \sum_{m=1}^{M} A_m \cos\left(\frac{2\pi}{T_m}(t - \tau_m)\right) \tag{B.13}$$

$$A_m^2 = a_m^2 + b_m^2$$

$$\tau_m = \frac{T_m}{2\pi}\arctan\left(\frac{b_m}{a_m}\right)$$

where A_m and τ_m are the amplitude and phase of the mth periodic or harmonic component of the time series. The a and b coefficients representing the time series can be determined form discrete values of ϕ at N times by minimization of the least squares functional

$$E = \sum_{n=1}^{N}\left(\phi(t_n) - a_0 - b_0 t - \sum_{m=1}^{M} a_m \cos\left(\frac{2\pi t_n}{T_m}\right) - \sum_{m=1}^{M} b_m \sin\left(\frac{2\pi t_n}{T_m}\right)\right)^2 \tag{B.14}$$

with respect to the a and b coefficients. The minimization results in a system of $2N+1$ equations for the a and b coefficients. For comparison of model

predictions with observations, harmonic coefficients are determined for both model-predicted and observed time series, and the amplitudes and phases appropriately compared for each harmonic component.

For two-dimensional vector time series, the vector components, *u* and *v*, are separately analyzed to determine the coefficients in the expansions

$$u(t) = u_0 + \sum_{m=1}^{M} uc_n \cos\left(\frac{2\pi t}{T_m}\right) + \sum_{m=1}^{M} us_n \sin\left(\frac{2\pi t}{T_m}\right) \tag{B.15a}$$

$$v(t) = v_0 + \sum_{m=1}^{M} vc_n \cos\left(\frac{2\pi t}{T_m}\right) + \sum_{m=1}^{M} vs_n \sin\left(\frac{2\pi t}{T_m}\right) \tag{B.15b}$$

The combined results can be cast in tidal velocity ellipse form with the major and minor axis amplitudes, the ellipse orientation, and the phase at which the velocity vector aligns with the major axis replacing the *uc*, *us*, *vc*, and *vs* coefficients for each constituent. The half-lengths, *ma* and *mi*, of the major and minor axes are given by

$$\begin{aligned} ma &= rp + rm \\ mi &= |rp - rm| \\ rp &= \sqrt{(uc + vs)^2 + (vc - us)^2} \\ rm &= \sqrt{(uc - vs)^2 + (vc + us)^2} \end{aligned} \tag{B.16}$$

for each constituent. The major axis orientation angle *ang*, in degrees counterclockwise from east, and the time phase *phe*, at which the velocity vector aligns with the major axis, are given by

$$\begin{aligned} ang &= \frac{90}{\pi}(ap + am) \\ phe &= \frac{T}{4\pi}(am - ap) \\ ap &= \tan^{-1}\left(\frac{vc - us}{uc + vs}\right) \\ am &= \tan^{-1}\left(\frac{vc + us}{uc - vs}\right) \end{aligned} \tag{B.17}$$

for each constituent.

An alternative method for comparing time series of observed and model predicted quantities is the use of spectral analysis techniques. Spectral analysis is particularly useful for comparing the frequency domain structure of observed and predicted responses to random external model forcings such as wind.

Spectral analysis can also be used for the analysis of time series composed of the sums of discrete harmonics and a random component. For a quantity s_k, observed or predicted at N discrete times $k\Delta t$ ($k = 0, N-1$) relative to a local time original, the discrete Fourier transform S_n is given by

$$S_n = \sum_{k=0}^{N-1} s_k \exp\left(\frac{2\pi ikn}{N}\right) \tag{B.18}$$

where i is the unit imaginary number. Note that the standard Fourier transform convention of defining N data points from indices 0 to $N-1$ is employed here (Press et al., 1992). The discrete transform is defined at discrete frequencies:

$$f_n = \frac{n}{N\Delta t} \quad ; \quad n = -\frac{N}{2}, \ldots 0 \ldots, \frac{N}{2} \tag{B.19}$$

with S_0 corresponding to the discrete 0 frequency, S_n ($n = 1, N/2-1$) corresponding to the first $N/2-1$ positive frequencies, and S_n ($n = N/2+1, N-1$) corresponding to the first $N/2-1$ negative frequencies in reverse order. At n equals $N/2$, S_n defines the value at both the positive and negative Nyquist critical frequencies,

$$f_c = f_{N/2} = \frac{1}{2\Delta t} \tag{B.20}$$

The inverse discrete transform is given by:

$$s_k = \frac{1}{N} \sum_{n=0}^{N-1} S_n \exp\left(\frac{2\pi ikn}{N}\right) \tag{B.21}$$

The power spectral density function, P_{ss}, of the quantity is defined, following Press et al. (1992), as

$$\begin{aligned} P_{ss}(0) &= P_{ss}(f_0) = \frac{1}{N^2}|S_0|^2 \\ P_{ss}(f_k) &= \frac{1}{N^2}\left(|S_k|^2 + |S_{N-k}|^2\right) \quad , \quad k = 1, \frac{N}{2} - 1 \\ P_{ss}(f_k) &= P_{ss}(f_{N/2}) = \frac{1}{N^2}|S_{N/2}|^2 \end{aligned} \tag{B.22}$$

for positive frequencies only and has the normalization property that its sum is equal to the mean square value of s.

$$\sum_{k=0}^{N/2} P_{ss}(f_k) = \frac{1}{N} \sum_{j=0}^{N-1} |s_j|^2 \tag{B.23}$$

When *s* is the water surface elevation, the summed spectral density function is readily identified as twice the mean potential energy divided by the acceleration for gravity:

$$\frac{2PE}{g} = \sum_{k=0}^{N/2} P_{\zeta\zeta}(f_k) \tag{B.24}$$

When *s* corresponds to velocity, the summed spectral density function is twice the component kinetic energy with the total kinetic energy defined by

$$2KE = \sum_{k=0}^{N/2} \left(P_{uu}(f_k) + P_{vv}(f_k)\right) \tag{B.25}$$

A useful measure of model performance is provided by the difference of observed and predicted power spectral density function of a particular quantity:

$$P_{dd}(f_k) = P_{oo}(f_k) - P_{pp}(f_k) \tag{B.26}$$

with *d*, *o*, and *p* denoting the difference, observed, and predict, quantities respectively.

Principal current direction

$$\theta_{PCD} = \frac{1}{2}\arctan\left(\frac{2\sum_{n=1}^{N}(u_n - \bar{u})(v_n - \bar{v})}{\sum_{n=1}^{N}(u_n - \bar{u})^2 - \sum_{n=1}^{N}(v_n - \bar{v})^2}\right) + m\frac{\pi}{2} \tag{B.27}$$

Where m is chosen to be 0 or 1, whichever maximizes

$$\begin{aligned} s^2 &= \cos^2\theta_{PCD}\sum_{n=1}^{N}(u_n - \bar{u})^2 + \sin^2\theta_{PCD}\sum_{n=1}^{N}(v_n - \bar{v})^2 \\ &+ \cos\theta_{PCD}\sin\theta_{PCD}\sum_{n=1}^{N}(u_n - \bar{u})(v_n - \bar{v}) \end{aligned} \tag{B.28}$$

Appendix C: Sediment and Contaminant Transport Model Dry Season Sensitivity Analysis

DRAFT

November 2008

Prepared for:
USEPA Region 9
Los Angeles Regional Water Quality Control Board

Prepared by:
Tetra Tech, Inc.

Introduction

A preliminary, dry season sensitivity analysis for the sediment and contaminant transport model predictions was conducted with respect to three types of model forcing functions and process parameterizations representing sediment and contaminant sources and sinks. The three types of conditions included: open boundary concentration levels, river and watershed loads, and sediment erosion rates. These three sensitivity options represent the range of controllability. For example, it is not practicable or feasible to control the open boundary concentration levels, representing ambient or background concentrations in San Pedro Bay. In this respect, demonstration of low sensitivity to open boundary concentration levels is desirable. In contrast, river and watershed loads are the primary controllable sediment and contaminant sources. A moderate to high sensitivity with respect to loads indicates that these sources are primarily responsible for observed levels of contamination. Another sensitivity analysis was performed to explore controlling sediment bed sources via sediment erosion rates. That is, lower erosion rates would reduce diffusive flux rates and overall net flux of sediment, metals, and organics from the bed to the water column. This could be achieved via controlling sediment bed sources by either covering contaminated sediment with clean sediment from land source controlled inflow or active capping or removal at hot spots.

The approach utilized in the sensitivity analysis involved simple system wide perturbations in the three types of forcing functions. Since a primary objective of TMDL development is reduction in contamination levels, the perturbations were based on 50 percent reductions or halving of the forcing functions. The model calibration simulation was repeated for each of the three sensitivity cases. Sensitivity was evaluated by comparison of dry season average model calibration predictions with sensitivity simulation predictions at the sixty 2006 sediment and overlying water sites (Figure 15). These sites were chosen for comparison since their locations represent a random sampling within the greater harbors area of interest.

Sensitivity to Open Boundary Conditions

The open boundary of the model domain can be either a source or sink with net transport of material into or out of the model domain. To investigate sensitivity with respect to open boundary concentrations, the calibration open boundary concentrations were reduced by a factor of one-half (0.5). Dry season average concentration predictions corresponding to the full and half calibration boundary values were compared at the sixty 2006 sediment and overlying water sites and are shown in Figures C-1 through C-7. A diagonal or unit slope plot, Figure C-1 for example, of black dots indicates low sensitivity in that model predictions are not affected by halving the boundary condition. A slope of less than unity, Figure C-6 for example, indicates sensitivity. The red dots indicate the difference

between the full boundary concentration and the half boundary concentration and are measured on the y-axis.

With respect to halving boundary conditions values, PAH was the only variable showing sensitivity as noted in Table C-1. With reference to Figure C-6, sites with low concentrations tend to be highly sensitive with concentrations approximately halved. Higher concentration sites are moderately sensitive.

Sensitivity to River and Watershed Loads

In the absence of significant point source loads, river and watershed loads are the primary controllable sediment and contaminant sources. A simple global loading sensitivity analysis was conducted by halving the inflowing concentration of sediment and contaminants, which corresponds to a 50 percent load reduction. Dry season average concentration predictions corresponding to the full and half calibration sediment and contaminant loads are compared at the sixty 2006 sediment and overlying water sites and are shown in Figures C-8 through C-14. The results indicate that sediment, copper, lead, DDT, and PAH predictions are relatively insensitive to halving loads. Zinc exhibits moderate or medium level sensitivity in Figure C-11. Figure C-14 shows model predicted PCB concentrations to exhibit a medium to high sensitivity with a halving of loads yielding a corresponding reduction in PCB concentrations.

Sensitivity to Sediment Erosion Rates

Existing contamination of bed sediment can be a significant source of water column contamination due to sediment erosion and diffusion of contaminants dissolved in pore water. To gain insight into the relative importance of the sediment bed as a source of water column contamination, the base sediment erosion rate was halved. Although halving the erosion rate does not represent a feasible harbor wide control approach, it does directly reveal the relative importance of the sediment bed as a source. Alternatively, halving of the erosion rate could be viewed as analogous to wide scale capping of coarse material making the sediment more resistant to hydrodynamic forces responsible for erosion, or mixing clean sediment from the inflows such that net erosion flux of contaminants is reduced. As might be expected, the water column sediment concentrations were significantly reduced as shown in Figure C-15. The concentrations of the three metals in the water column were also reduced, Figures C-16 through C-18. Copper and lead, which have higher partition coefficients than zinc, showed corresponding higher sensitivities to erosion, as expected, due to their strong affinity for the particulate phase. The three organic contaminants showed a range of sensitivities to sediment erosion (Figures C-19 through C-21).

Summary

With respect to contaminated sediment TMDL development for the greater harbors, the sensitivity analysis suggests that a reduction of watershed and river inflows of contaminated sediments, but not necessarily clean sediment, provides a feasible pollution control strategy in combination with localized capping or sediment removal. For the organics and, to a certain extent, zinc, reduction of land-derived loads was shown to result in lower levels of water column contamination. Gradual replacement of incoming contaminated sediment with clean sediment would yield lower contaminant exposure levels to living organisms in either water column or bed sediments, since the new deposited cleaner sediment would ultimately reduce contaminant flux from the sediment bed.

Table C-1. Summary of Sensitivity Analysis

Contaminant	Sensitivity to Halving Open Boundary Conditions	Sensitivity to Halving River and Watershed Loads	Sensitivity to Halving Sediment Erosion Rate
Sediment	Low	Low	High
Copper	Low	Low	High
Lead	Low	Low	High
Zinc	Low	Medium	Medium
DDT	Low	Low	Medium
PAH	Low to Medium	Low	Medium to High
PCB	Low	Medium to High	Low to Medium

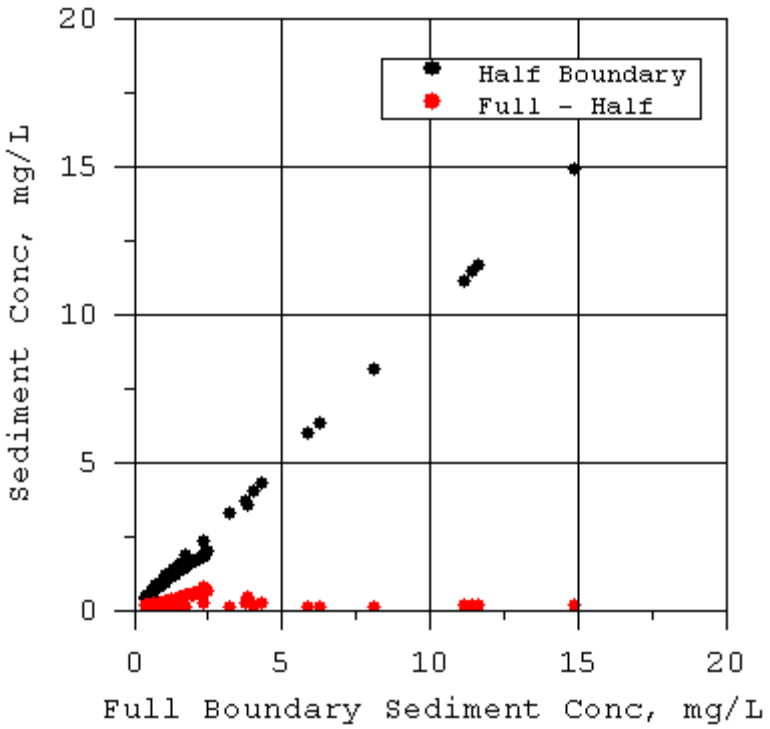

Figure C-1. Sensitivity of sediment concentration to halving sediment and contaminant open boundary conditions

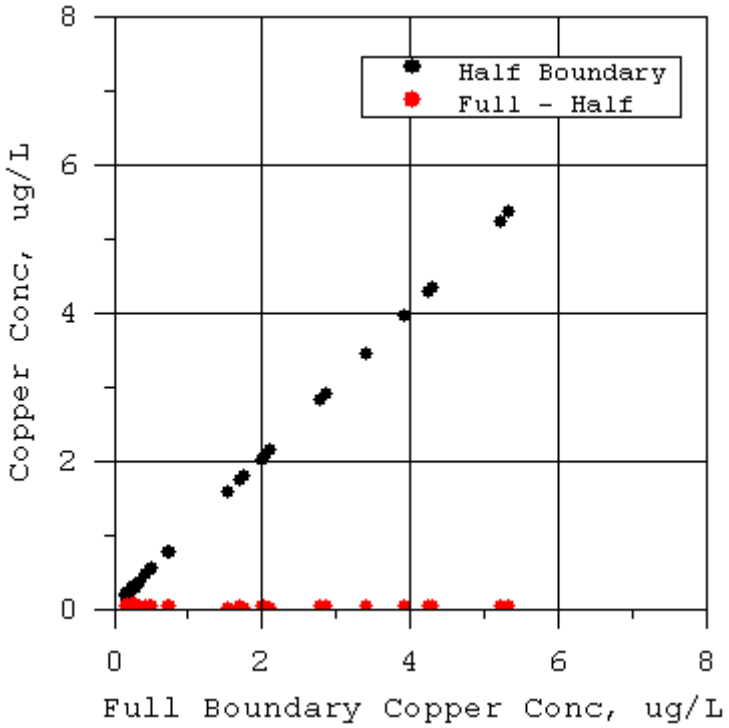

Figure C-2. Sensitivity of copper concentration to halving sediment and contaminant open boundary conditions

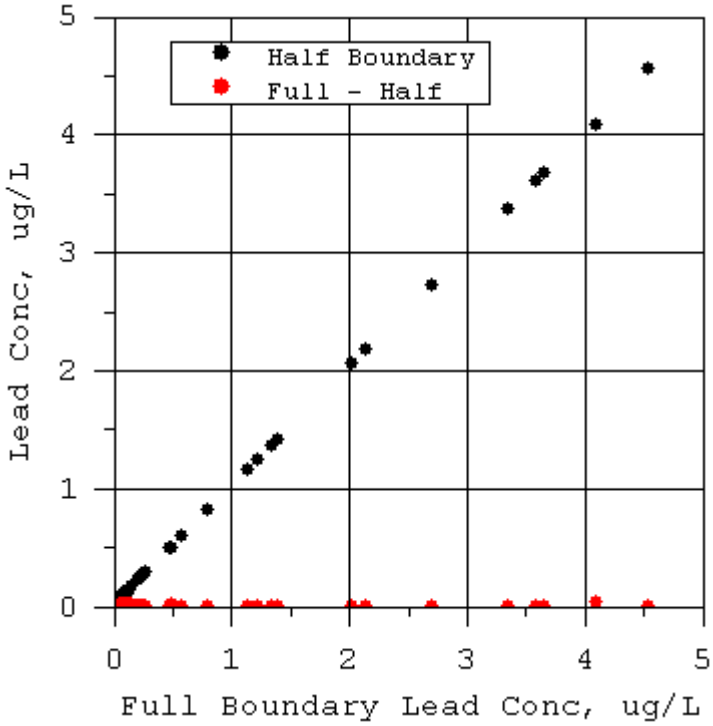

Figure C-3. Sensitivity of lead concentration to halving sediment and contaminant open boundary conditions

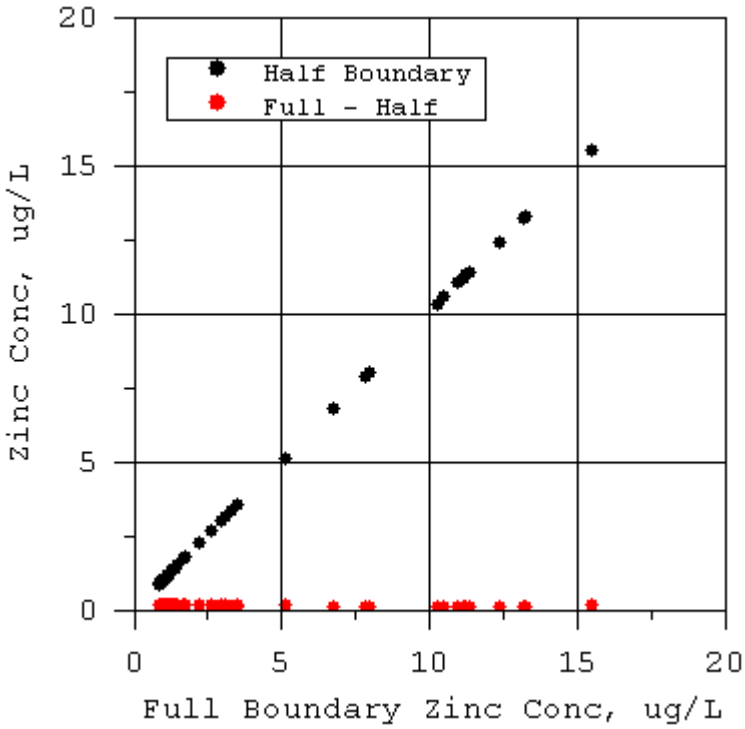

Figure C-4. Sensitivity of zinc concentration to halving sediment and contaminant open boundary conditions

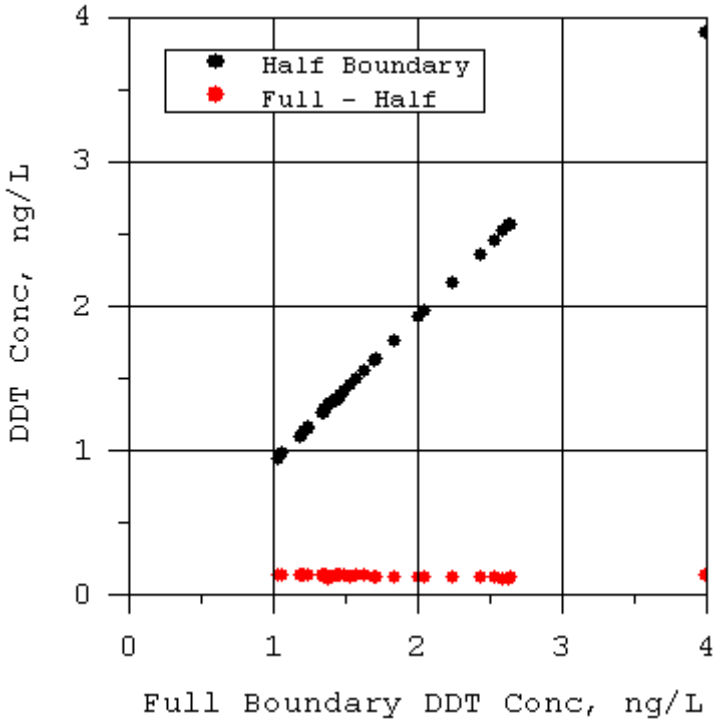

Figure C-5. Sensitivity of DDT concentration to halving sediment and contaminant open boundary conditions

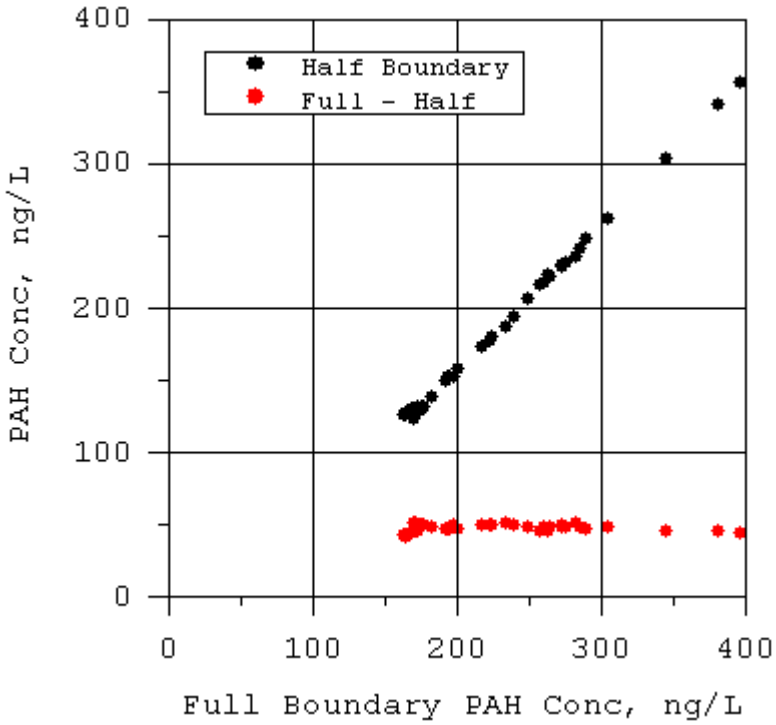

Figure C-6. Sensitivity of PAH concentration to halving sediment and contaminant open boundary conditions

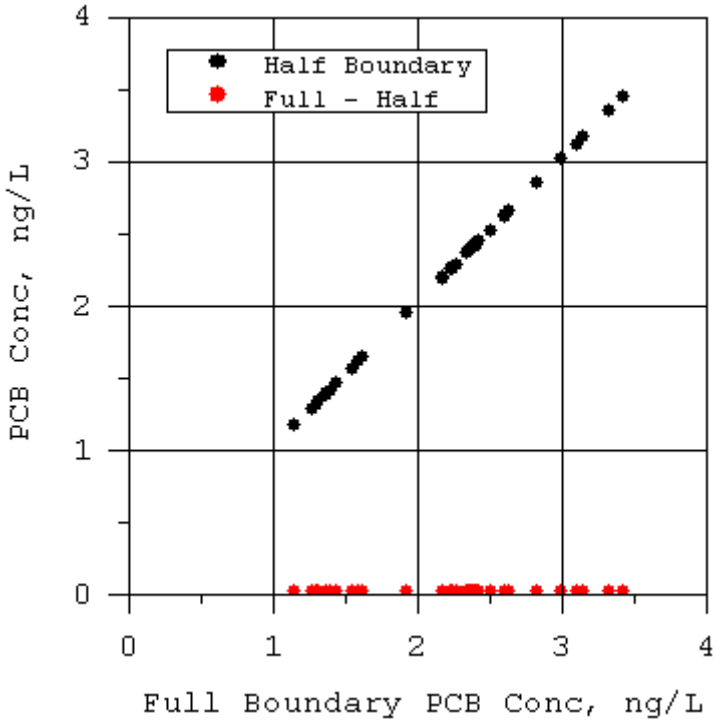

Figure C-7. Sensitivity of PCB concentration to halving sediment and contaminant open boundary conditions

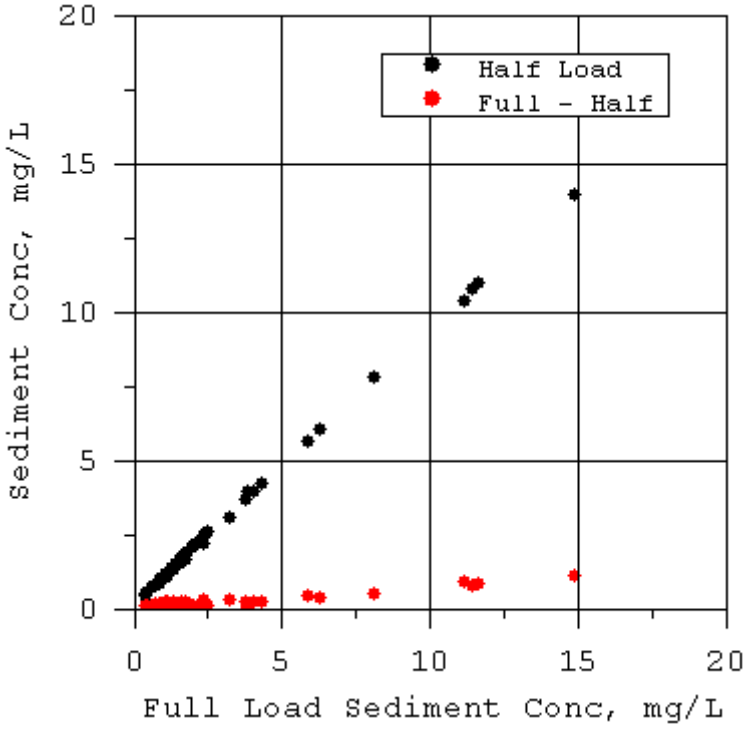

Figure C-8. Sensitivity of sediment concentration to halving sediment and contaminant loads

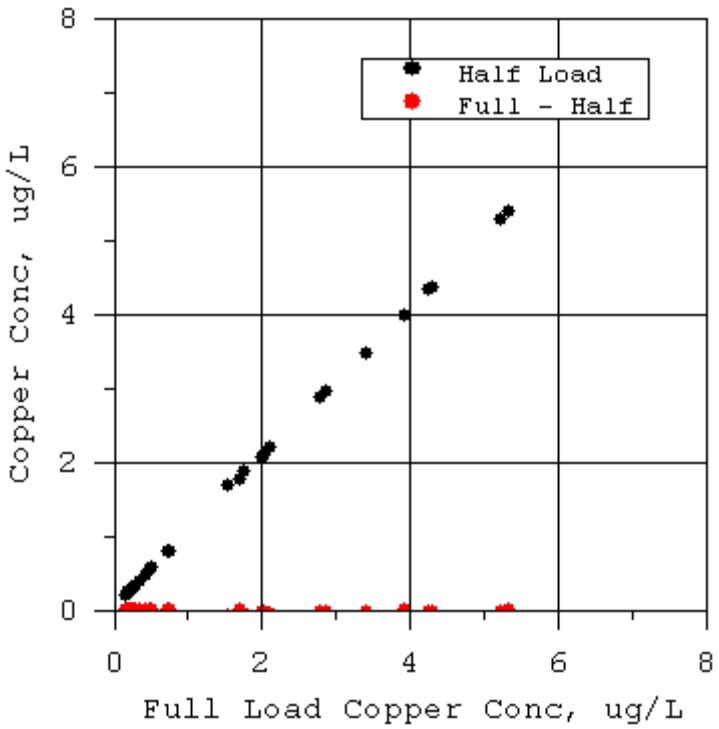

Figure C-9. Sensitivity of copper concentration to halving sediment and contaminant loads

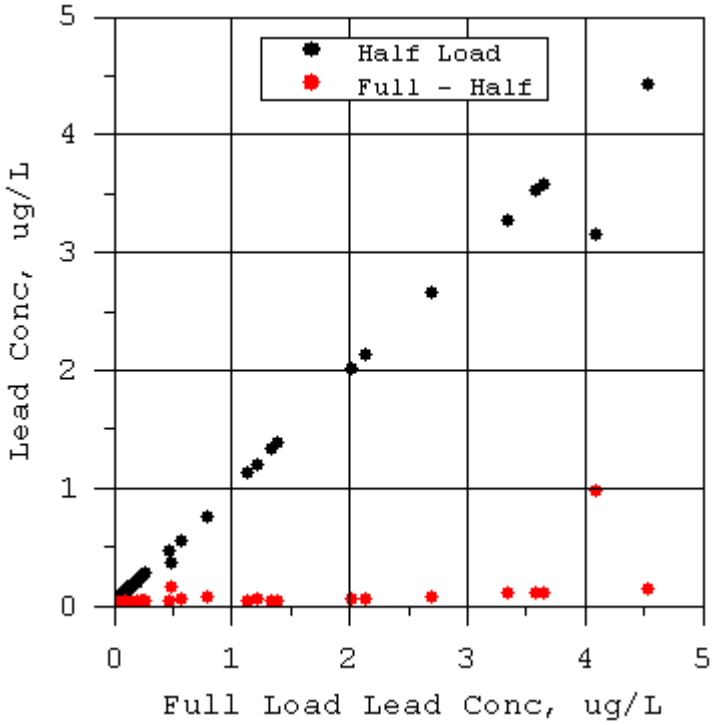

Figure C-10. Sensitivity of lead concentration to halving sediment and contaminant loads

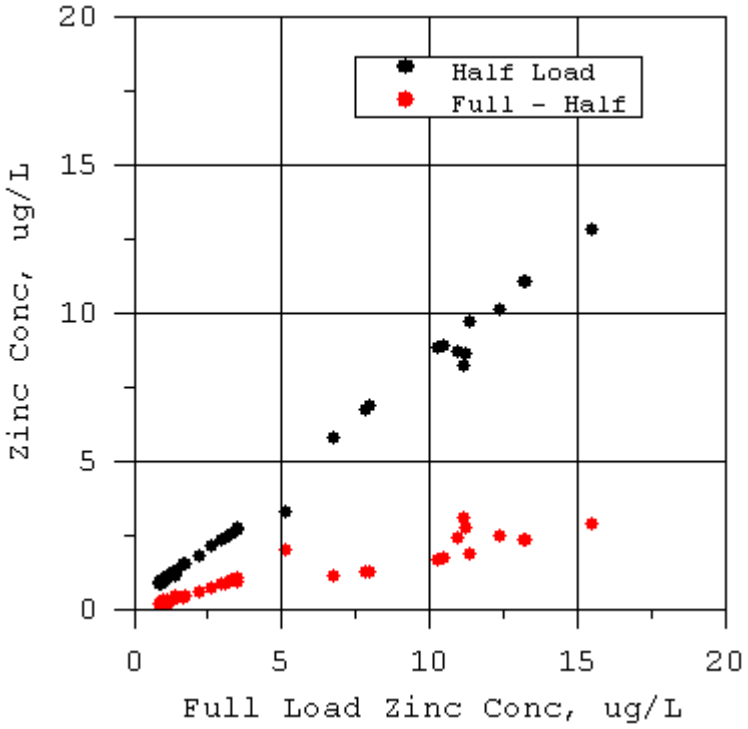

Figure C-11. Sensitivity of zinc concentration to halving sediment and contaminant loads

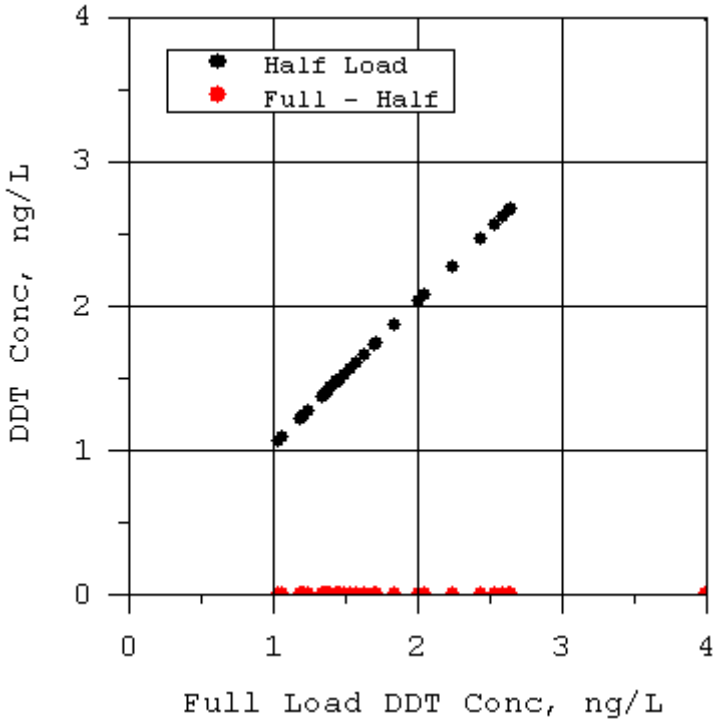

Figure C-12. Sensitivity of DDT concentration to halving sediment and contaminant loads

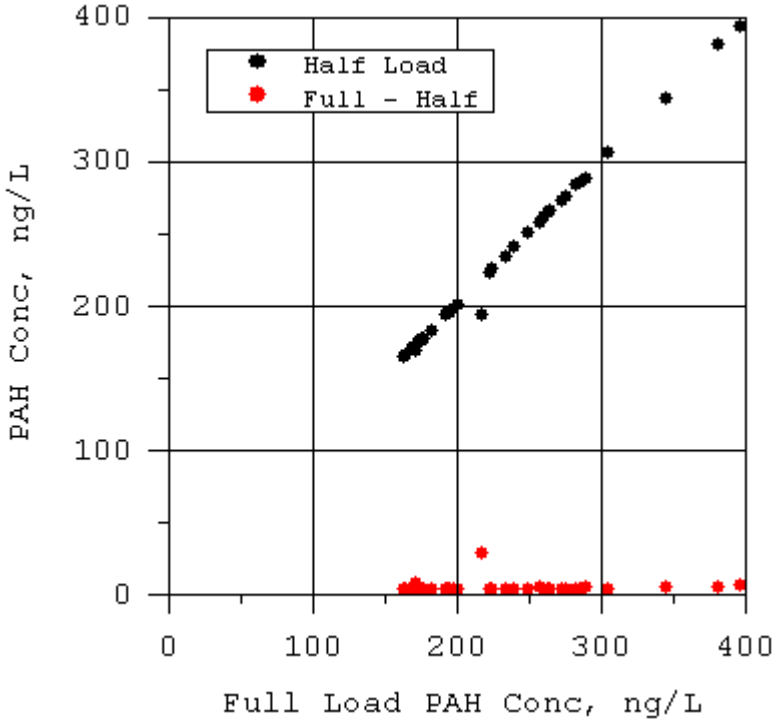

Figure C-13. Sensitivity of PAH concentration to halving sediment and contaminant loads

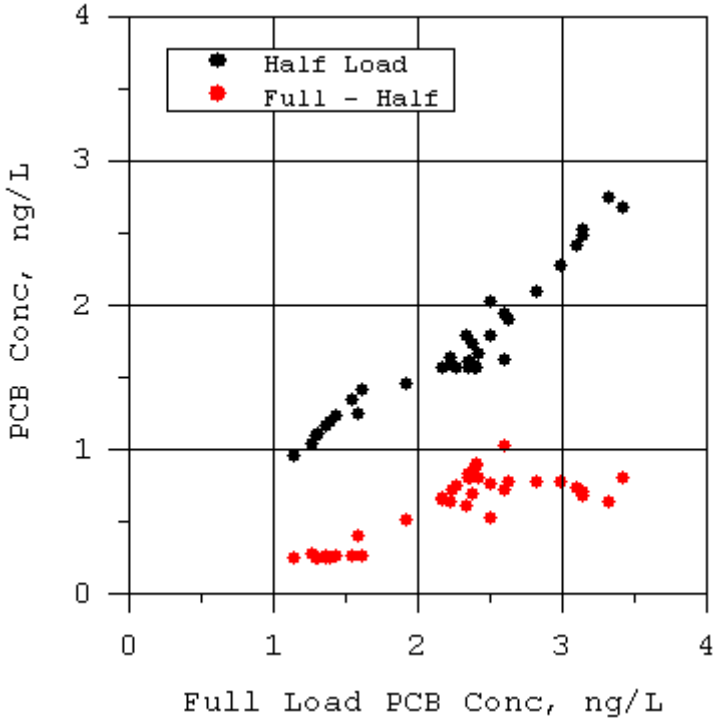

Figure C-14. Sensitivity of PCB concentration to halving sediment and contaminant loads

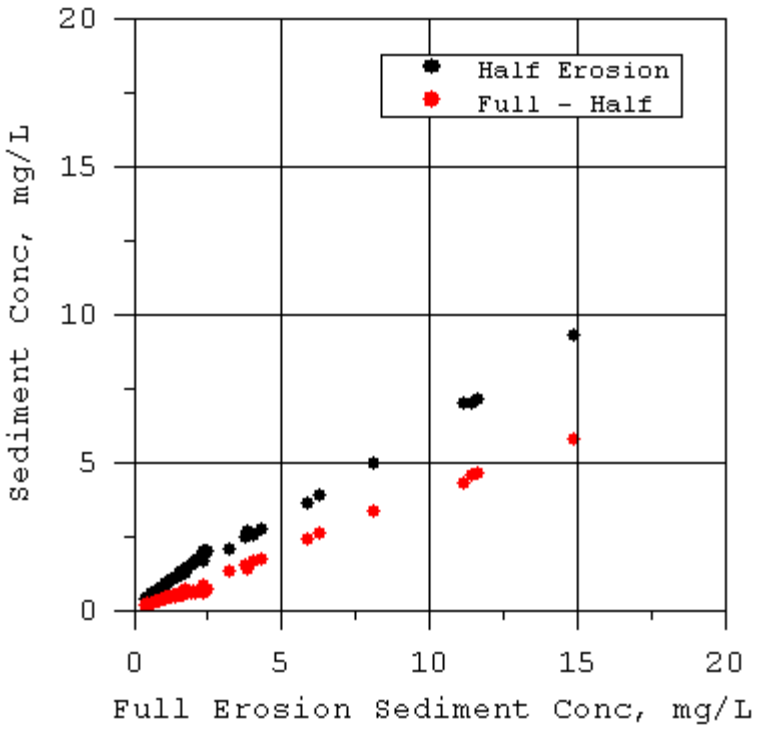

Figure C-15. Sensitivity of sediment concentration to halving sediment erosion rate

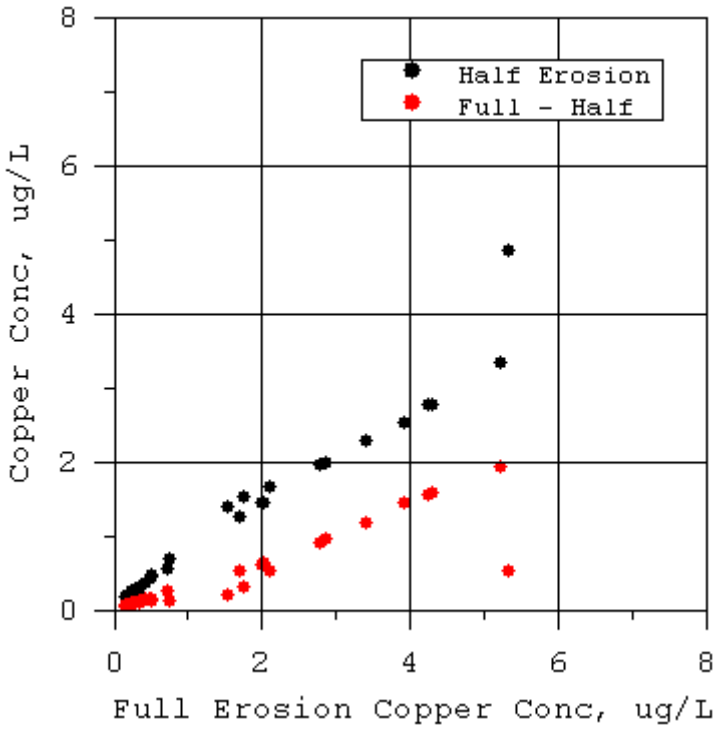

Figure C-16. Sensitivity of copper concentration to halving sediment erosion rate

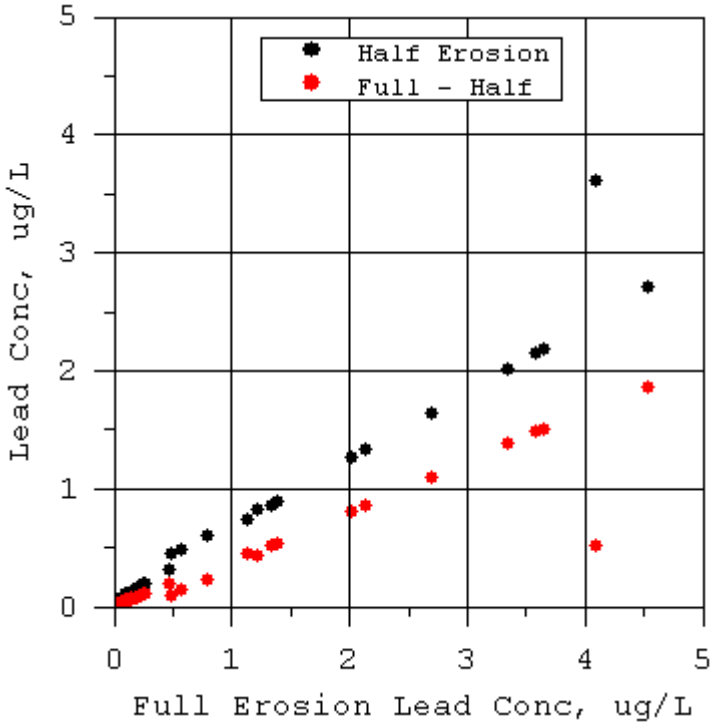

Figure C-17. Sensitivity of lead concentration to halving sediment erosion rate

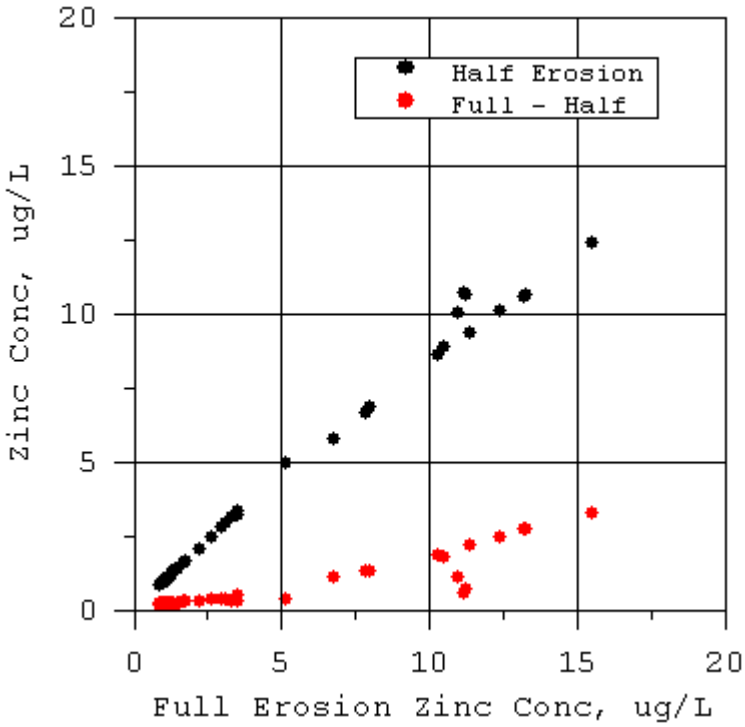

Figure C-18. Sensitivity of zinc concentration to halving sediment erosion rate

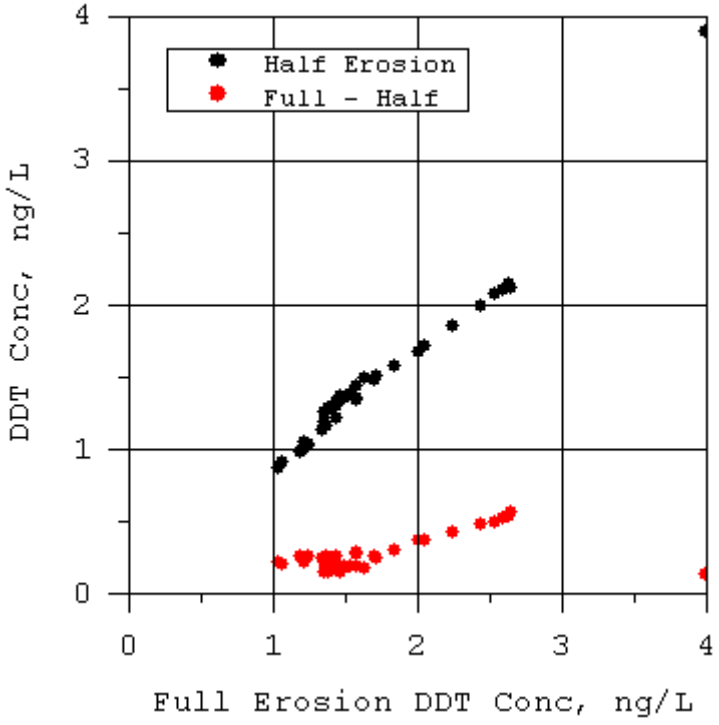

Figure C-19. Sensitivity of DDT concentration to halving sediment erosion rate

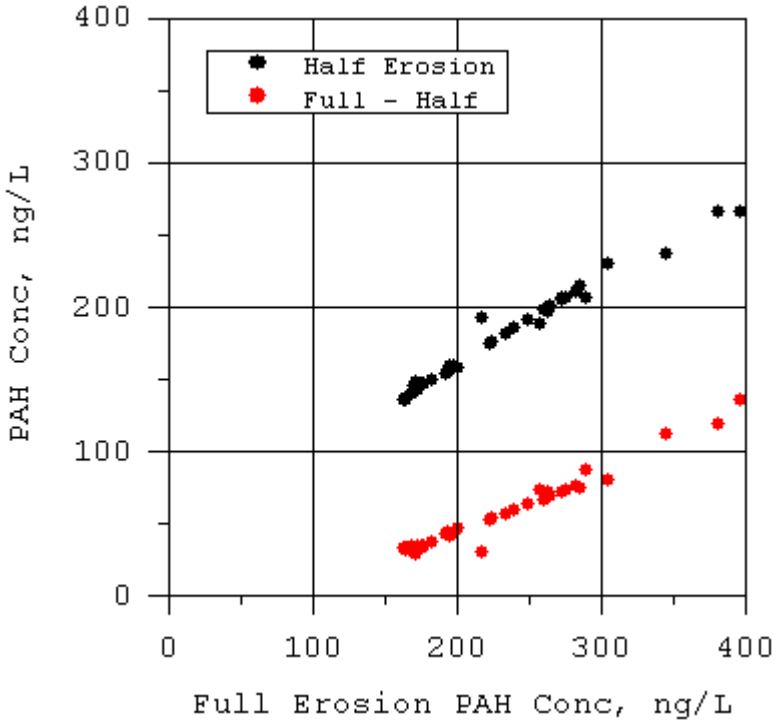

Figure C-20. Sensitivity of PAH concentration to halving sediment erosion rate

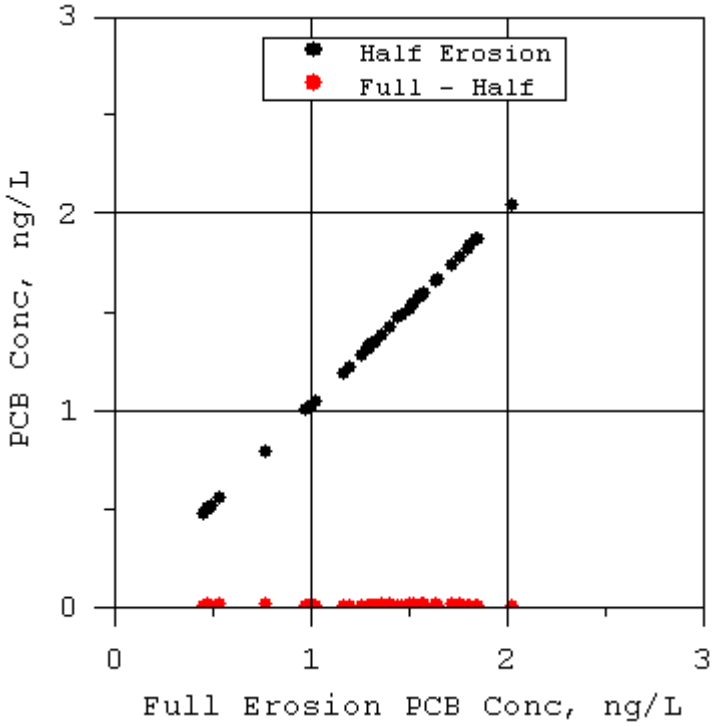

Figure C-21. Sensitivity of PCB concentration to halving sediment erosion rate

Appendix D: Sediment and Contaminant Transport Model Sensitivity to Long-Term Load Reductions

DRAFT

November 2008

Prepared for:
USEPA Region 9
Los Angeles Regional Water Quality Control Board

Prepared by:
Tetra Tech, Inc.

Introduction

Two simulations were conducted to investigate the sensitivity of the sediment and contaminant model predictions to long-term load reductions. Both simulations spanned a four year period from 2002 through 2005. This period includes significant wet season inflow events as illustrated by the Los Angeles River flow shown in Figure D-1. The first (or baseline) simulation used watershed model estimated sediment and contaminant loads. The second (or load reduction) simulation used sediment and contaminant loads which were reduced by 50 percent for both rivers and near shore watersheds. The sensitivity analysis results are presented in both time series graphs and maps illustrating changes in contaminant level over the four year period, as described below.

Time series of water column and sediment bed concentrations provide qualitative insight into the long-term response at three spatially diverse stations selected from the 60 sites visited in the Ports' 2006 study (Figure 15 and Figure D-2). Water column and sediment bed concentration time series for copper, zinc, DDT, and PAHs are shown for three stations: LA Inner Harbor (8); LB Inner Harbor (42) and Outer Harbor (54) (circled in blue on Figure D-2). These results also provide insight into water column and sediment bed concentration responses during wet weather inflow events. Concentrations in these graphs are defined as mass per unit volume (ug/L or ng/L) for both the water column and sediment bed surface. This provides a true measure of mass associated with the sediment bed and therefore illustrates the changes in total concentration.

Analysis of the simulation results focuses on the change in sediment bed surface contaminant levels over the four-year period. Three sets of spatial maps were generated to illustrate (1) the changes at the end of the four year simulations for the base and load reduction simulations and (2) the relative change for the load reduction simulation. The three maps presented for each contaminant are defined as:

> **Areal Concentration Change in Baseline Simulation Over Time** = Final Areal Concentration using Baseline Conditions in 2005 (after 4 years) – Initial Areal Concentration using Baseline Conditions in 2002 (beginning of simulation period)
>
> **Areal Concentration Change from Load Reduction Simulation** = Final Areal Base Simulation Concentration in 2005 – Final Areal Load Reduction Concentration in 2005 (based on 50 percent load reduction from the rivers and nearshore watersheds)
>
> **Relative Change in Load Reduction Simulation** = Relative Change in Load Reduction Change (normalized by initial top bed layer concentration)

Note: Areal concentration is the mass per unit area in top layer of sediment bed

The “Areal Concentration Change in Baseline Simulation” is presented for comparative purposes only. Specifically, the “Areal Concentration Change from Load Reduction Simulation” results can be compared with the “Areal Concentration Change in Baseline Simulation” to evaluate the impacts of reducing the watershed and river loads by 50 percent after a four year period.

Copper and Zinc Results

Water column and sediment bed concentration time series for total copper are shown in Figures D-3 through D-5 for Stations 8, 42, and 54 (these stations are circled in blue on Figure D-2). Corresponding results for zinc are shown in Figures D-6 through D-8. The top panel of the time series figures shows the results for the Baseline Simulation (i.e., using baseline loads from the watersheds), while the lower panel illustrates the concentrations associated with the Load Reduction Simulation (i.e., river and near shore watershed loads were reduced by 50 percent). Results for both copper and zinc indicate decreases in water column concentrations during periods of high flow, when comparing the baseline conditions with the 50 percent load reduction scenario. Although the load reductions were 50 percent, there is not a corresponding 50 percent reduction in water column concentrations.

In general, sediment bed contaminant concentrations tend to increase in response to high freshwater flows, which is expected since more sediments are transported by inflows from the watershed under high flow conditions. Over a four-year period, additional sediment is added to the system due to freshwater inputs and other transport factors; therefore, there is an expected net increase in sediment bed contaminant concentrations (assuming no dredging or other pollutant-reduction activities have occurred). The net increases in sediment bed contaminant concentrations were compared between the Baseline Simulation and the Load Reduction Simulation. Overall, the net increase in copper and zinc concentrations over the four year period are substantially lower for the Load Reduction Simulation. Specifically, for stations 8 and 54 (Figures D-3 and D-5), the copper reductions observed at the end of the four-year period were approximately 1,000 ug/L (station 42 [Figure D-4] showed minimal change in copper concentrations). Sediment bed zinc concentrations at station 8 (Figure D-6) decreased by approximately 15,000 ug/L after four years in the Load Reduction Simulation, while stations 42 (Figure D-7) and 54 (Figure D-8) had smaller zinc reductions at the end of the four-year period (approximately 1,000 ug/L and 3,500 ug/L, respectively).

Figures D-9 through D-11 present the three maps associated with sediment bed copper results, while Figures D-12 through D-14 present sediment bed zinc results. For comparative purposes, the Areal Concentration Change in Baseline Simulation results are shown first and exhibit a similar spatial pattern for the two metals (Figures D-9 and D-12). These results are followed by the maps of the

Areal Concentration Change from Load Reduction Simulation. Overall, reduction of incoming loads by 50 percent results in a system-wide reduction in sediment bed copper and zinc concentrations (Figures D-10 and D-13, respectively). Recall that these figures represent the difference between the end of the simulation period under baseline conditions and the end of the simulation period for the load reduction scenario (not the change over time between the beginning and end of the load reduction simulation period). Therefore, all positive values indicate a reduction in copper and zinc sediment bed concentrations. Reductions in sediment bed copper concentrations due to the load reduction simulation ranged from over 1,000 mg/m^2 near the Consolidated Slip to less than 100 mg/m^2 by the breakwater. Similarly, zinc reductions ranged from over 10,000 mg/m^2 near the Consolidated Slip to less than 800 mg/m^2 by the breakwater. These correspond to relative copper reductions of approximately 10 percent (a factor of 0.10) in the Consolidated Slip region to nearly 1 percent (a factor of 0.01) in many of the other harbor areas (Figure D-11). Relative reductions associated with the load reduction simulations for zinc were even higher (Figure D-14), ranging from 40 percent (a factor of 0.4) to 2 percent (a factor of 0.02) throughout most of the area inside the breakwater.

DDT and PAH Results

Water column and sediment bed concentration time series for total DDT are shown for Stations 8, 42, and 54 (circled in blue on Figure D-2) in Figures D-15 through D-17. Corresponding results for PAH are shown in Figures D-18 through D-20. As described above for the metals, the top panel of the time series figures shows the results for the Baseline Simulation (i.e., using baseline loads from the watersheds), while the lower panel illustrates the concentrations associated with the Load Reduction Simulation (i.e., river and near shore watershed loads were reduced by 50 percent). The results indicate that DDT and PAH concentrations in the water column decrease during periods of high flow when comparing the baseline conditions with the 50 percent load reduction scenario, as was the case for the two metals.

Sediment bed contaminant concentration behavior is more spatially varied with DDT concentrations decreasing at Station 8 (Figure D-15) at approximately the same rate and similar magnitude for both scenarios. At the other two stations, DDT concentrations in the sediment bed do not change significantly. Specifically, almost no change in concentration is observed at Station 42 (Figure D-16) when comparing the two simulations. Station 54 shows a slight increasing trend in sediment concentrations over time in both simulations; however, the load reduction simulation has a lower concentration after four years by about 500 ng/L (Figure D-17). Bed concentration tendencies for PAH are somewhat more consistent with those for metals, but do not exhibit large relative changes. Station 8 (Figure D-18) shows a 10,000 ng/L decrease in sediment bed concentrations when comparing the base simulation results with the 50 percent load reduction simulation. Station 42 does not present a change in concentration

(Figure D-19), while there is an approximately 700 ng/L decrease in sediment concentration at Station 54 when comparing the two simulations (Figure D-20).

Spatial maps associated with sediment bed DDT results are presented in Figures D-21 through D-23, while maps for PAH levels are illustrated in Figures D-24 through D-26. Similar to the metals, for comparative purposes, the Areal Concentration Change in Baseline Simulation results are shown first (Figures D-21 and D-24) and these results are followed by the maps of the Areal Concentration Change from Load Reduction Simulation (Figures D-22 and D-25). The Areal Concentration Change in Baseline Simulation maps illustrate the change in sediment bed concentrations over a four-year period using the baseline conditions. The spatial pattern is somewhat similar for the two pollutants, with the most significant changes occurring in the inner harbors and near the Los Angeles River inflow (Figures D-21 and D-24). Review of the Load Reduction Simulation maps for DDT and PAH (i.e., the areal concentration change between the end of the simulation period under baseline conditions and the end of the simulation period for the load reduction scenario) indicates that the reduction of incoming loads by 50 percent results in a system-wide reduction in sediment bed DDT and PAH levels (Figures D-22 and D-25, respectively). These reductions are illustrated by the positive values in sediment bed concentrations. Reductions in areal sediment bed DDT concentrations due to the load reduction simulation ranged from over 1,000 $\mu g/m^2$ near the Los Angeles River to less than 100 $\mu g/m^2$ by the breakwater. Similarly, PAH reductions ranged from approximately 20,000 $\mu g/m^2$ near the Consolidated Slip to less than 200 $\mu g/m^2$ by the breakwater. These correspond to relative DDT reductions of approximately 40 percent (a factor of 0.40) in the Los Angeles River and San Gabriel River regions to 2 percent (a factor of 0.02) throughout most of the area inside the breakwater (Figure D-23). Relative reductions associated with the load reduction simulations for PAH were low (Figure D-26), ranging from 6 percent (a factor of 0.06) in Alamitos Bay, 4 percent (a factor of 0.04) near the Los Angeles River, and approximately 0.5 percent (a factor of 0.005) throughout most of the area inside the breakwater.

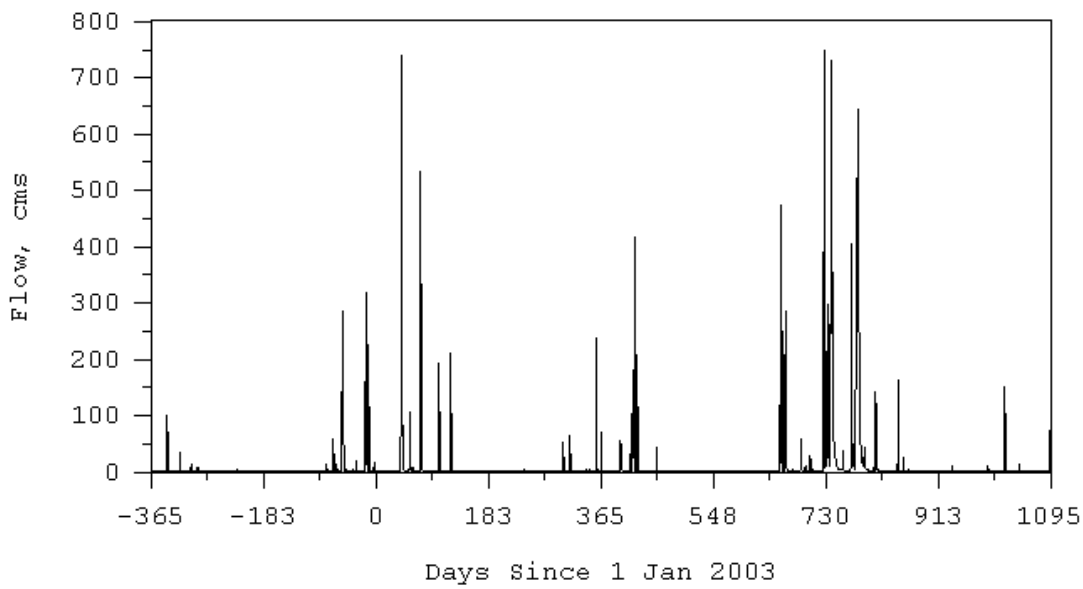

Figure D-1. Los Angeles River flow during long-term simulation period

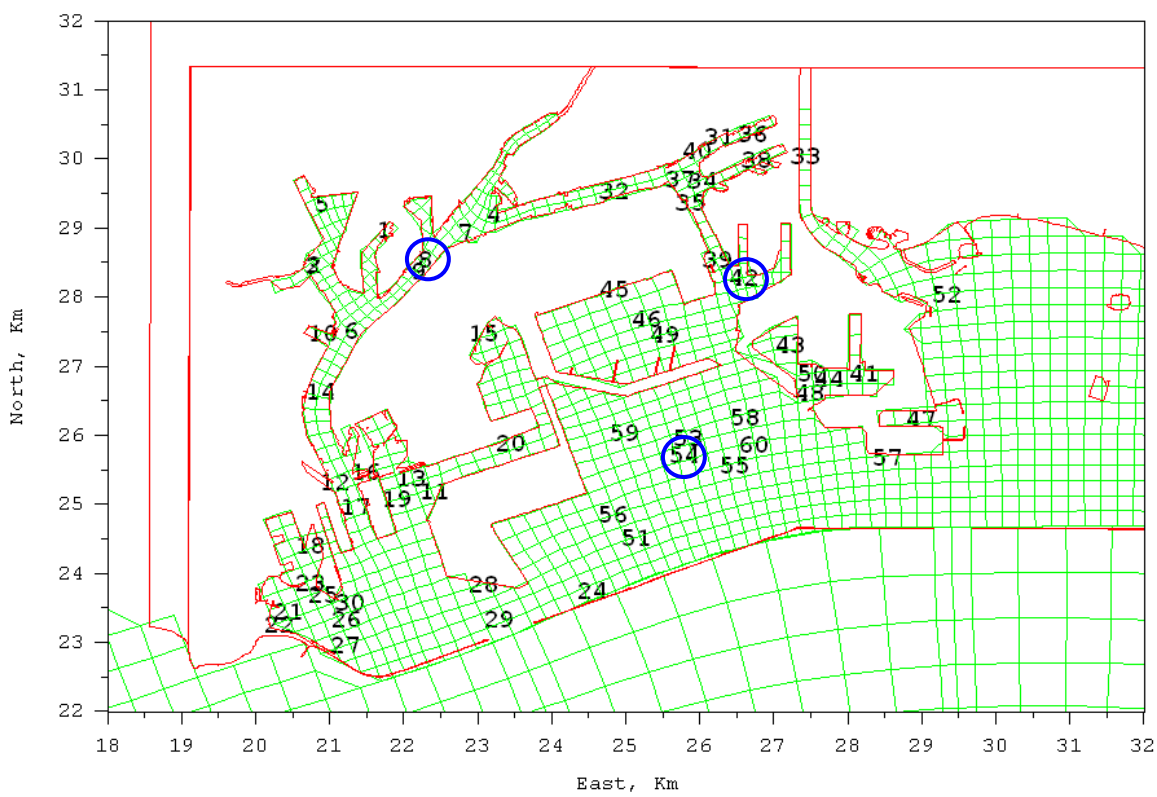

Note: Long-term sensitivity results are presented for the three stations circled in blue.

Figure D-2. Location of 2006 sediment and overlying water sampling locations

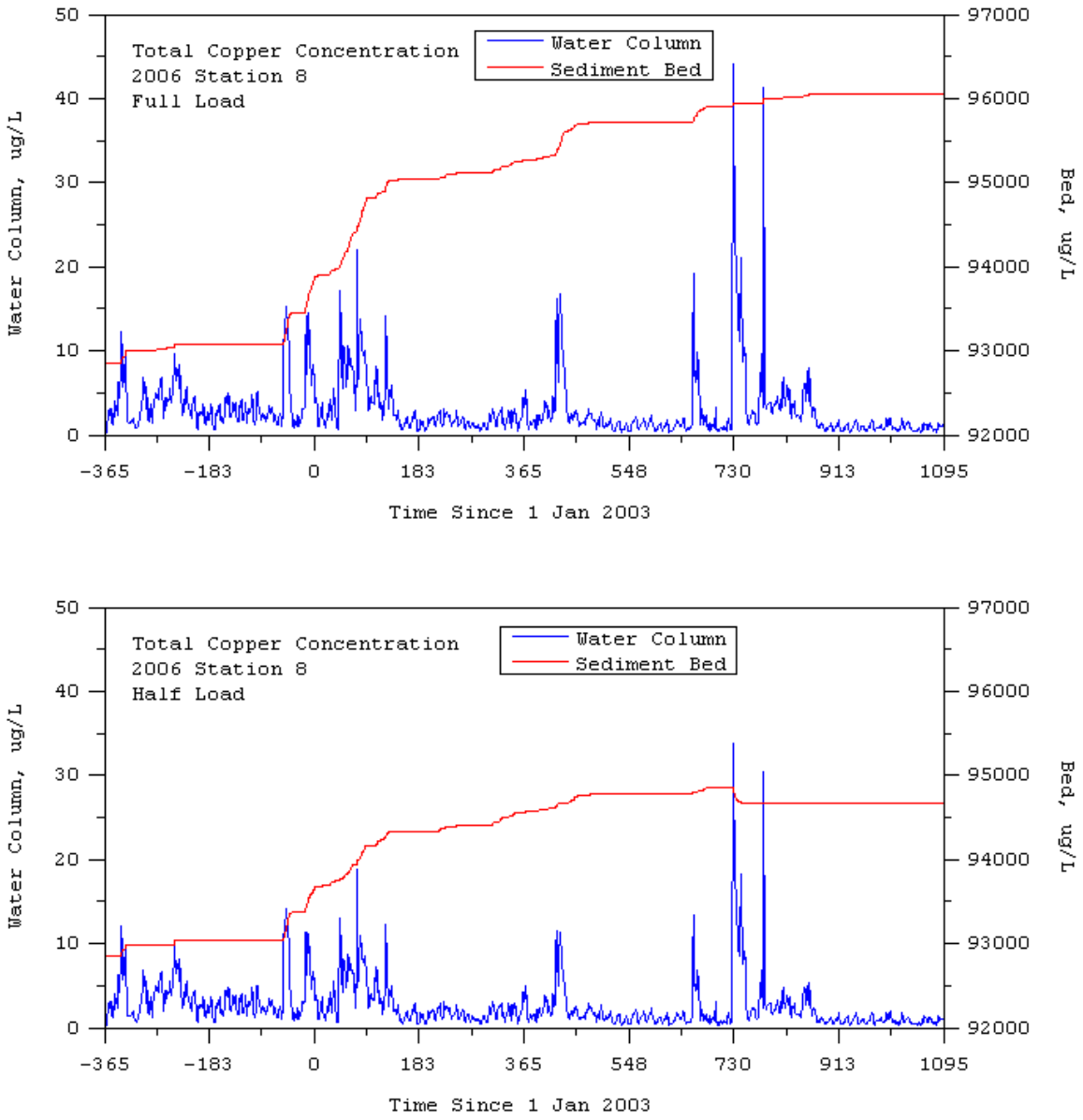

Figure D-3. Total copper concentration in water column and at sediment bed surface for Station 8 (see Figure D-2 for location)

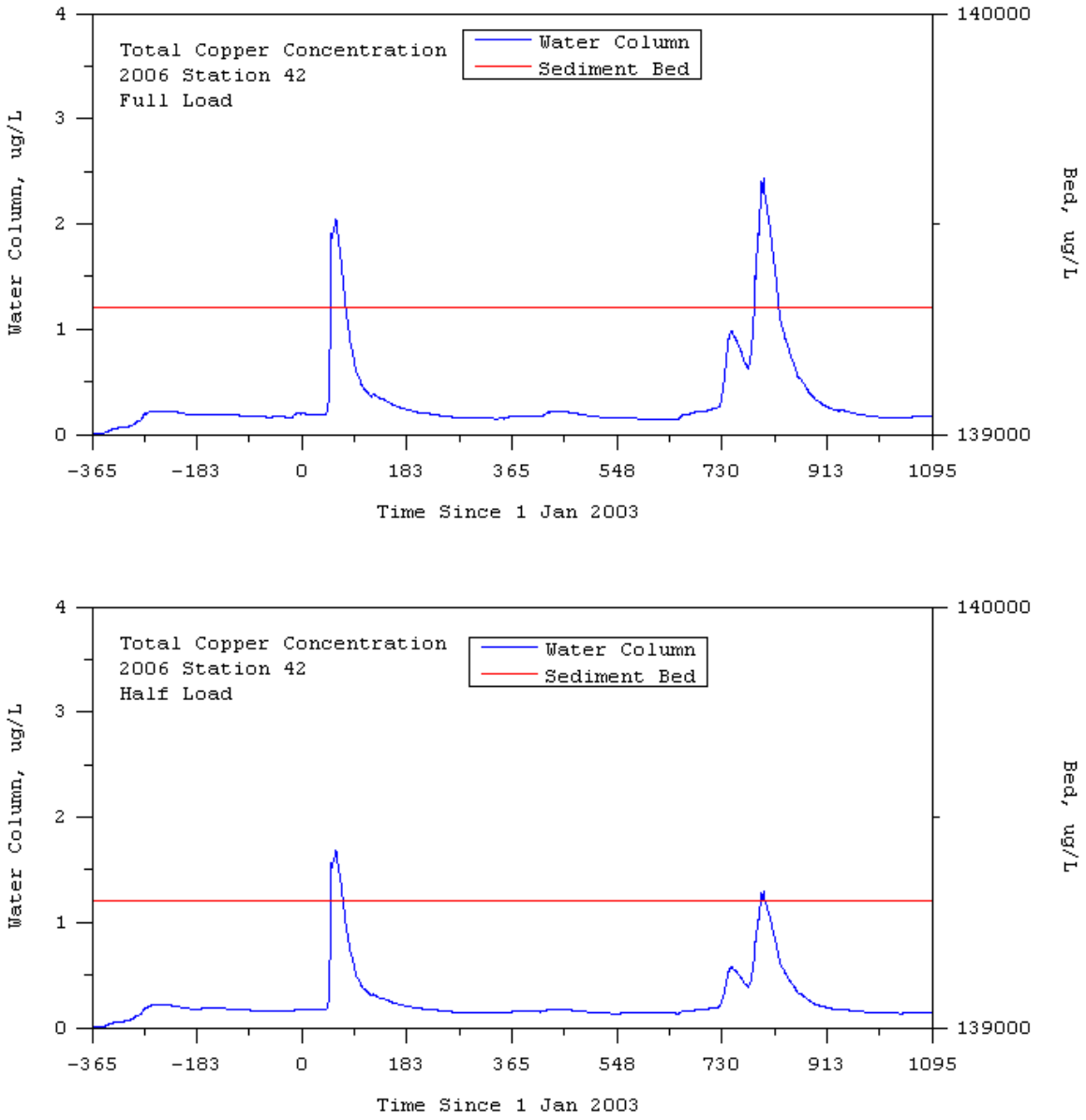

Figure D-4. Total copper concentration in water column and at sediment bed surface for Station 42 (see Figure D-2 for location)

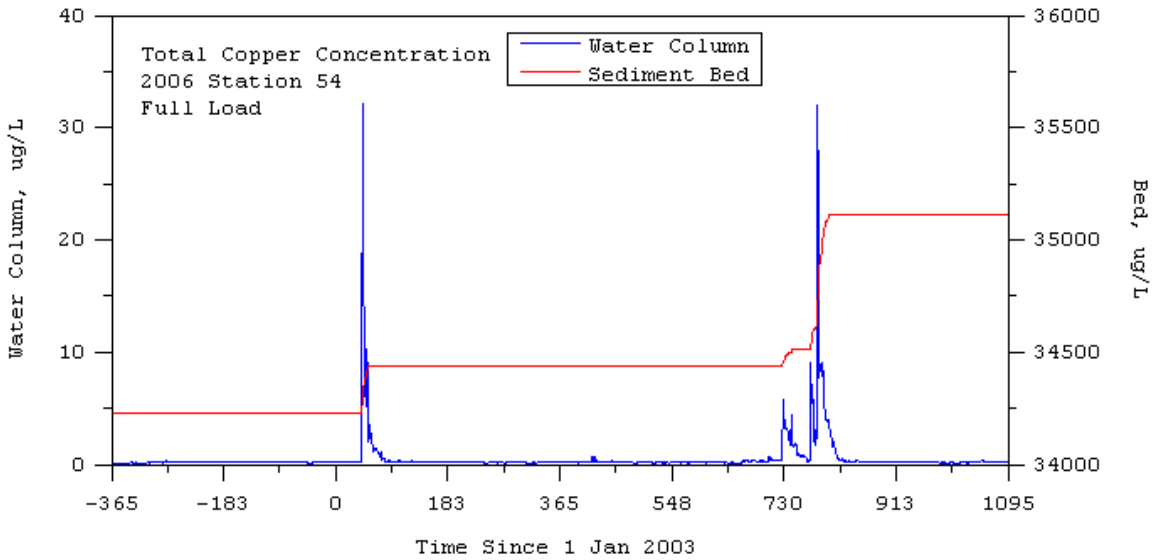

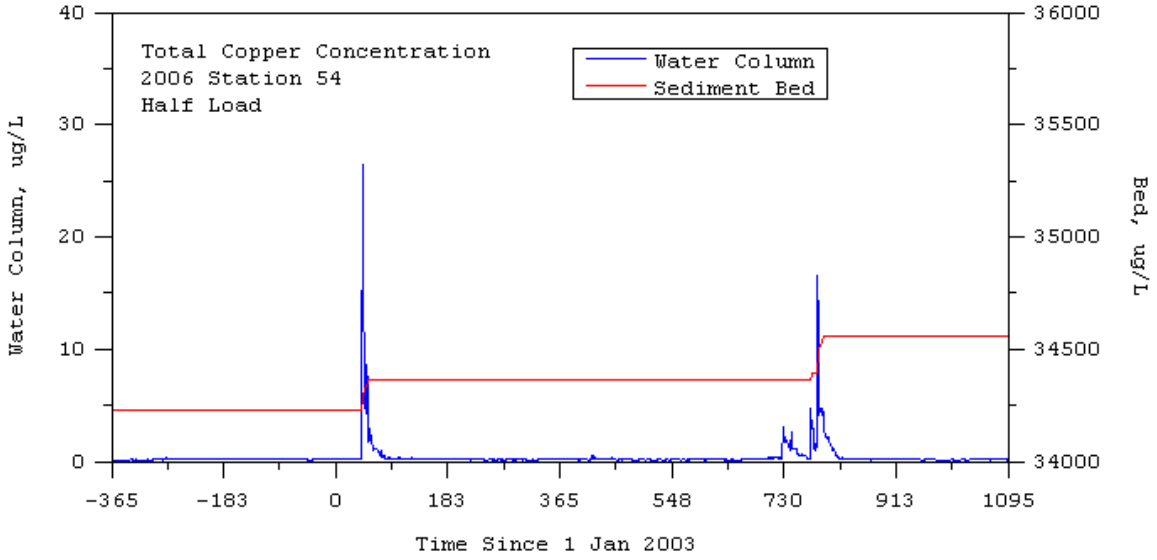

Figure D-5. Total copper concentration in water column and at sediment bed surface for Station 54 (see Figure D-2 for location)

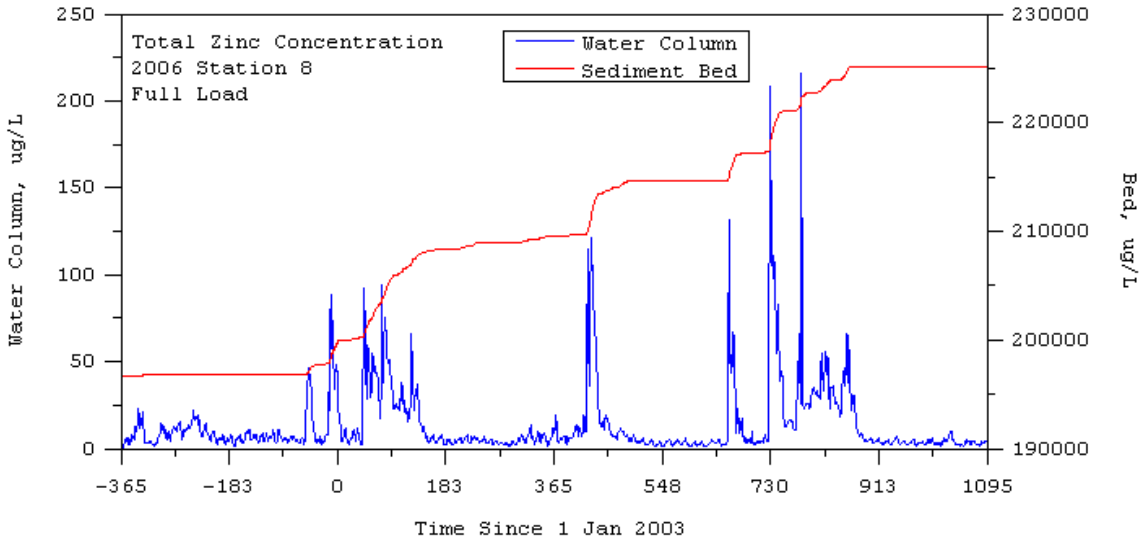

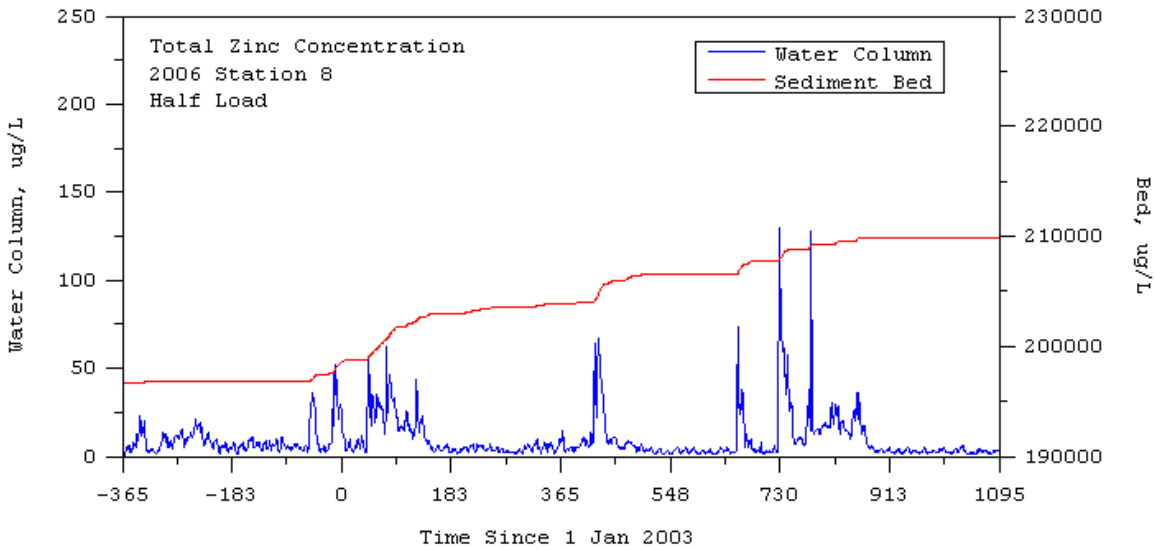

Figure D-6. Total zinc concentration in water column and at sediment bed surface for Station 8 (see Figure D-2 for location)

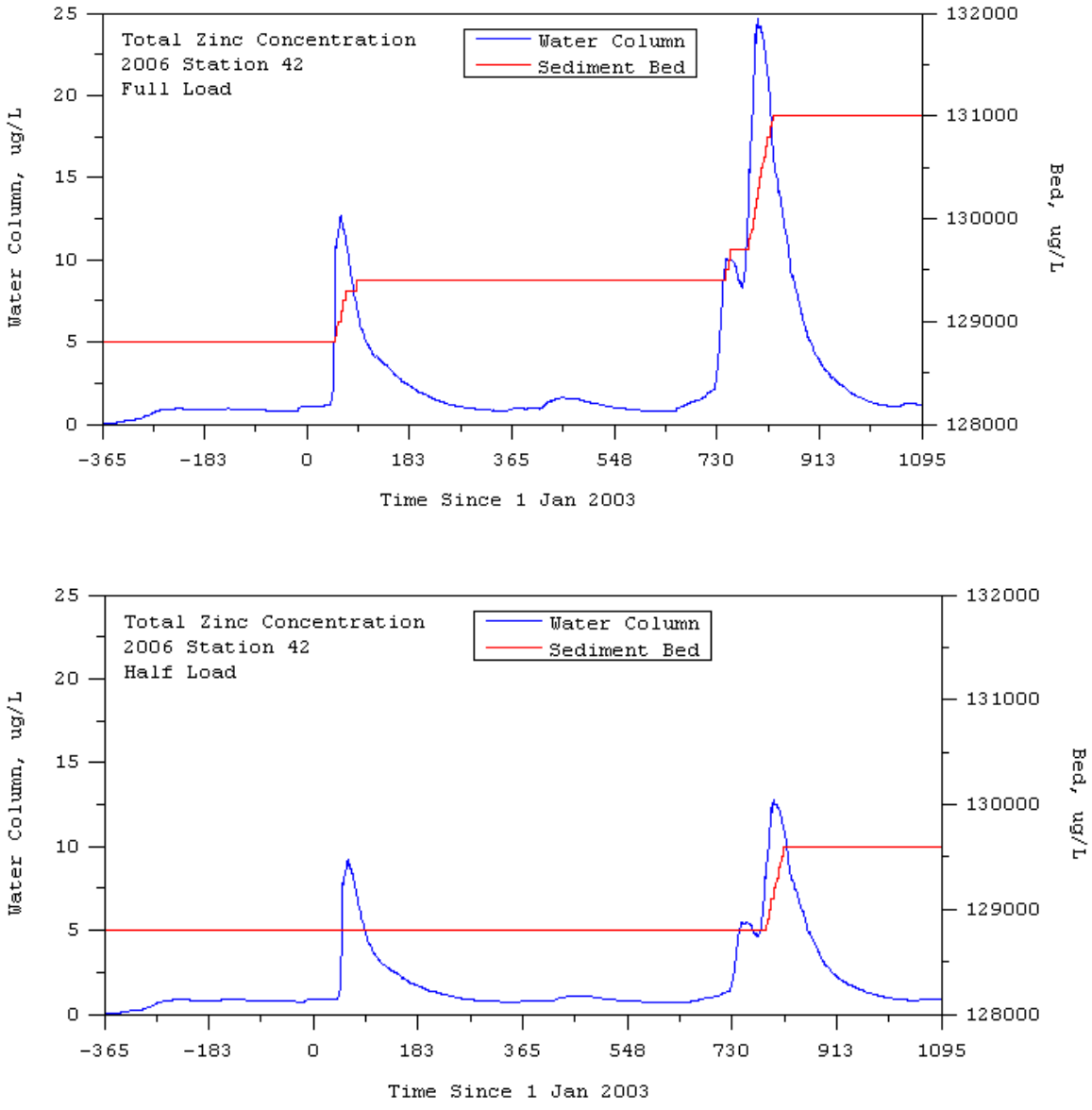

Figure D-7. Total zinc concentration in water column and at sediment bed surface for Station 42 (see Figure D-2 for location)

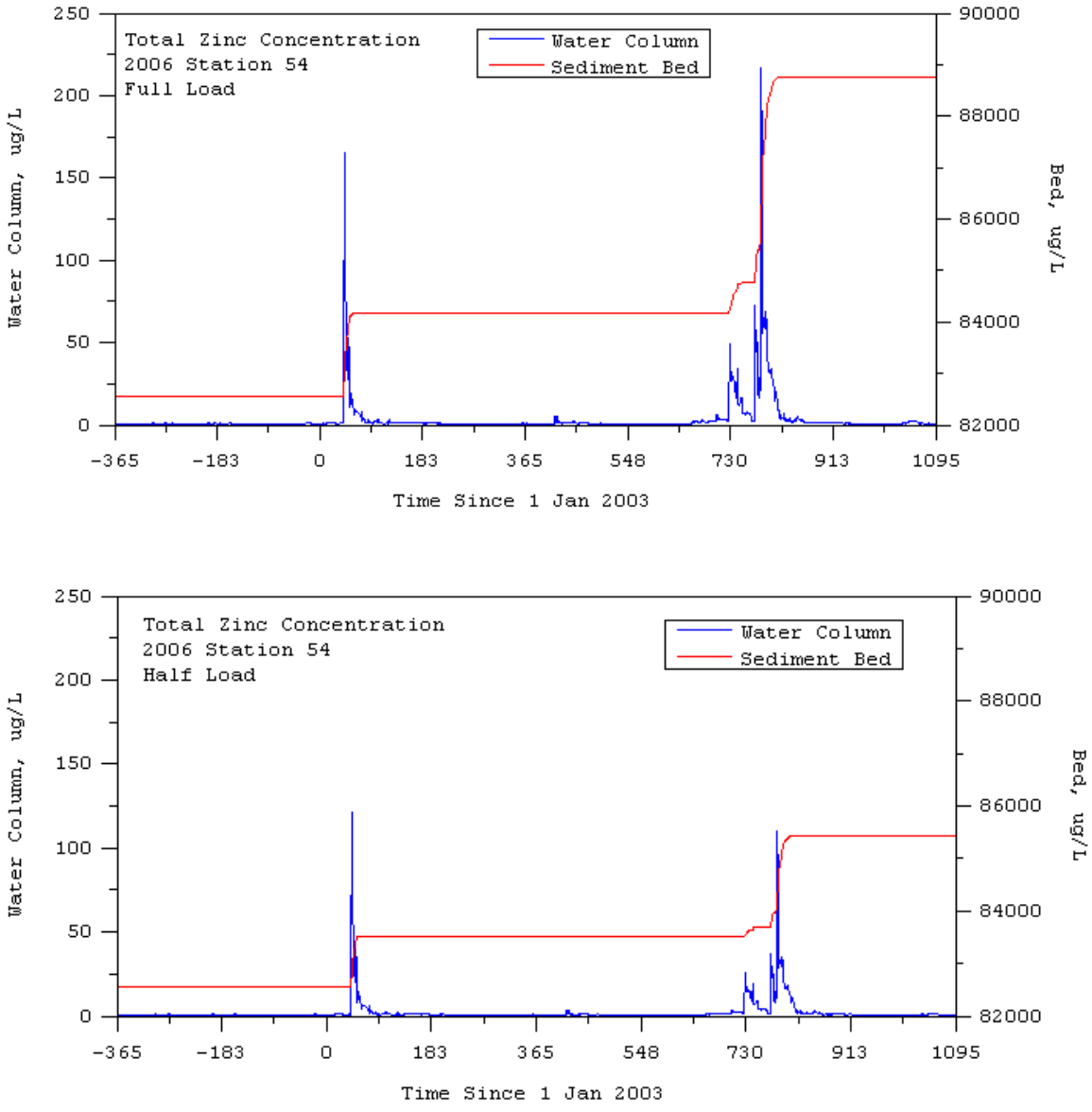

Figure D-8. Total zinc concentration in water column and at sediment bed surface for Station 54 (see Figure D-2 for location)

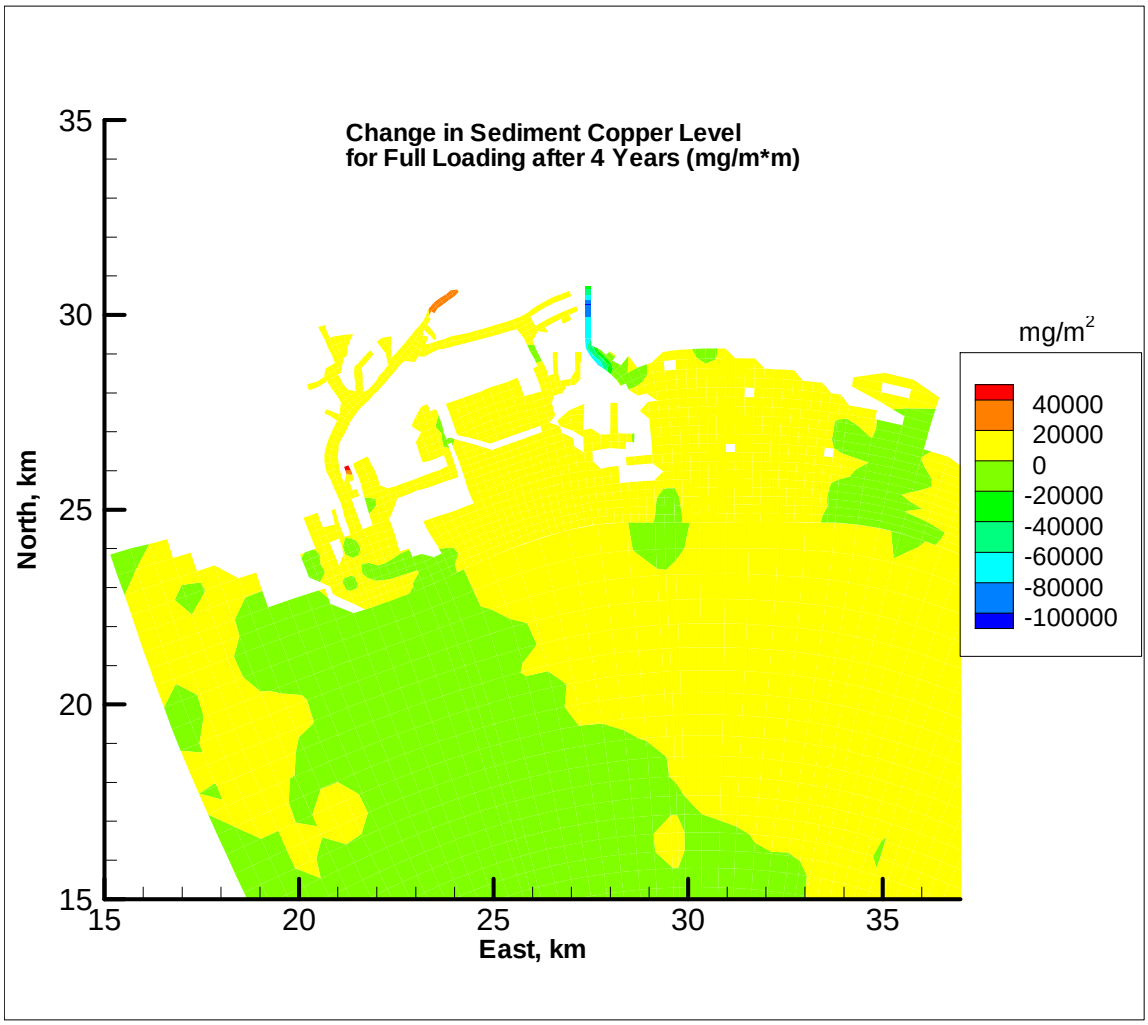

Note: Areal Concentration Change in Baseline Simulation Over Time = Final Areal Concentration using Baseline Conditions in 2005 (after 4 years) – Initial Areal Concentration using Baseline Conditions in 2002 (beginning of simulation period). Results are presented in mg/m^2.

Figure D-9. Areal concentration change in baseline simulation over time (after four years) – copper

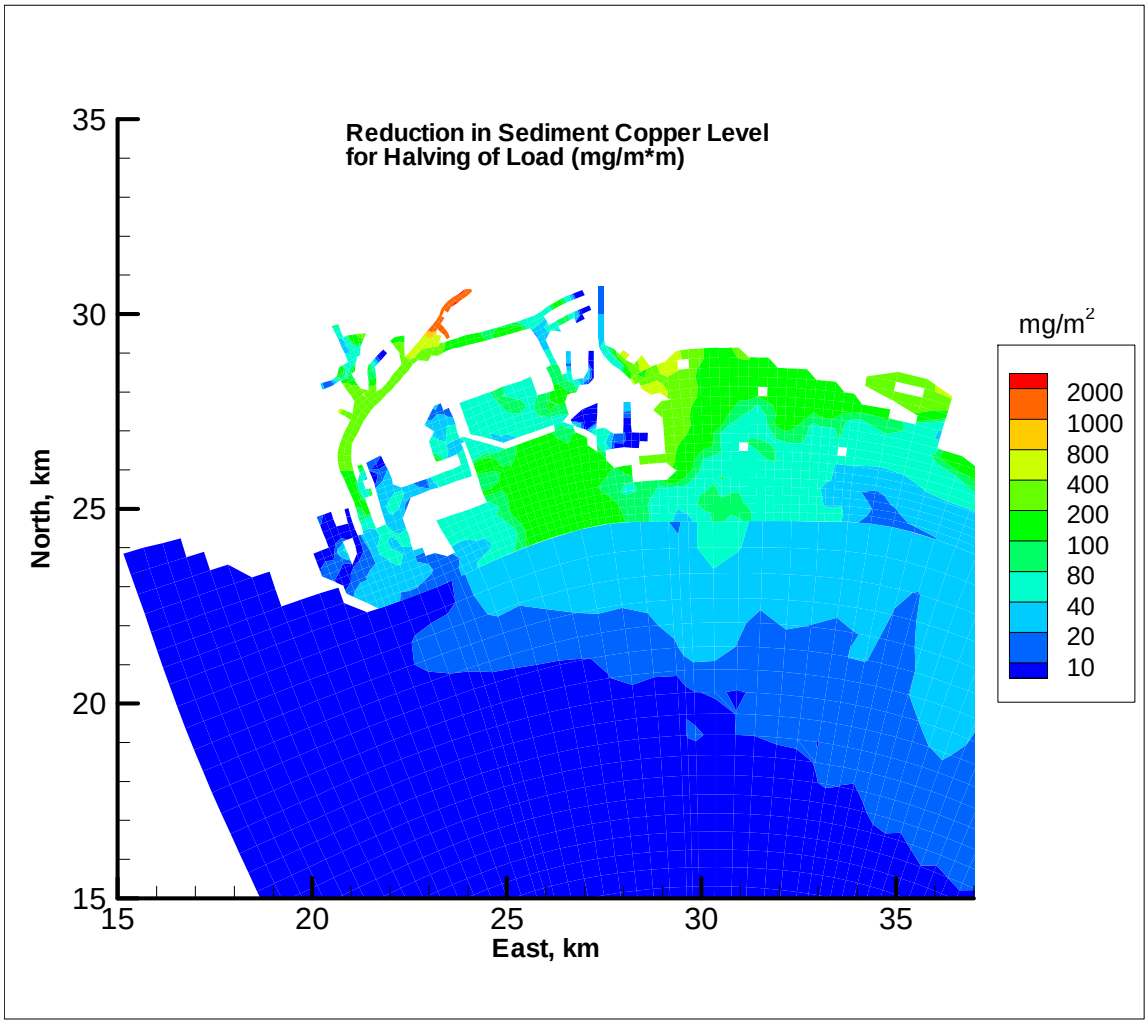

Note: Areal Concentration Change from Load Reduction Simulation = Final Areal Baseline Simulation Concentration in 2005 – Final Areal Load Reduction Concentration in 2005 (based on 50 percent load reduction from the rivers and nearshore watersheds). Results are presented in mg/m^2.

Figure D-10. Areal concentration change from load reduction simulation – copper

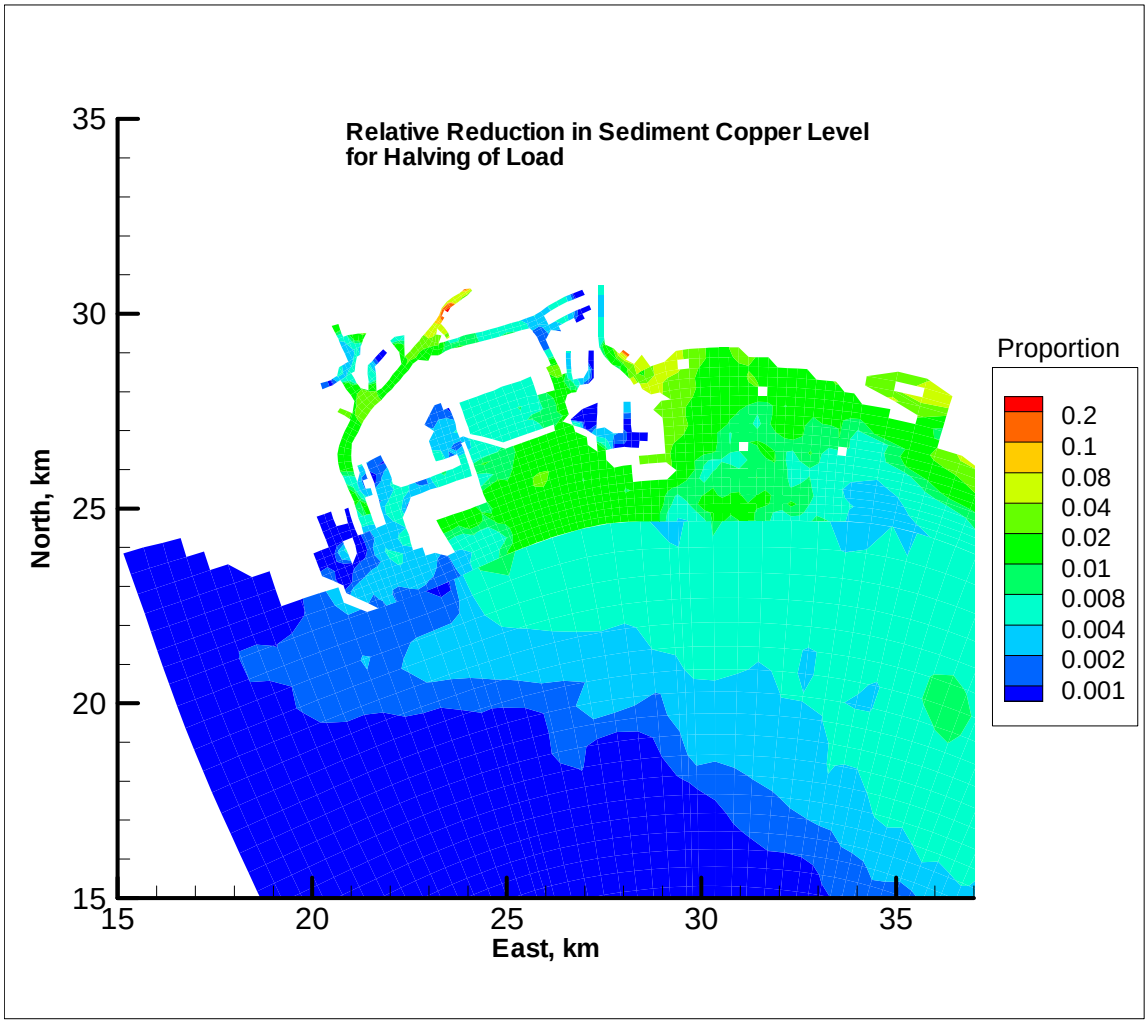

Note: Relative Change in Load Reduction Simulation = Relative Change in Load Reduction Change (normalized by initial top bed layer concentration). Results are proportions and can be multiplied by 100 to obtain percent.

Figure D-11. Relative change in load reduction simulation – copper

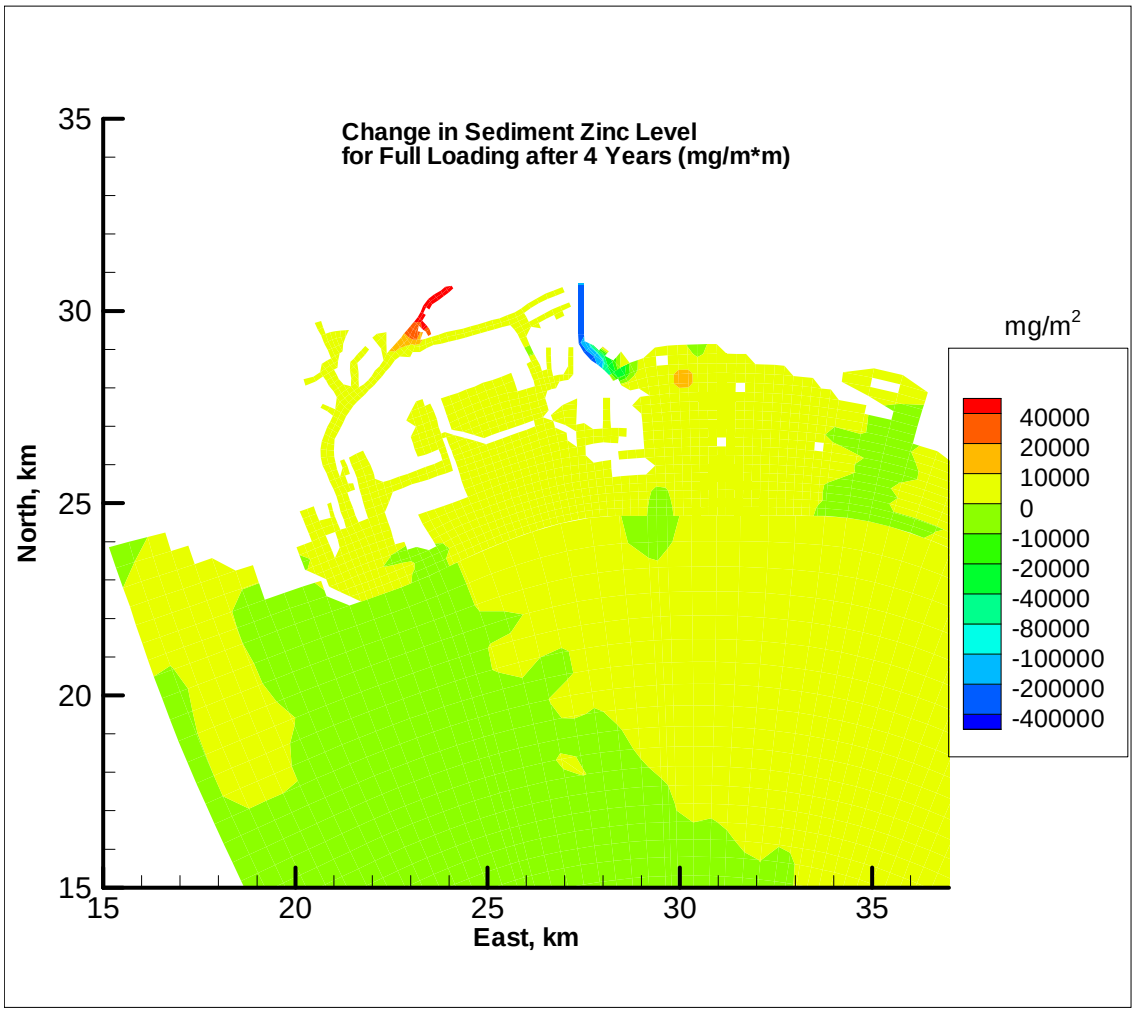

Note: Areal Concentration Change in Baseline Simulation Over Time = Final Areal Concentration using Baseline Conditions in 2005 (after 4 years) – Initial Areal Concentration using Baseline Conditions in 2002 (beginning of simulation period). Results are presented in mg/m^2.

Figure D-12. Areal concentration change in baseline simulation over time (after four years) – zinc

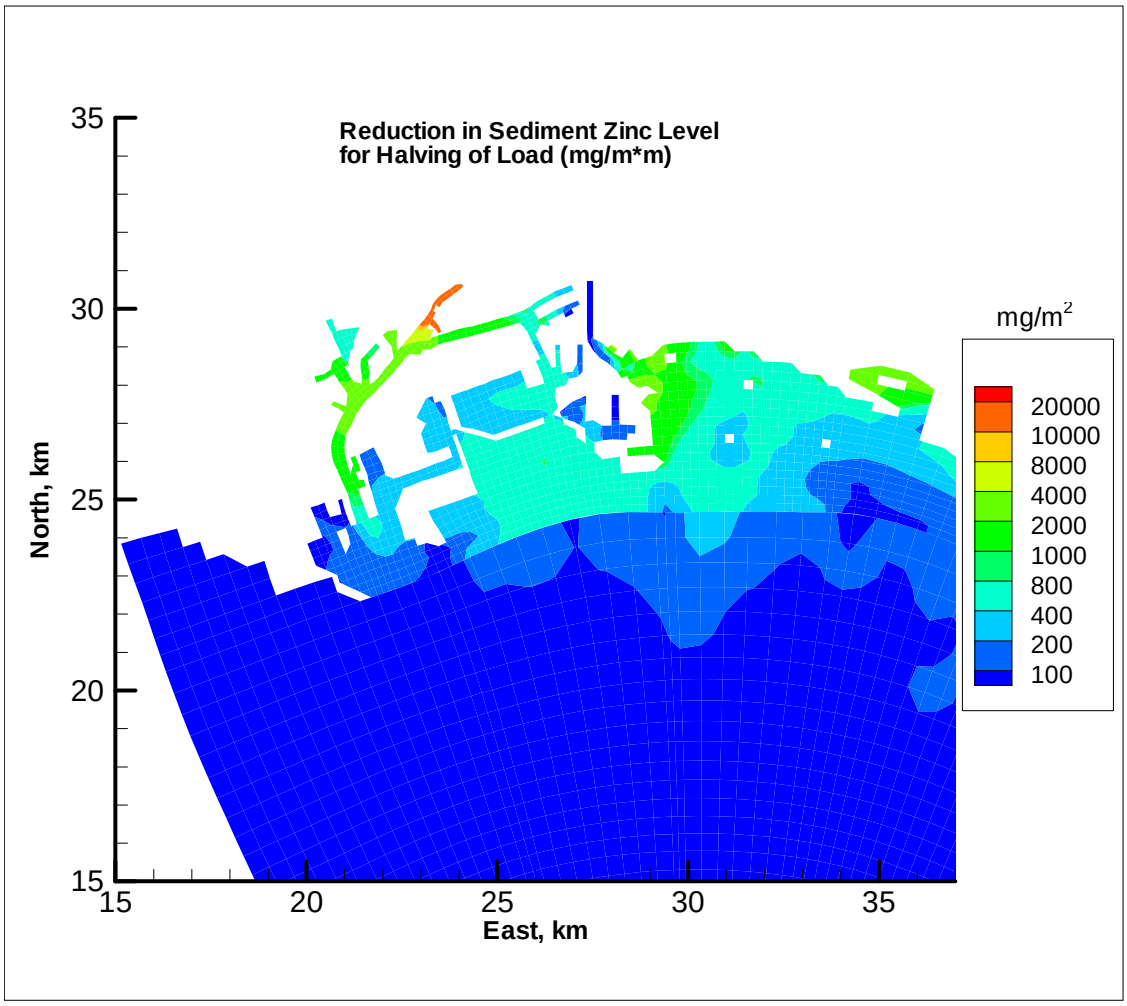

Note: Areal Concentration Change from Load Reduction Simulation = Final Areal Baseline Simulation Concentration in 2005 – Final Areal Load Reduction Concentration in 2005 (based on 50 percent load reduction from the rivers and nearshore watersheds). Results are presented in mg/m^2.

Figure D-13. Areal concentration change from load reduction simulation – zinc

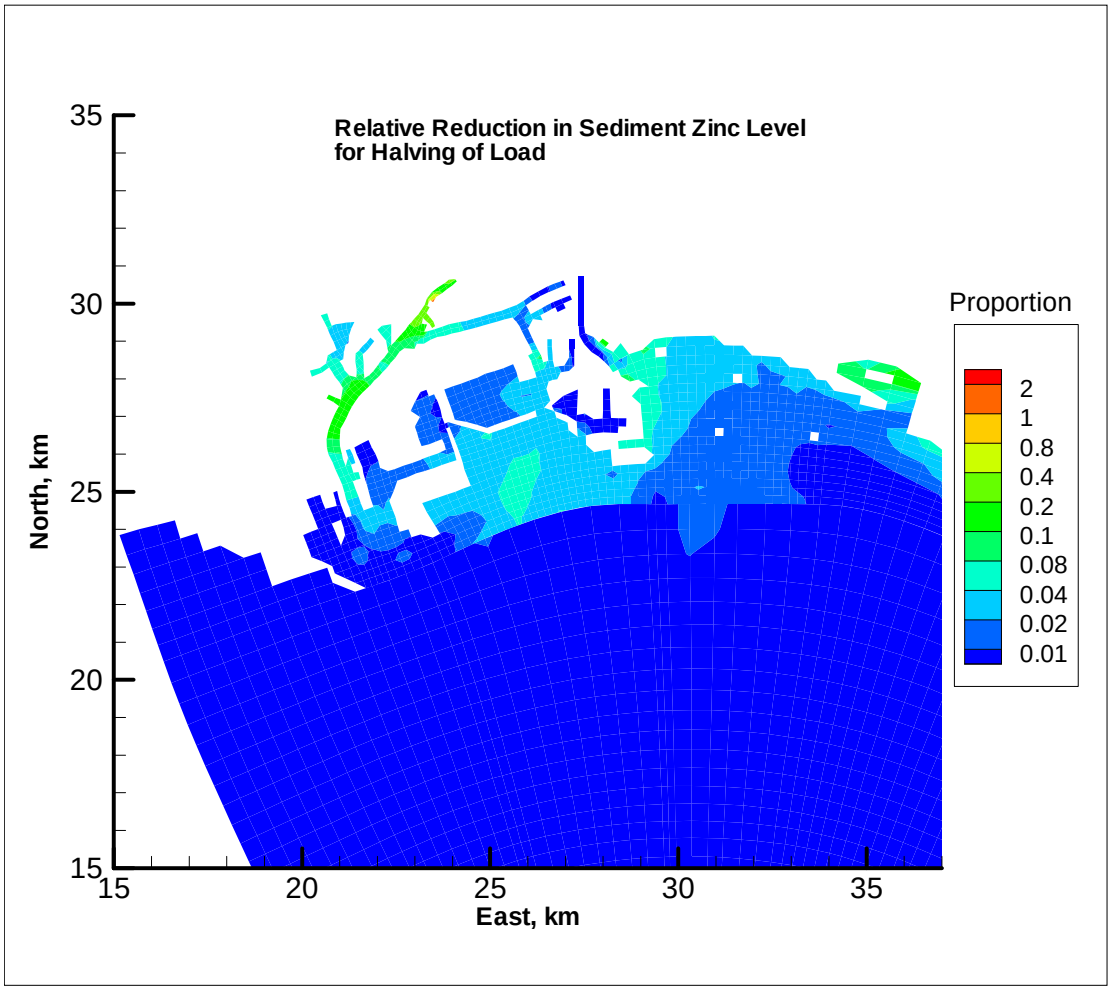

Note: Relative Change in Load Reduction Simulation = Relative Change in Load Reduction Change (normalized by initial top bed layer concentration). Results are proportions and can be multiplied by 100 to obtain percent.

Figure D-14. Relative change in load reduction simulation – zinc

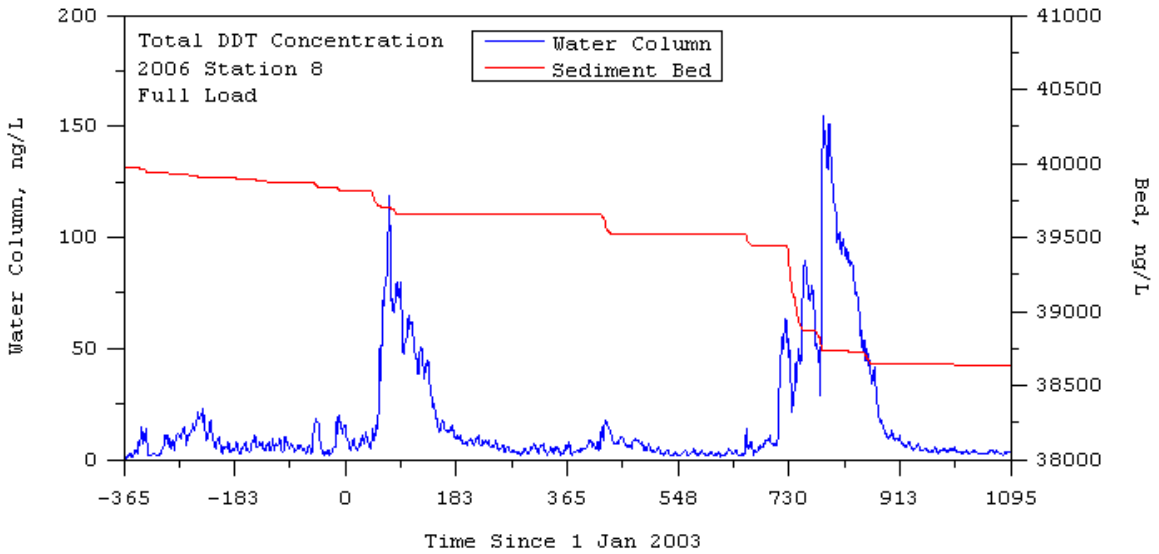

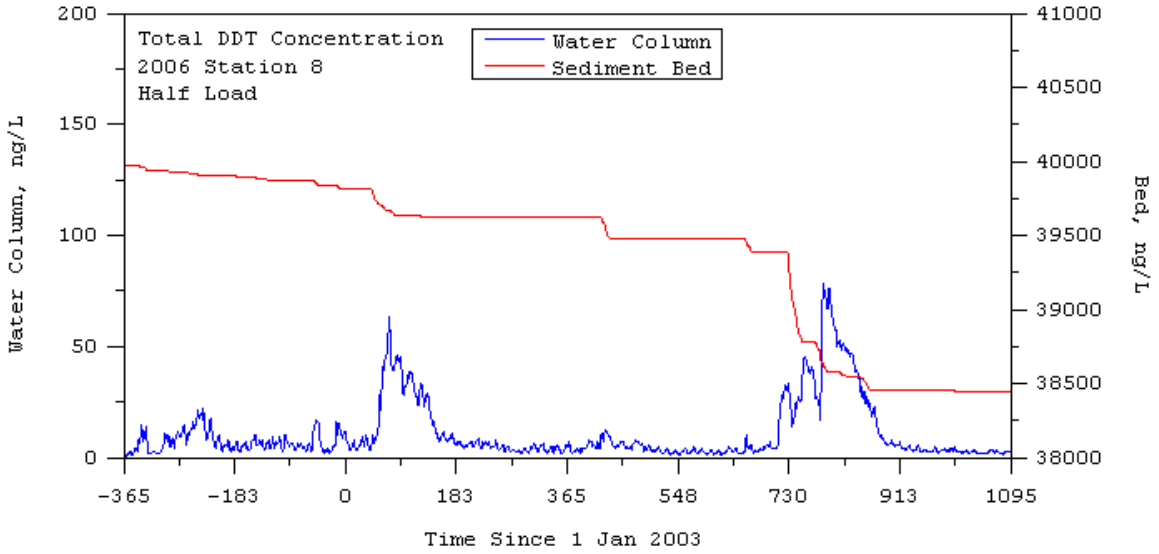

Figure D-15. Total DDT concentration in water column and at sediment bed surface for Station 8 (see Figure D-2 for location)

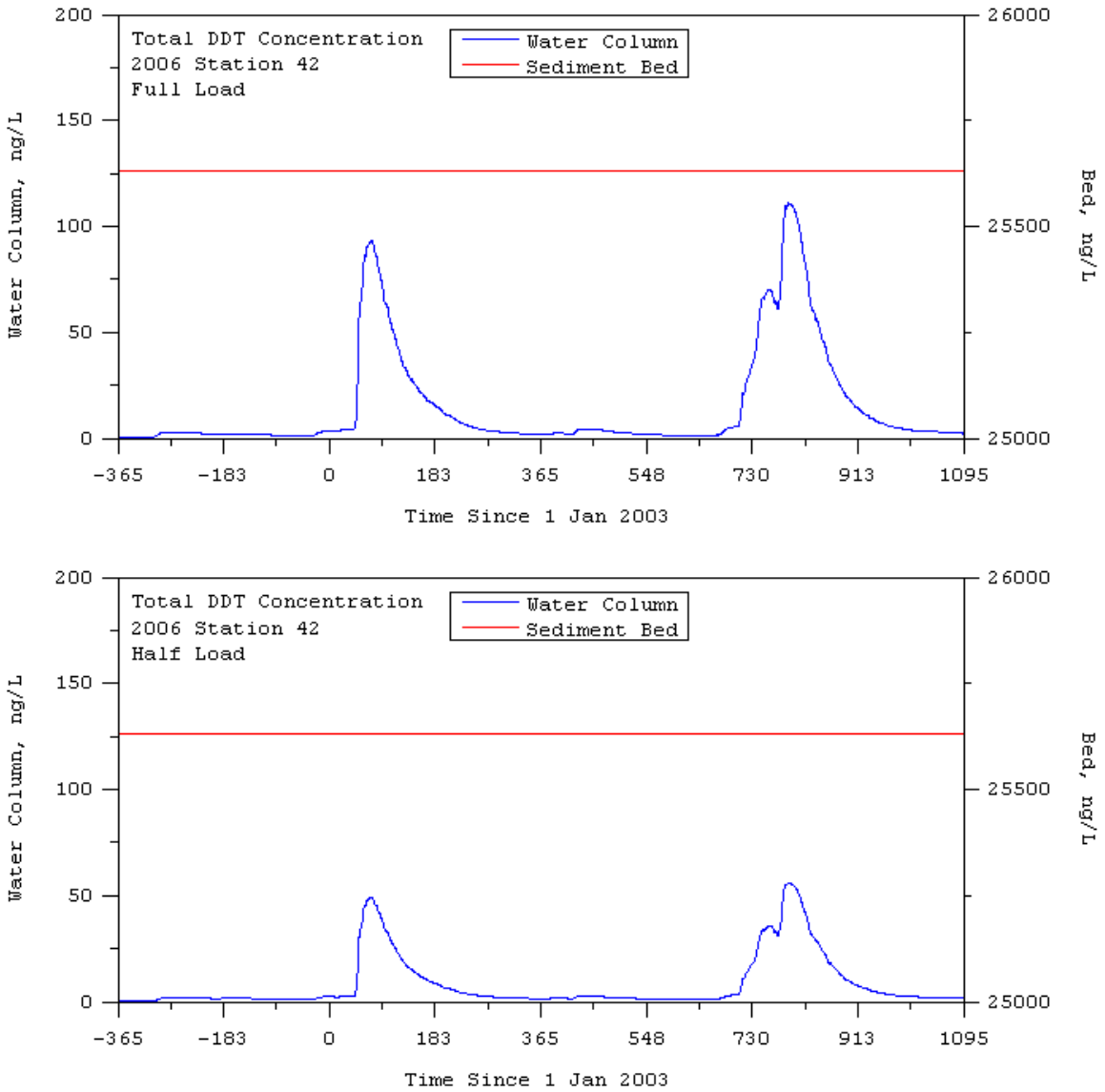

Figure D-16. Total DDT concentration in water column and at sediment bed surface for Station 42 (see Figure D-2 for location)

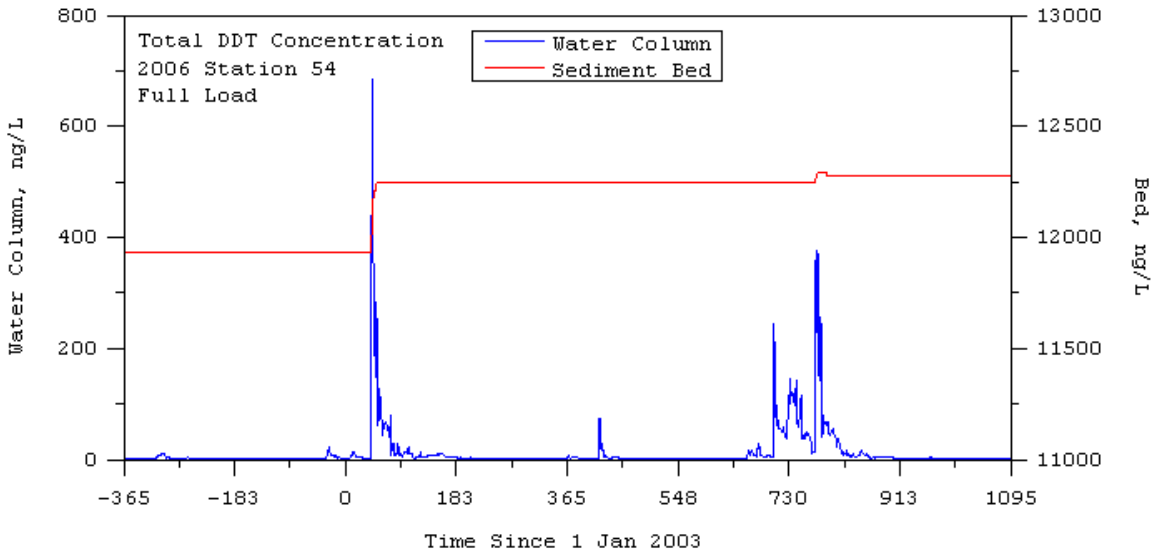

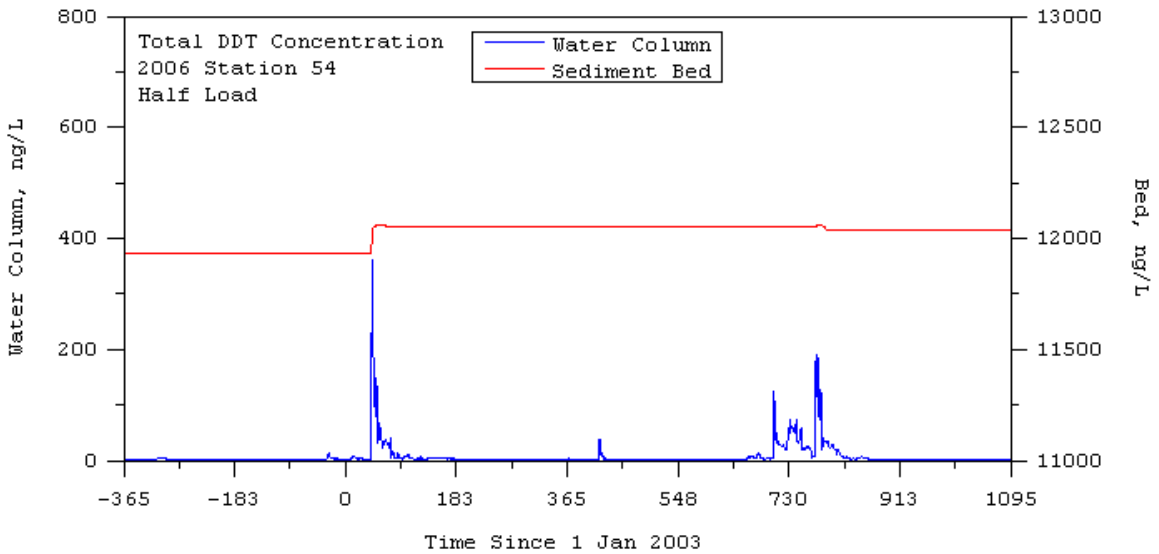

Figure D-17. Total DDT concentration in water column and at sediment bed surface for Station 54 (see Figure D-2 for location)

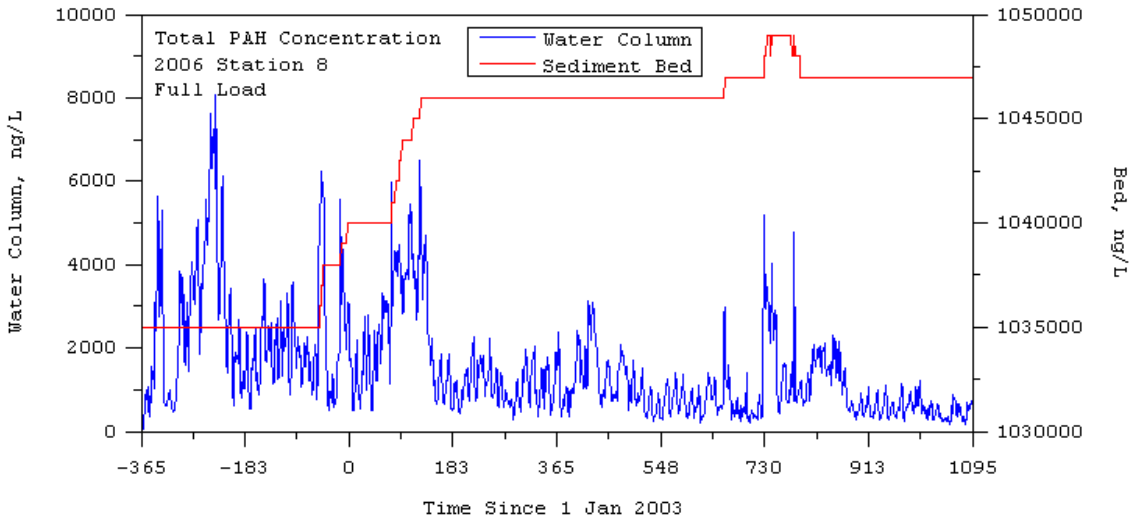

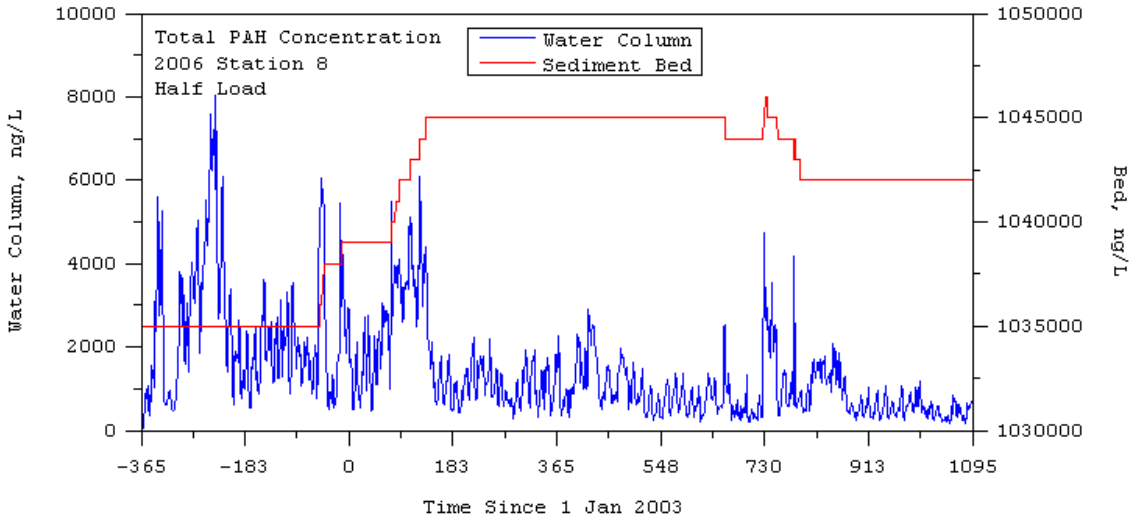

Figure D-18. Total PAH concentration in water column and at sediment bed surface for Station 8 (see Figure D-2 for location)

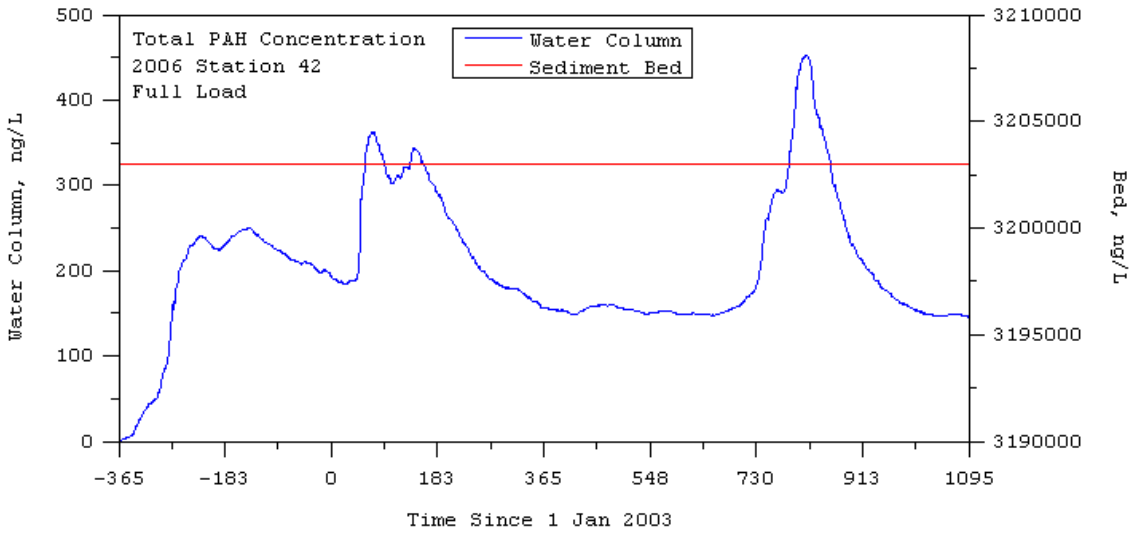

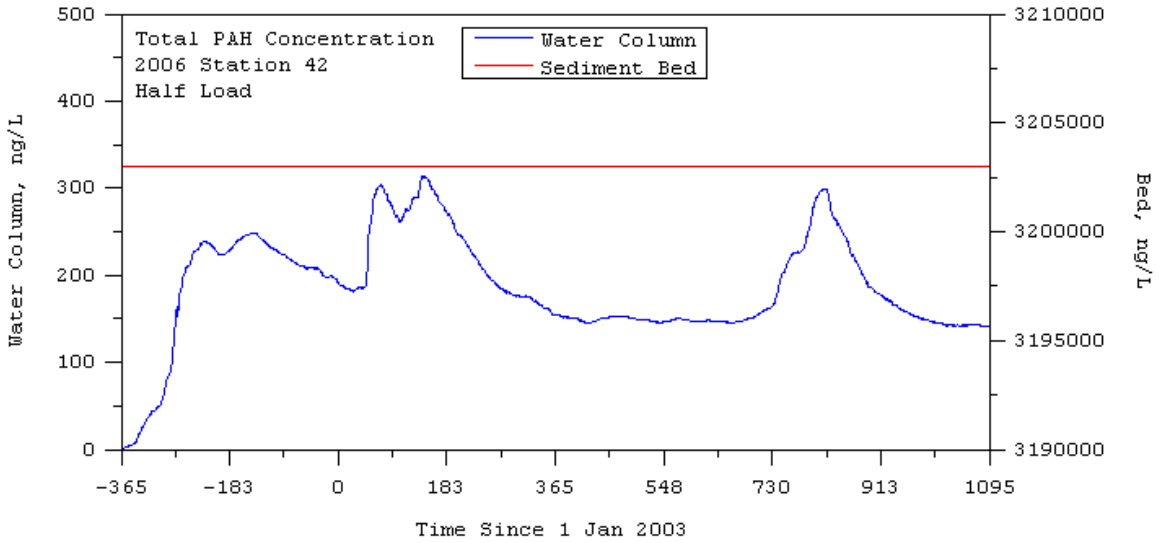

Figure D-19. Total PAH concentration in water column and at sediment bed surface for Station 42 (see Figure D-2 for location)

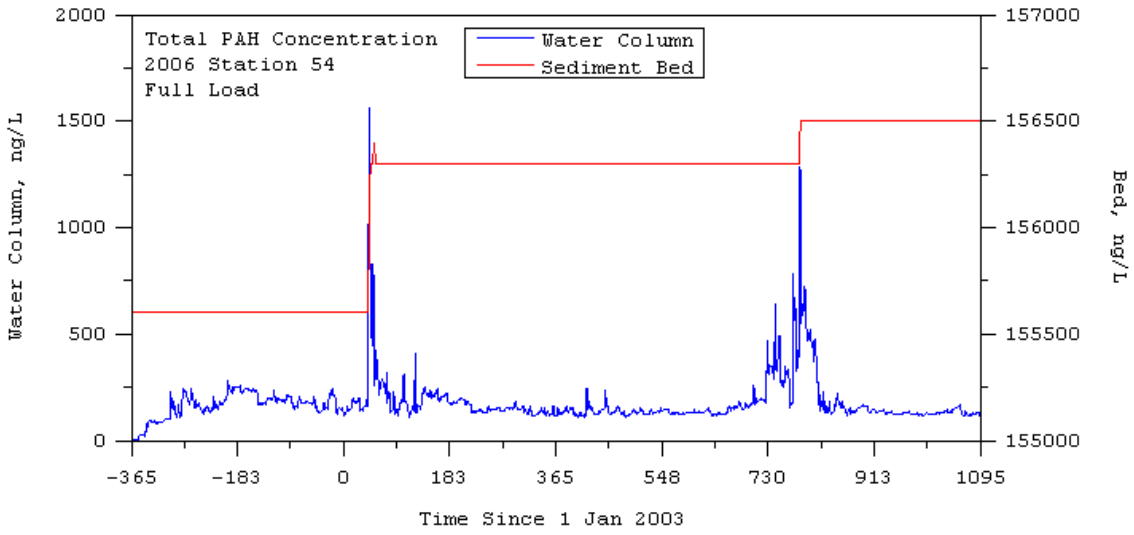

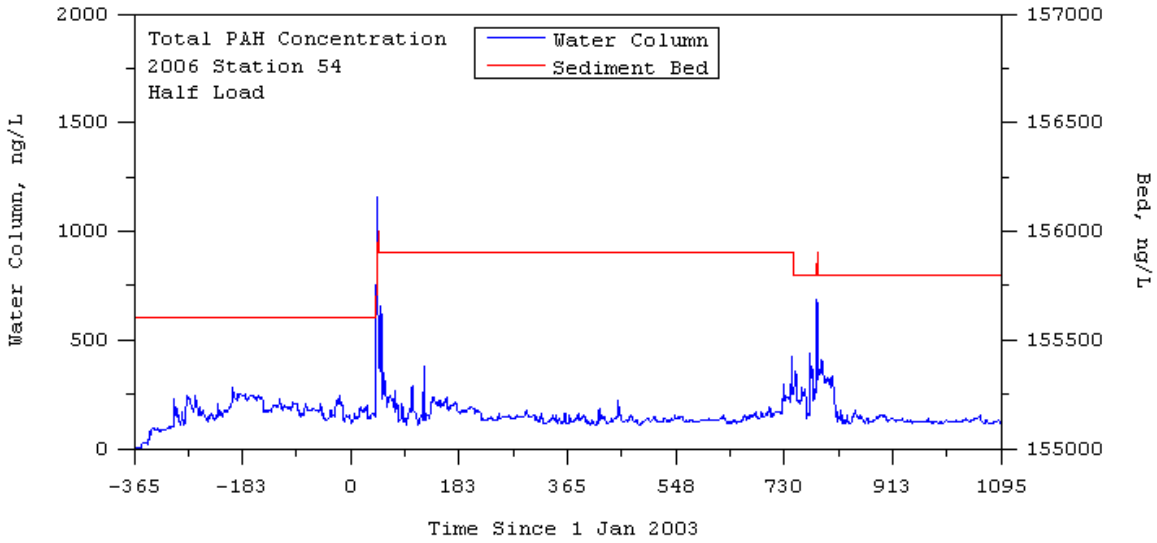

Figure D-20. Total PAH concentration in water column and at sediment bed surface for Station 54 (see Figure D-2 for location)

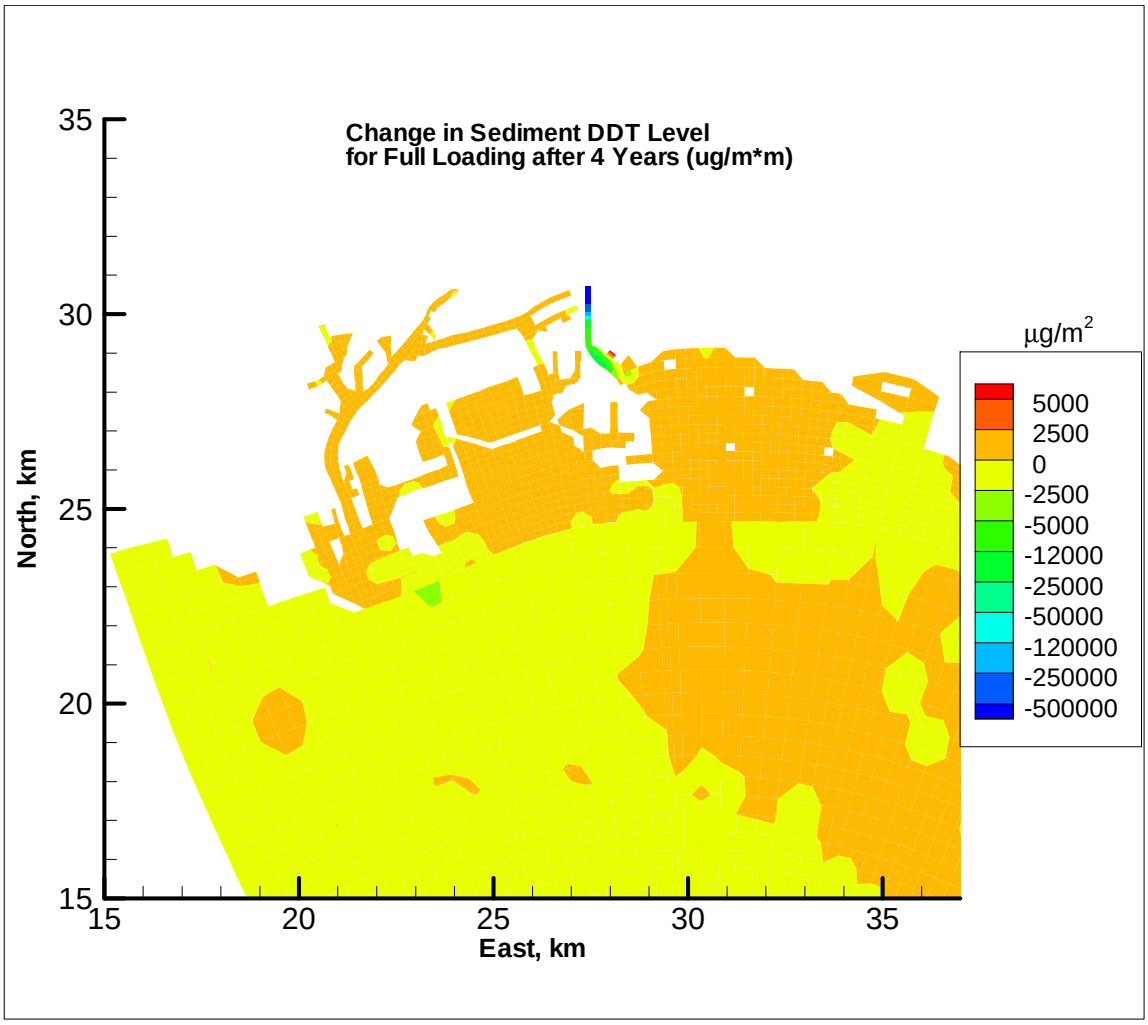

Note: Areal Concentration Change in Baseline Simulation Over Time = Final Areal Concentration using Baseline Conditions in 2005 (after 4 years) – Initial Areal Concentration using Baseline Conditions in 2002 (beginning of simulation period). Results are presented in $\mu g/m^2$.

Figure D-21. Areal concentration change in baseline simulation over time (after four years) – DDT

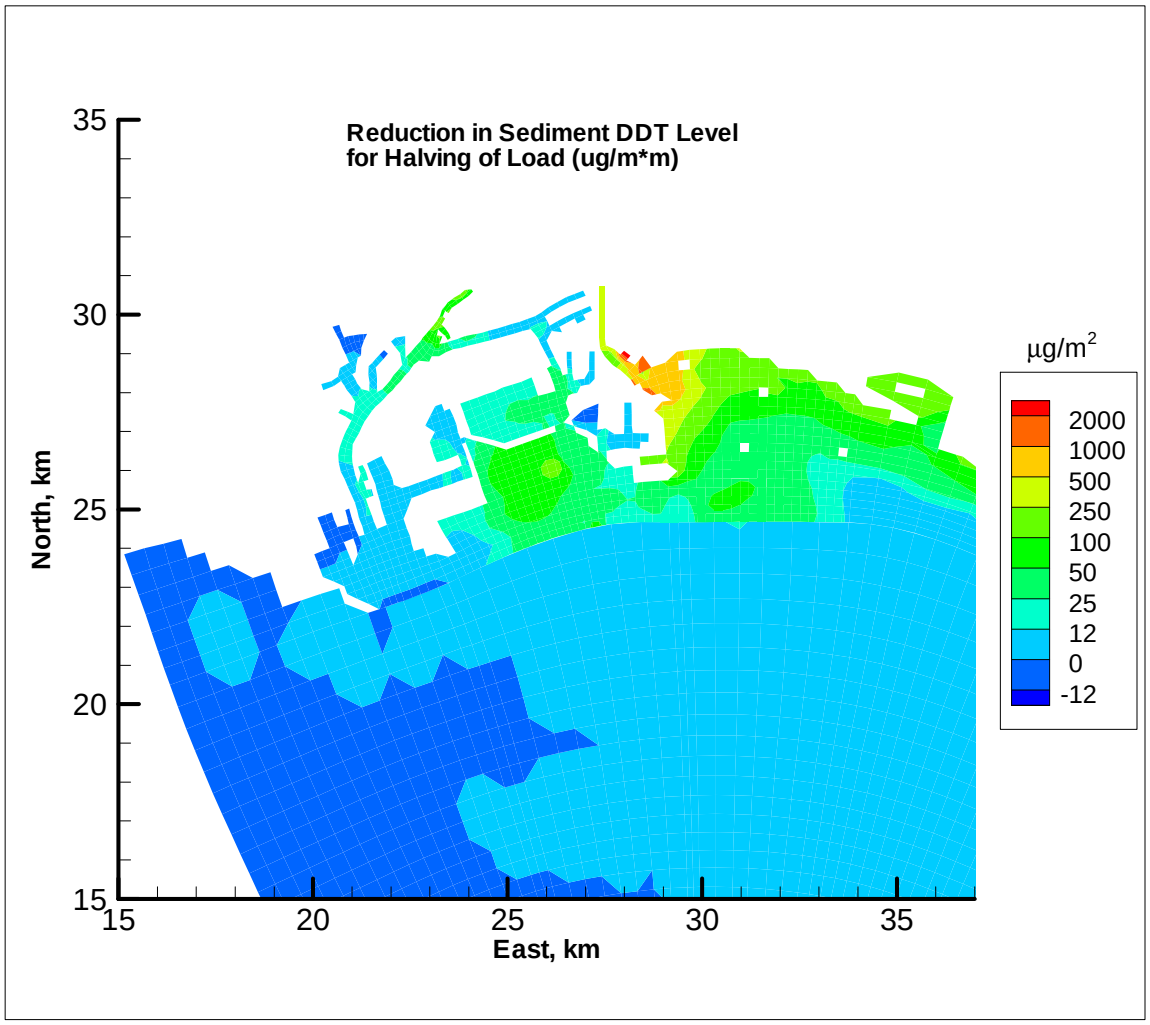

Note: Areal Concentration Change from Load Reduction Simulation = Final Areal Baseline Simulation Concentration in 2005 – Final Areal Load Reduction Concentration in 2005 (based on 50 percent load reduction from the rivers and nearshore watersheds). Results are presented in $\mu g/m^2$.

Figure D-22. Areal concentration change from load reduction simulation – DDT

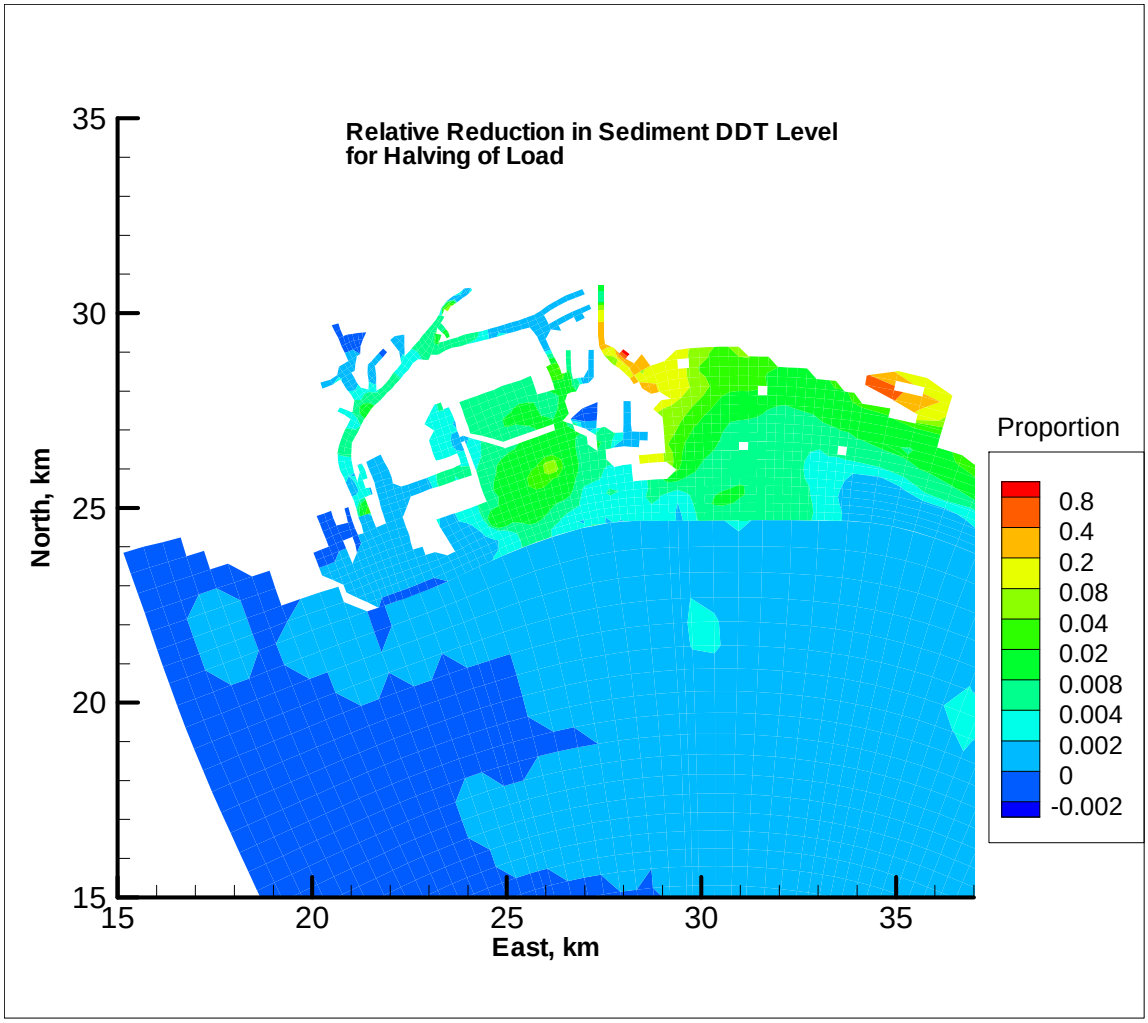

Note: Relative Change in Load Reduction Simulation = Relative Change in Load Reduction Change (normalized by initial top bed layer concentration). Results are proportions and can be multiplied by 100 to obtain percent.

Figure D-23. Relative change in load reduction simulation – DDT

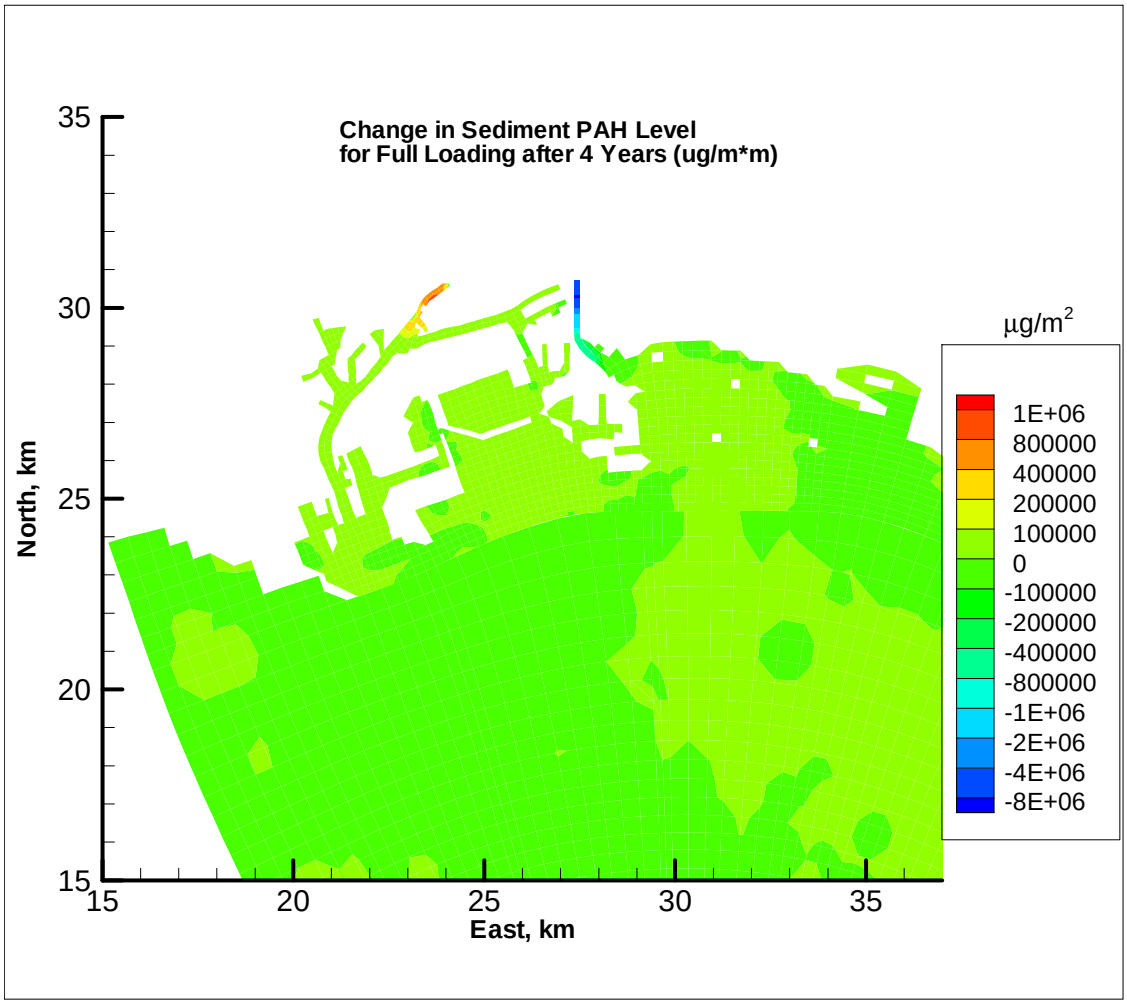

Note: Areal Concentration Change in Baseline Simulation Over Time = Final Areal Concentration using Baseline Conditions in 2005 (after 4 years) – Initial Areal Concentration using Baseline Conditions in 2002 (beginning of simulation period). Results are presented in $\mu g/m^2$.

Figure D-24. Areal concentration change in baseline simulation over time (after four years) – PAH

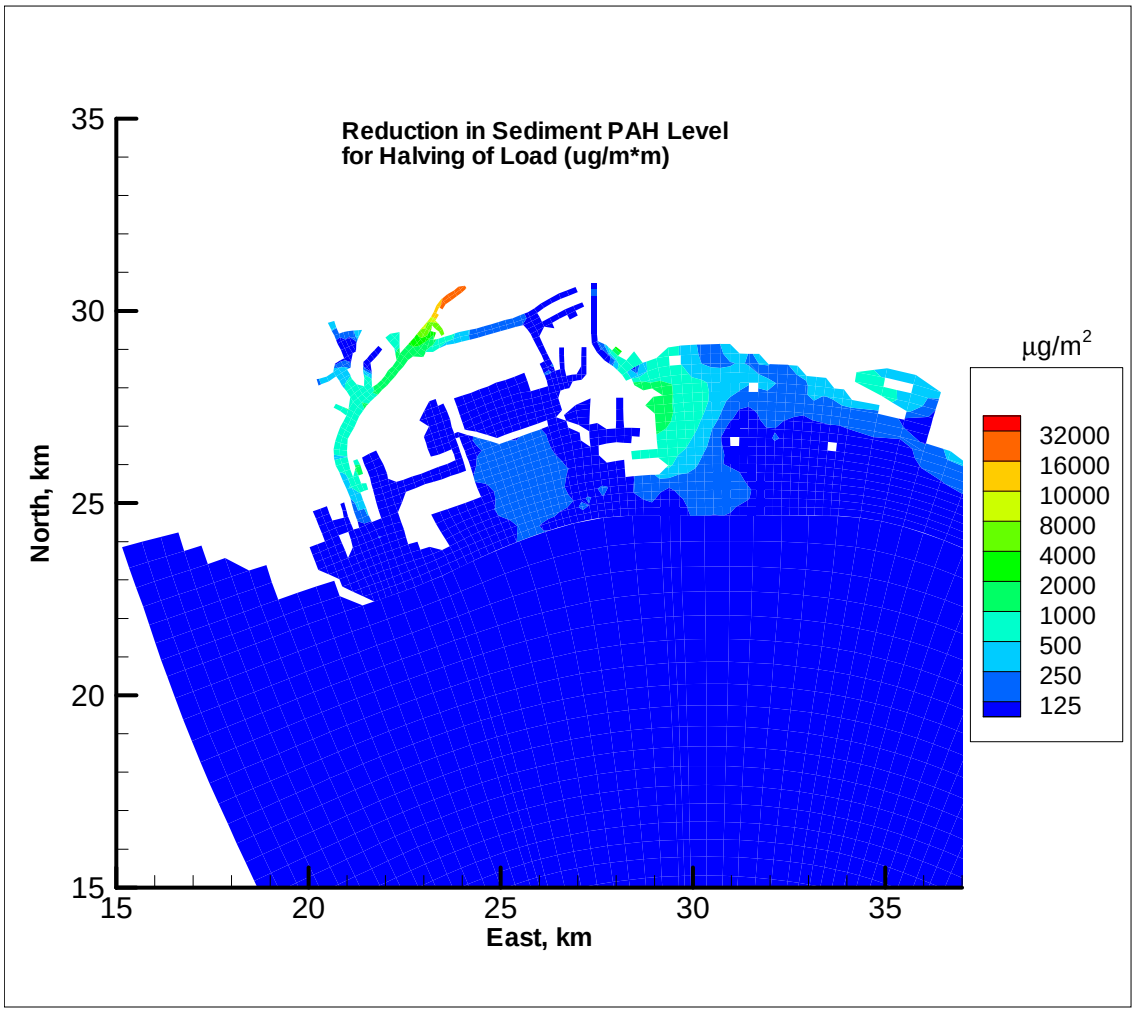

Note: Areal Concentration Change from Load Reduction Simulation = Final Areal Baseline Simulation Concentration in 2005 – Final Areal Load Reduction Concentration in 2005 (based on 50 percent load reduction from the rivers and nearshore watersheds). Results are presented in µg/m^2.

Figure D-25. Areal concentration change from load reduction simulation – PAH

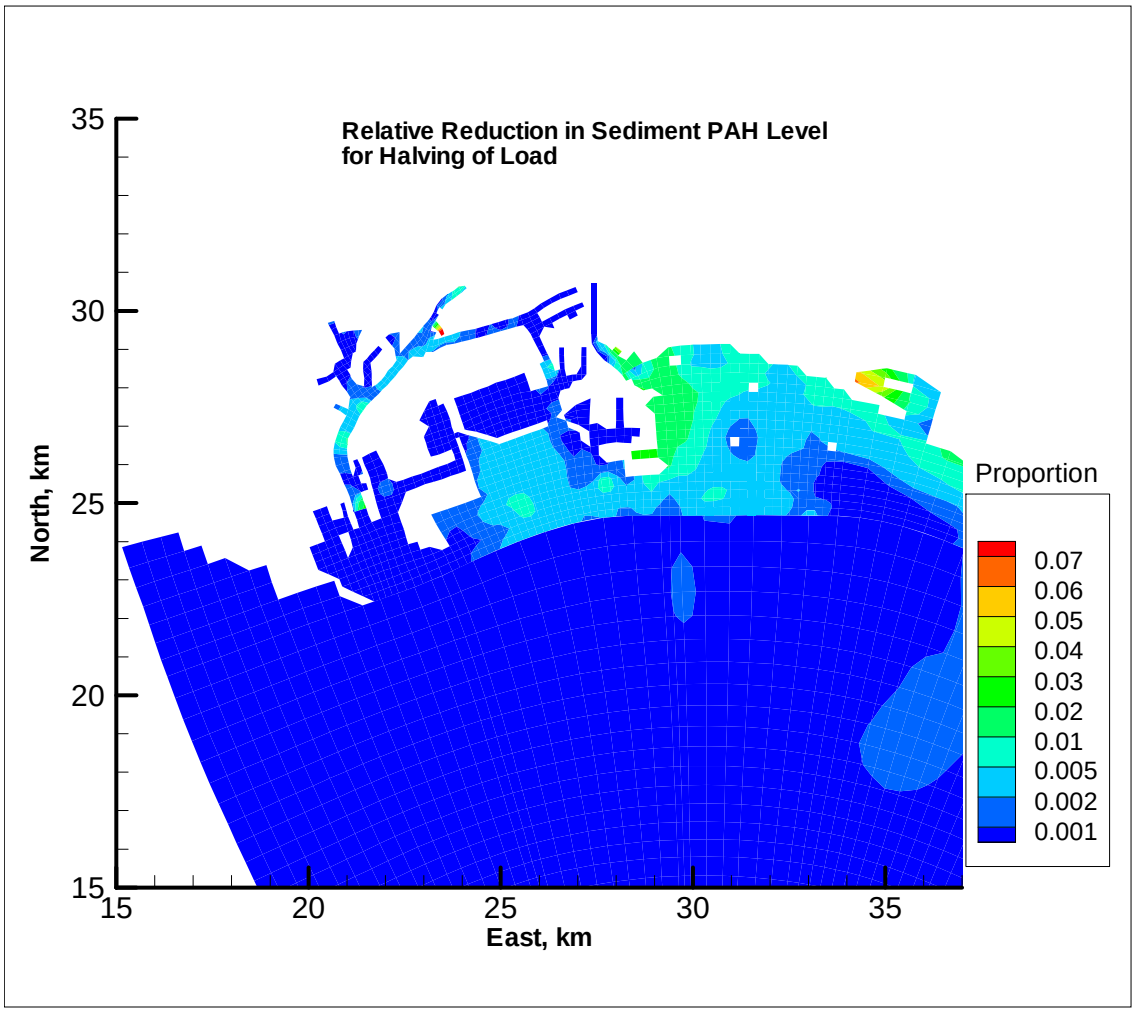

Note: Relative Change in Load Reduction Simulation = Relative Change in Load Reduction Change (normalized by initial top bed layer concentration). Results are proportions and can be multiplied by 100 to obtain percent.

Figure D-26. Relative change in load reduction simulation – PAH

Appendix E: Analysis of Additional Water Column Metals and Suspended Solids Data

DRAFT

November 2008

Prepared for:
USEPA Region 9
Los Angeles Regional Water Quality Control Board

Prepared by:
Tetra Tech, Inc.

Introduction

Subsequent to conducting the calibration and sensitivity simulations for metals, described in Chapter 8 and Appendix C, using water column partition coefficients in column 5 of Table 21, additional water column metals and sediment concentration data sets became available. These data sets include dissolved and total metals data collected during January and March 2006 and dissolved and total metals and suspended solids data collected in January 2008. The locations of these data sets correspond to the 2005 locations shown in Figure 25. The following sections present, analyze, and discuss these data sets.

Water Column Metals Data: 2006

Dissolved and total metals concentrations were reported for 66 mid-water column sampling locations in January and March of 2006 in waters of the Port of Los Angeles. For comparison with the 2005 POLA and 2006 POLB data, these data were used to determine the ratio of the particulate to dissolved fraction, which also corresponds to the product of the equilibrium partition coefficient and suspended solids concentration according to

$$K_p \bullet P = \frac{C_p}{C_d} \qquad (6)$$

where P is the suspended sediment concentration. Figure E-1 shows scatter plots of the ratio for copper, lead, and zinc. Table E-1 summarizes the average values of the ratios and compares them with results for 2005 POLA and 2006 POLB stations (Figure 26 and Table 21, fourth column). The concentration ratios for the three metals, copper, lead, and zinc, are very consistent between the two data sets. The range of average partition coefficients corresponding to an assumed range of sediment concentrations is shown in the fourth column of Table E-1.

Water Column Metals and Suspended Solids Data: 2008

Dissolved and total metals concentrations and total suspended solids were reported for 43 mid-water column sampling locations in January 2008 in waters of the Port of Los Angeles. For comparison with the 2005 POLA and 2006 POLB data, these data were used to determine the partition coefficient with the following equation:

$$K_p = \frac{1}{P}\frac{C_p}{C_d} \qquad (5C)$$

where P is the suspended sediment concentration. Figure E-2 shows the partition coefficients for copper, lead, and zinc as function of the suspended sediment concentration. The fifth column of Table E-1 summarizes the average values of the partition coefficients. These can be compared to the range estimated using the POLA 2006 particulate to dissolved concentration ratio.

For comparison, the model calibration and sensitivity simulations (Chapter 8 and Appendix C) conducted before these data became available used partition coefficients of 0.25, 1.25, and 0.05 L/mg for copper, lead, and zinc, respectively. The model simulation values used for copper and lead, 0.25 and 1.25, are very consistent with the observation-based values of 0.17 and 1.5. The model simulation value for zinc (0.05 L/mg) is significantly less than the average observation-based value, but still within the range of shown for zinc in Figure E-1 and Table E-1.

Table E-1. Equilibrium Partition Coefficients and Particulate to Dissolved Concentration Ratios for Metals

Contaminant	**Water Column Particulate to Dissolved Concentration Ratio *POLA2005 POLB2006***	**Water Column Particulate to Dissolved Concentration Ratio *POLA2006***	**Range of Partition Coefficients, L/mg Corresponding to TSS range of 1 to 10 mg/L (based on *POLA2006*)**	**Average Partition Coefficients, L/mg for *POLA2008***
Copper	0.51	0.72	0.05 to 0.7	0.17
Lead	7.12	6.28	0.6 to 7	1.5
Zinc	0.20	0.19	0.02 to 0.2	0.20

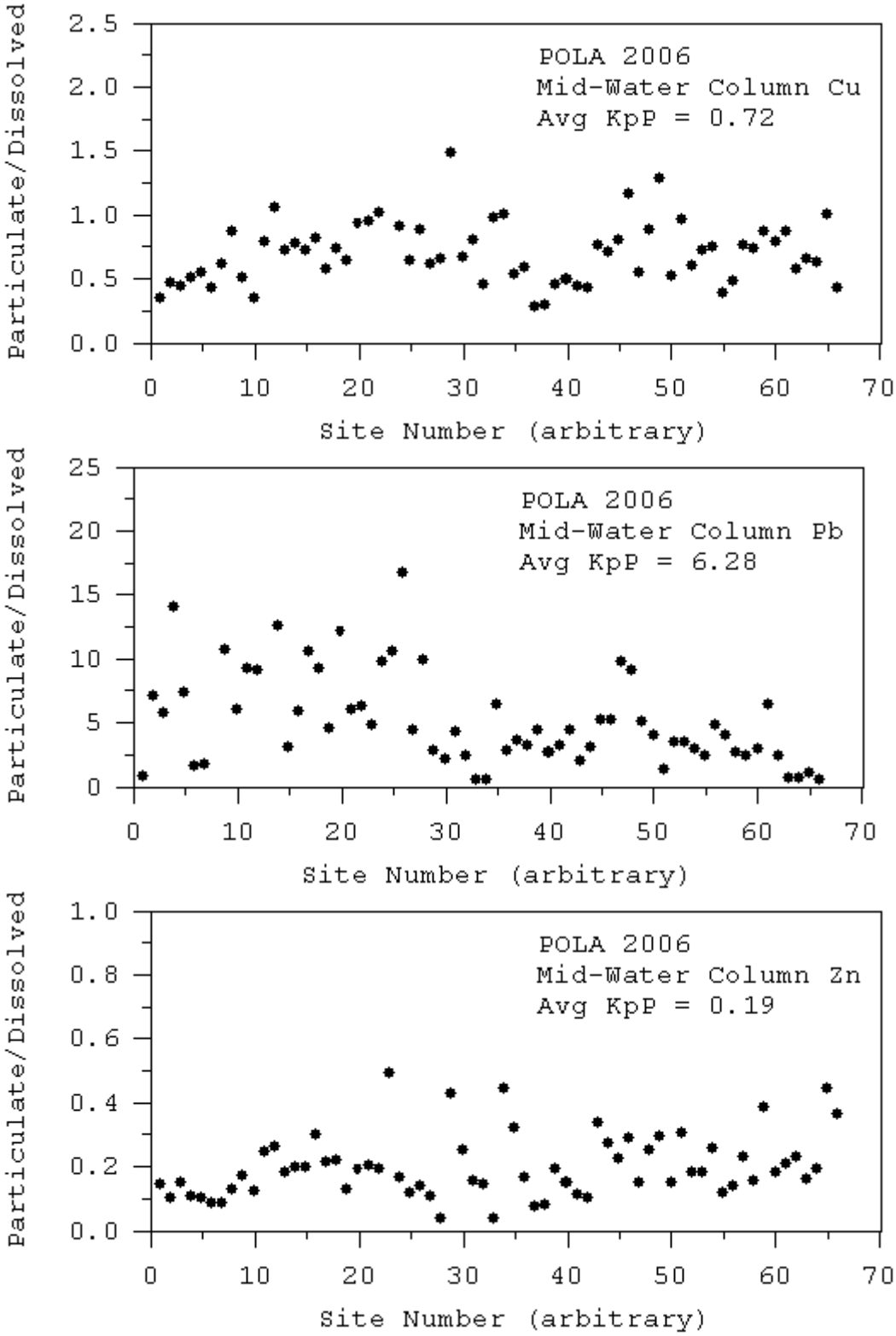

Figure E-1. Particulate to dissolved concentration ratio (equal to product of partition coefficient and adsorption site particle concentration) for 2006 POLA mid-water column metals samples

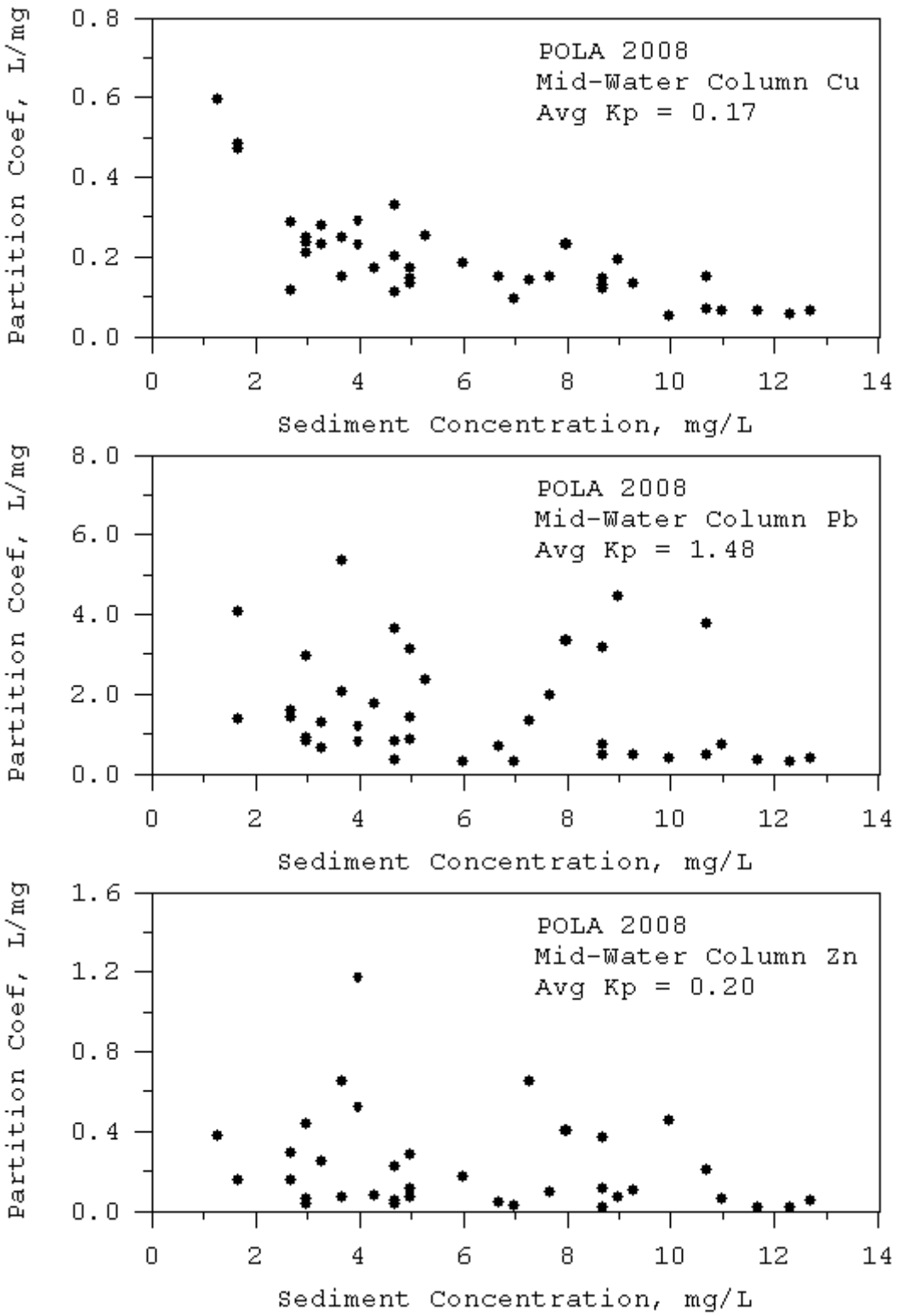

Figure E-2. Partition coefficients for copper, lead, and zinc as a function of suspended sediment concentration for 2008 POLA mid-water column samples